Title

Synthesis and Development of Biologically and Environmentally Stimulated Polymers

Author

Fruehauf, Krista

Publication Date

2020

UNIVERSITY OF CALIFORNIA,
IRVINE

Synthesis and Development of Biologically and Environmentally Stimulated Polymers

DISSERTATION

submitted in partial satisfaction of the requirements
for the degree of

DOCTOR OF PHILOSOPHY

in Chemistry

by

Krista Rose Fruehauf

Dissertation Committee:
Professor Kenneth J. Shea, Chair
Professor Jennifer Prescher
Professor Zhibin Guan

2020

DEDICATION

In memory of my mother.

TABLE OF CONTENTS

CHAPTER 1: Metabolite Responsive Nanoparticle–Protein Complex

CHAPTER 2: Polymers of Intrinsic Microporosity for Water Filtration

CHAPTER 3: Progress Towards Photodegradable Polymethylene

LIST OF FIGURES

LIST OF SCHEMES

ACKNOWLEDGMENTS

First, I want to thank Professor Kenneth Shea for being my advisor. You have taught me a lot of things, both chemistry and life related. I don't think I'm able to put into words how grateful I am for your support these past five years. Thanks for always telling me that your students are like family and pushing me to be more confident in myself. You always wanted me to succeed and knew that I could, which helped me do just that.

I would like to thank my committee members, Professor Jennifer Prescher and Professor Zhibin Guan for their guidance and suggestions. I would like to thank Professor Szu-Wen Wang for her guidance, ideas on my project, and giving me the opportunity to publish something I'm proud of. Thanks to Professor Joseph Patterson for his assistance with my TEM experiments and guidance both in and out of the lab. Thanks to Professor Jose Eduardo Baez for his mentorship, advice about life, and assistance with polyhomologation as well as the polymers of intrinsic microporosity. Thanks to Dr. Darryl Sasaki for his cleaning tendencies as well as general advice on things both chemistry and life related. Thanks to the LDOS team, especially Sandra Tsing-Loh, for helping me see a larger picture of communication and the world outside of graduate school.

I want to thank my dad, from the bottom of my heart and with my whole heart. You have been my number one supporter in all things. You tirelessly listened to me complain, cry, whine, and yell about anything and everything these past five years. But you also made sure that I felt loved and supported regardless of what decisions I was making. You are the reason I went to grad school and the reason I finished. I have learned so much from you and I hope I can keep on making you proud. My success is thanks to you!

I want to thank my mom, even though she wasn't able to watch me grow as a scientist and a person. Although she passed away at the very beginning of my graduate school journey, I never stopped feeling her love and support. I miss you Mama. This is for you.

I have many friends to thank. Thank you to my friends from UCSB who supported me when times were so tough, I wasn't sure I was going to make it through. Thank you to my friends at UCI, who accepted and helped me through many difficult times no matter how busy they were with their own lives and research. I know I've made some of the best friends I will have for the rest of my life. Thank you to my friends from Sender One who helped create a place for me to be silly, relax, and have fun outside of school. All of you have made a huge difference in my life in the last five years and I wouldn't be writing this without you.

In addition, I would like to thank UCI facilities, especially Dr. Dima Fishman and Dr. Xiaofeng Liu for their patience and assistance on many projects when I wasn't sure what instrument to use or how to use it. I would also like to thank Dr. Ben Katz and Dr. Felix Grun for their assistance in the mass spec facility. Thanks to the MCP program for providing me an opportunity to find my passion in science and for supporting me in my first year at UCI. I want to thank the School of Physical Sciences for funding me and giving me an opportunity to be the first SciComm Fellow from Chemistry. Thank you to the UCI

Chemistry Department for their assistance with all things related to paperwork, room reservations, and in general.

I thank the American Chemical Society for permission to include Chapter One of my dissertation, which was originally published in Biomacromolecules. Financial support was provided by the University of California, Irvine

CURRICULUM VITAE

Krista R. Fruehauf

Education

University of California, Irvine (UCI) (September 2015 – June 2020)
PhD in Chemistry
Advisor: Professor Kenneth J. Shea.
Research focuses:

1. Developing polymer hydrogel nanoparticle-protein conjugates as a metabolite responsive drug delivery system.
2. Synthesis of intrinsically porous polymer membranes for water purification.
4. Developing a photolabile polymer for photodegradable commodity plastic applications.
5. Synthesizing polymer hydrogel nanoparticles and linear polymers as abiotic protein affinity reagents for use as inexpensive alternatives for biomacromolecule purification.
6. Synthesizing polymers with protein affinity for electrospinning as a potential membrane for protein purification.

University of California, Santa Barbara (UCSB) (September 2011 – March 2015)
B.S. in Physiology.
Advisor: Professor Javier Read de Alaniz.
Research focuses:

1. Synthesis of an aza-spirocycle motif of natural products stemonamine and omacetaxine mepesuccinate.
2. Direct conversion of phenols to anilines and nitrosobenzenes.

Skills and Training

- Expertly trained in small molecule and polymer synthesis requiring water and air sensitive reaction conditions.
- Extensive experience in small molecule, polymer, and material characterization techniques including NMR, MS, DLS, GPC, High Temperature GPC, SEC-MALS, FTIR, DSC, MALDI-TOF, physical adsorption.
- Highly experienced in evaluation of protein-polymer nanoparticle interactions using UV-Vis, Equilibrium Dialysis, Fluorescence, Circular Dichroism.
- Mentored undergraduate student researchers.
    - Planned experiments and discussed future research directions with students.
    - Trained undergraduates to perform organic small molecule and polymer synthesis.
    - Revised papers as well as oral and poster presentations.
- Teaching Assistant for undergraduate lecture discussion and laboratory sections.
    - Prepared discussion materials, assisted in writing exams, advised students on laboratory procedures.
    - Teaching experience in undergraduate labs and lectures
        - Advanced materials

            - Organic chemistry

Leadership

- Managing Editor for the KPCC podcast “The Loh Down on Science” (April 2019 – May 2020)
    - Work with writers to review scripts and offer feedback or final edits before recording.
    - Organize and assist producer and host during studio recording sessions
- Vice President of Iota Sigma Pi, Calcium Chapter (June 2018 – June 2020)
    - Support and assist the club members in routine club activities and events
    - Volunteering at local outreach events, such as at the Santa Ana Zoo with ACS for National Chemistry Week and partnering with United Cerebral Palsy of Orange County to perform demos with small groups of children
    - Participate in resumé or fellowship workshops and panels to educate and discuss undergraduates and younger graduate students about graduate school
- Safety Officer for the Shea lab (January 2016 – June 2020)
    - Maintain chemical inventory of the lab
    - Train all new members on safety standards of the lab
    - Ensure all members understand and follow safety rules and regulations
    - Attend various department and campus-wide safety workshops and walk-throughs with other labs to stay current with potential hazards and how to handle different situations
- Vice President and President of Global Water Brigades, UCSB Chapter (October 2013 – March 2015)
    - Lead club meetings, organized fundraising events, and planned trips to Honduras where our club worked with the local, rural community to build sustainable water systems. These systems helped bring clean, running water to their homes for the first time. Educated communities about water sanitation and hygiene.

Extracurricular Activities

- Science Coach through ACS Science Coaches Program (October 2019 – June 2020)
    - Paired with one teacher throughout the school year as a volunteer to help advance chemistry education and interest
    - Assisted in planning lesson plans and executing demos
- Science Fair judge at the Irvine Unified School District Science Fair (2018)
    - Evaluated the elementary level science fair competition
    - Interacted and asked the students questions about their proposed projects and what they enjoyed most about the process
- Writer for the KPCC podcast “The Loh Down on Science” (April 2018 – May 2019)
    - Find new and exciting research ranging from psychology to physics to communicate to the public. Write short scripts (less than 200 words) for the average, non-scientific listener.
    - Scripts recorded to date: “Fantastic Plastic, “Sweet Bee”, “Hummingbird Hustle”, “Deep Dive”, “Achy Breaky Joints”, “Silky Secrets”, “Quiet Creativity”,

        “The Tooth is Out There”, “Water Wonder”, “Mighty Methane Munchers”, “Vision Quest”, “Photo Finish”, “Tangled Tongues”, “Toxic Baby Food”, “Rice Cooker”, “Relephant Factors”, “Bar-B-Q-rius”, “Tooth Toughener”, “Scent of a Mosquito”

- Outreach Volunteer with the UCI Chemistry Outreach Program (2016 – 2018)
    - Visit elementary, middle, and high schools in Orange County to perform chemistry demonstrations

Oral Presentations

Fruehauf, K; Shea, K.J. *Division of Polymer Chemistry, 258th ACS National Meeting and Exposition*, August 25-29, 2019, San Diego, CA.

“Separating the Left from the Right: A Chemist’s Challenge”, *Brews and Brains*, March 5, 2019, Costa Mesa, CA.

Fruehauf, K.; Kim, T.I.; Pham, Q.; Wang, S.W.; Shea, K.J., *Division of Polymeric Materials Science and Engineering, 256th ACS National Meeting and Exposition,* August 19-23, 2018, Boston, MA.

Fruehauf, K.; Kim, T.I.; Wang, S.W.; Shea, K.J., *99th Annual Meeting of the Pacific Division of the American Association for the Advancement of Science*, June 12-15, 2018, Pomona, CA.

Fruehauf, K.; Kim, T.I.; Wang, S.W.; Shea, K.J., *3rd Annual University of California Symposium for Chemical Sciences*, March 26-28, 2018, Lake Arrowhead, CA.

Fruehauf, K.; Kim, T.I.; Wang, S.W.; Shea, K.J., *27th Student Research Conference by Graduate Women in Science*, December 2, 2017, Orange, CA.

Publications.

St. Amant, A.H.; Frazier C.P.; Newmeyer B.; **Fruehauf K.R**.; Read de Alaniz, J. "Direct synthesis of anilines and nitrosobenzenes from phenols." *Org. Biomol. Chem*. **2016**, *14*, 5520-5524.

Fruehauf, K.R.; Kim, T.I.; Patterson, J.P.; Nelson, E.; Wang, S.W.; Shea, K.J. “Metabolite responsive nanoparticle-protein complex.” *Biomacromolecules* **2019**, *20*, 2703-2712.

Yoshimatsu, K.; **Fruehauf, K.R.**; Zhu, Q.; Weisman, A.; Fan, J.; Xue, M.; Bierle, J.M.; Shea, K.J. “Metal-free affinity medium for selective purification of His$_6$-tagged proteins.” Manuscript in preparation.

Onogi, S.; Lee, S.H.; **Fruehauf, K.R.**; Shea, K.J. “pH dependent multivalent interactions between polymer hydrogel nanoparticles and proteins.” Manuscript in preparation.

O’Brien, J.; Onogi, S.; Yuan, Z.; **Fruehauf, K.R.**; Shea, K. “Rapid evaluation of polymer – biomacromolecule interactions. A discovery platform for nanoparticle – biomacromolecule affinity pairs.” Manuscript in preparation.

Fellowships and Awards

- School of Physical Sciences Science Communication Fellow - Chemistry (January 2020 – August 2020)
- First Place Ph.D. Student Oral Presentation at the 27th Student Research Conference hosted by the Orange County chapter of Graduate Women in Science (2017)
- Robert H. DeWolfe Undergraduate Research Award (2014)

Patents

Metabolite Responsive Hybrid Materials, Tech ID 30162, UC Case 2019-076-0

ABSTRACT OF THE DISSERTATION

Synthesis and Development of Biologically and Environmentally Stimulated Polymers

By

Krista Fruehauf

Doctor of Philosophy in Chemistry

University of California, Irvine, 2020

Professor Kenneth J. Shea, Chair

Stimuli responsive polymers have been used for a plethora of applications. In this consolidated work, it has been used for two different applications. The first application is for drug delivery of hydrophobic therapeutics. To eliminate non-specific interactions in the body, a metabolite responsive nanoparticle that will enable more precise and specific delivery of therapeutic agents. Separately, the growing accumulation of plastics in the environment is troubling. Another stimuli responsive polymer, found in the third chapter, explores developing a photodegradable analogue to poly(ethylene), one of the most popular commodity plastics. An additional problem examined in this dissertation is water purification. The second chapter encompasses work done to develop a polymer of intrinsic microporosity for aqueous applications, specifically filtering out virus particles. Although these topics do not overlap, the main focus is on human health and interactions with the environment.

Chapter 1: Metabolite Responsive Nanoparticle-Protein Complex

Preface

Stimuli responsive polymers have been developed to target a variety of diseases. These specific disease states are chosen based on their distinct microenvironments or the way they significantly alter normal physiology. These changes may lead to an increase in reductive or oxidative environments, a decrease in pH, an increase in temperature, alterations in ion or small molecule concentrations, heightened mechanical forces, higher expression of certain enzymes or proteins, and even structural changes to the surrounding tissue. All of these altered environments can be used as triggers to design stimuli-responsive polymer systems.1 However, the goal continues to be the ability to selectively target a specific site located in the body to eliminate non-specific response by the polymer systems. We believe we have achieved such an advance by developing a cancer metabolite responsive system, an approach which has rarely been explored and less frequently realized by the scientific community.

References

(1) Lu, Y.; Aimetti, A. A.; Langer, R.; Gu, Z. Bioresponsive materials. *Nature Reviews Materials*, **2017**, *2*, 1–17.

Introduction

Drug delivery has been a high priority for researchers in academia and industry alike. Challenges arise from solubilizing drugs, maximizing bioavailability, and ensuring selectivity toward the tissues and organs that are to be treated. However, combining these traits into a single vehicle remains elusive and has been a driving force for research. Methods devised to address these problems include developing stimuli-responsive materials. This strategy addresses the challenges of selectivity and, if designed appropriately, can help increase bioavailability.

Various strategies have been investigated including systems responsive to changes in pH,[1−10] reducing or oxidizing environments,[11] disease-associated enzymes[12−16] or small molecules,[17] hypoxic environments,[18] mechanical cues,[19,20] and temperature.[21,22] However, the relatively low incidence of clinical success would suggest there are still opportunities to improve performance.[23,24] Other methods draw inspiration from biology. Protein−polymer conjugates have made an impact in the scientific community as an attractive approach to address drug delivery. These strategies consist of noncovalent, covalent, and supramolecular interactions between polymers and proteins. Some examples involve protein cages, formation of polymer micelles around proteins, and synthesis of nanoparticles incorporating proteins into the backbone.[25−32] All of these strategies have been used to enhance the success and selectivity of delivering biological agents as well as drugs.

The versatility of nanoparticles allows for a range of approaches to be employed. Protein−nanoparticle complexes are of particular interest as treatments for various diseases, especially cancer. The stimuli response of protein−nanoparticle complexes has depended on many of the previously mentioned strategies. These studies have included adenosine-5′-triphosphate (ATP) and glucose-responsive systems.[33] Both the ATP and glucose systems rely on a concentration gradient or an intra- and intercellular difference in concentration of these molecules. The specificity of these systems is lacking in the sense that ATP and glucose are found throughout the body. High local concentration of a specific molecule or metabolite that is a signature of a disease can provide a chemospecific target for therapeutic intervention. However, there remains a compelling need to develop a responsive polymer−protein conjugated system designed around a specific disease associated metabolite. Designing a protein−nanoparticle complex that responds to a metabolite of disease could provide an effective solution to the issue of selectivity. By focusing on a molecule or metabolite that has distinctively high concentrations in the local area of disease, side effects can be minimized while maximizing therapeutic effects.

There have been many studies describing the Warburg effect in cancer progression. This phenomenon describes an accumulation of lactate, leading to a decrease in pH within the cancer microenvironment.[34−36] The phenomenon is attributed to cancer cells that predominantly utilize anaerobic glycolysis instead of oxidative phosphorylation.34−36 Cancer usually exists under low oxygen, or hypoxic, conditions so cells must compensate for this impediment to energy production. This leads to a lactate concentration higher than what is found under normoxic conditions. Anaerobic glycolysis is performed in healthy tissues as well, most notably during exercise when a buildup of lactic acid occurs. Healthy tissues have lactate concentrations between 0.5 and 2 mM,[37−39] while concentrations in tumor tissues range from 10 to 20 mM[40−43] and up to 40 mM.[35,40] The almost 10-fold increase in lactic acid lowers the pH from 7.4 to 6.0−7.0,[44] an effect that has been taken advantage of by designing polymers that release anticancer drugs under acidic conditions.[34−36] However, there are organs with regions of low pH that are not associated with cancer, most notably the stomach and kidney. A more chemospecific trigger, such as one that responds to high lactate concentrations, would be more effective.

In this report, we describe hydrogel nanoparticles (NP) that are responsive to lactate at physiologically relevant concentrations. To achieve this, we incorporated a known inhibitor of lactate dehydrogenase (LDH), oxamate, into the backbone of a hydrogel polymer. The polymer-bound oxamate was used to bind LDH, present as a homomeric tetramer, noncovalently to the polymer and function as a cross-linker between the polymer NP and LDH. We utilized *N*-isopropylacrylamide (NIPAm) as the base monomer. NIPAm was chosen due to its low affinity for plasma proteins, this minimizes any nonspecific binding of proteins other than the one of interest.[45] NIPAm polymers exhibit a lower critical solution temperature (LCST) at approximately 32 °C. Below this temperature, the polymer is solvent swollen. Increasing the temperature beyond 32 °C desolvates the particle, leading to a volume reduction. Our design strategy was to incorporate LDH into the polymer in its solvent swollen state (<32 °C) before raising the temperature to physiological conditions.

Our LDH was based on the protein sequence of *Bacillus stearothermophilus* LDH, a thermally stable and well-characterized protein that would be compatible with experimental conditions. LDH is a homomeric tetramer with four binding sites and provides a nexus for cross-linking by the polymer bound oxamate (Figure 1.1). This enzyme converts pyruvate into lactate, this is done at higher than normal rates within the tumor microenvironment so the cancer cells can utilize lactate fermentation. However, this enzymatic reaction is reversible, and lactate can be converted back into pyruvate with the same enzyme. The polymer-bound oxamate will noncovalently bind LDH; when more than one oxamate binds to the homomeric tetramer, the result is cross-linking. These cross-links will be competitively displaced by lactate upon entering an environment with elevated lactate levels. The decreased cross-linking of the polymer to LDH endows the particle with a lactate responsiveness that results in NP swelling. At appropriate loadings of inhibitor and LDH, one can tune the lactate responsiveness of the NP to the relevant physiological range of lactate in the local cancer environment.

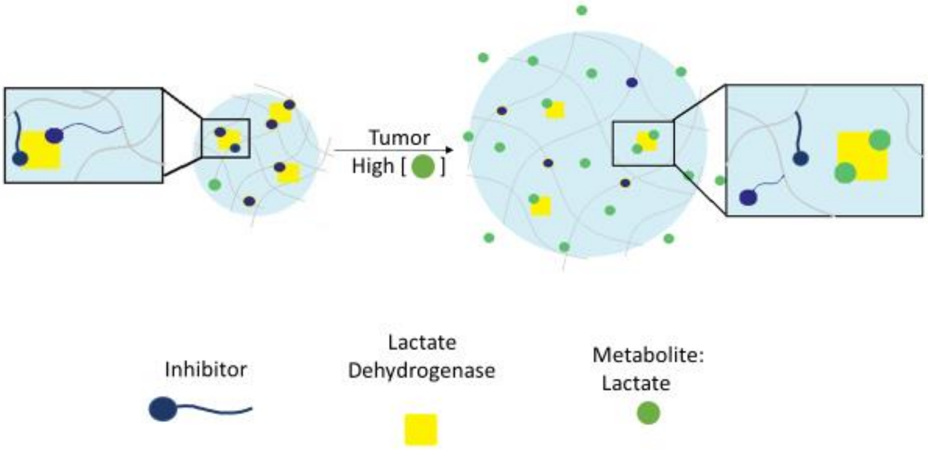

Figure 1.1: Lactate responsive nanoparticle. An inhibitor for LDH is incorporated into the NP. When LDH is introduced, the inhibitor acts as a cross-linker between the particle and protein leading to a decrease in NP size. Once the complex is introduced to lactate, the inhibitor is displaced and the cross-linking is eliminated. This leads to a swelling of the particle.

Experimental Section

^{1}H NMR spectra were recorded at 500 MHz, using a Bruker DRX 500 spectrometer. ^{13}C NMR spectra were recorded at 125 MHz, using a Bruker DRX CRYO500 spectrometer. ^{1}H and ^{13}C NMR spectra were run in $CDCl_3$ with shifts reported as δ values in ppm and referenced to residual solvent proton or carbon. Splitting patterns are abbreviated as follows: s = singlet, d = doublet, dd = doublet of doublets, t = triplet, q = quartet, quint = quintet, sext = sextet, sep = septet, m = multiplet, br = broad.

General Procedures.

Methylene chloride was obtained from a dry Solvent Dispensing System. Chloroform was distilled and kept under nitrogen. Amine bases were freshly distilled over CaH_2 from a ketal still. NIPAm was recrystallized from hexanes. All other commercial reagents were used as received. Reactions were monitored by thin layer chromatography using glass-backed EM Science Silica Gel 60 PF254 Plates. Flash chromatography was performed using EM Science Silica Gel 60 (230−400 mesh). All volatile solvents were removed, in vacuo, under reduced pressure using a Büchi rotary evaporator.

Inhibitor Synthesis.

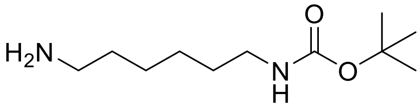

1-Boc-1,6-Hexanediamine ***2***. A solution of 1,6-hexanediamine (11g, 100 mmol) in chloroform (26 mL) was cooled to 0 °C with an external ice bath then treated via dropwise addition over 2 h with a solution of Boc anhydride (4.4 g, 20 mmol) in chloroform (20 mL). Reaction was removed from ice and allowed to warm to room temperature. After reacting overnight, the solution was filtered, filtrate concentrated in vacuo, re-dissolved in ethyl acetate, washed with brine (3×), dried over $MgSO_4$, filtered, and then concentrated in vacuo. Flash column chromatography was performed and eluted with methylene chloride treated with an equal volume of methanol:ammonium hydroxide solution then concentrated in vacuo to yield 4.5 g (81%) of a thick white oil. ^1H, ^{13}C NMR, and HRMS matched the literature values.[46]

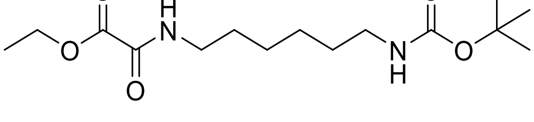

*Oxamide Ester **3***. To a cooled solution of ethyl chlorooxoacetate (0.08 mL, 0.75 mmol) in chloroform (2 mL) at 0 °C, a solution of 2 (165 mg, 0.75 mmol) and Hünig's base (0.2 mL, 1.125 mmol) in chloroform (3 mL) was added. Reaction turned from clear to light yellow. After completion by TLC, solution was washed with 0.1 N HCl (1×), washed with DI water (1×), dried over $MgSO_4$, filtered, and concentrated in vacuo. Flash column chromatography was performed eluting with 4:6 hexanes to ethyl acetate to yield 156.6 mg (66%) of a light yellow oil. ^{1}H NMR ($CDCl_3$-*d* + 0.05% TMS, 500 MHz): δ/ppm = 7.21 (s, 1H, NH), 4.57 (s, 1H, NH), 4.39 (q, 2H, CH_2–O), 3.39 (q, 2H, CH_2–NH), 3.16 (d, 2H, CH_2–NH), 1.5 (m, 12H, CH_3), 1.35–1.47 (m, 8H, CH_2–CH_2); ^{13}C NMR ($CDCl_3$-*d* + 0.05% TMS, Cryo 500 MHz): δ 160.9, 156.6, 156.0, 63.3, 40.3, 39.7, 30.0, 29.1, 28.4, 26.3, 26.2, 14.0, 13.9; HRMS (ESI-TOF): m/z Calcd for $C_{15}H_{28}N_2O_5$ $[M + Na]^+$, 339.1896; found, 339.1892.

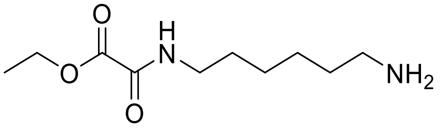

*Boc Deprotection **4***. A solution of compound **3** (24 mg, 0.079 mmol) in methylene chloride (0.3 mL) was treated with TFA (0.2 mL, 2.7 mmol) at room temperature. The reaction was monitored by TLC and finished in 30 min. Solvent was removed to produce a TFA salt, 20 mg (80% yield). ^{1}H NMR (CDCl3-*d* + 0.05% TMS, 500 MHz): δ/ppm = 4.42 (q, 2H), 3.43 (m, 2H), 3.17 (m, 2H) 1.79–1.54 (m, 13H); 13C NMR (CDCl3-*d*, Cryo 500 MHz): δ 158.8, 158.5, 117.0, 114.7, 62.1, 62.0, 61.9, 54.4, 54.1, 13.35; HRMS (ESI-TOF): m/z Calcd for $C_{10}H_{20}N_2O_3$ $[M + H]^+$, 217.1552; found, 217.1550.

*Acryloylation **5***. Et_3N (0.65 mL, 4.5 mmol) was added to compound **4** (125 mg, 0.38 mmol) at 0 °C. Then, a solution of acryloyl chloride (36 μL, 0.45 mmol) in CH_2Cl_2 (5 mL) was added and stirred for 1 h at 0 °C. The reaction then came to rt and left to stir o/n. Reaction was complete by TLC (ethyl acetate, Rf = 0.25) and washed with NH_4Cl (1×), $NaHCO_3$ (1×), NaCl (1×), then dried over $MgSO_4$, filtered, and concentrated in vacuo. Flash column chromatography in EtOAc was performed to produce 54.8 mg (53% yield). ^1H NMR ($CDCl_3$-*d* + 0.05% TMS, 500 MHz): δ/ppm = 7.22 (1H, b), 6.33 (dd, 1H, CH_{sp2}), 6.16 (dd, 1H, CH_{sp2}), 5.69 (dd, 1H, CH_{sp2}), 4.41 (d, 1H, NH), 3.39 (q, 2H, CH_2−O), 1.65−1.45 (m, 11H, CH_2−CH_2); ^{13}C NMR ($CDCl_3$-*d* + 0.05% TMS, Cryo 500 MHz): δ 130.9, 126.3, 63.2, 39.5, 39.2, 29.4, 29.0, 26.2, 14.0; HRMS (ESI-TOF): m/z Calcd for $C_{13}H_{22}N_2O_4$ $[M + Na]^+$, 293.1477; found, 293.1475.

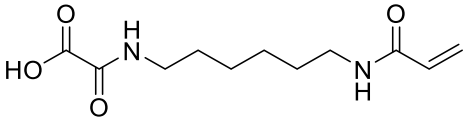

*Ester Hydrolysis **6***. KOH (18 mg, 0.32 mmol) was added to a solution of **5** (43 mg, 0.16 mmol) in MeOH (2 mL) at rt. Reaction complete by TLC (ethyl acetate) after 10 min (Rf = 0). Reaction mixture was acidified with 5 N HCl. Solvent removed to produce a white solid (quantitative yield). ^1H NMR ($CDCl_3$-*d* + 0.05% TMS, 500 MHz): δ/ppm = 8.83 (s, 1H), 8.11 (s, 1H), 6.2 (dd, 1H, CH_{sp2}), 6.09 (dd, 1H), 5.58 (dd, 1H, CH_{sp2}), 3.11 (m, 4H, CH_2) 1.44−1.28 (m, 8H, CH_2); ^{13}C NMR (CDCl3-*d* + 0.05% TMS, Cryo 500 MHz): δ 128.8, 31.9. 29.4, 28.47, 26.1, 22.7, 14.1; HRMS (ESI-TOF): m/z Calcd for $C_{11}H_{18}N_2O_4$ $[M - H]^-$, 241.1188; found, 241.1188.

OxNP Characterization.

DLS was run using OxNPs diluted 10-fold into nanopure water. Samples at 37 °C were equilibrated for 2 min before measuring. Molecular weight of nanoparticles was determined using SEC-MALS (Malvern Viskotek GPC/SEC triple detection system). The system was run in PBS (10 mM phosphate, 50 mM NaCl). The column (Viscotek A7000) was heated to 30 °C and the system was calibrated to a 500 kDa pullulan standard. Nanoparticle samples were prepared by dialyzing in PBS overnight. The OxNP sample was diluted into PBS (2.5 mg/mL) and injected onto the column. Injections of 40 μL were used with a flow rate of 1 mL/min. The M_n was determined to be 2.276×10^8 and M_w was 2.863×10^8 with a PDI of 1.26.

Cloning of LDH Gene.

DNA encoding wtLDH from *B. stearothermophilus* with a N-terminal His6X tag was synthesized by Integrated DNA Technologies using sequences optimized for *E. coli* expression. *B. stearothermophilus* LDH was selected due to its structural stability at elevated temperature. The gene was ligated into Blunt Topo vector, transformed into *E. coli* (DH5α) cells, and sequence confirmed with standard Sanger's sequencing (GeneWiz). wtLDH fragment of the wtLDH-TOPO vector was digested with *Bam* HI and *NdeI*, extracted from a 0.7% agarose gel (GeneJET kit), and ligated into a *Bam* HI- and *NdeI*-digested pET11a vector. The ligated plasmid was cotransformed into BL21(DE3) *E. coli* cells together with a pGRO7 chaperone protein plasmid.

Purification of LDH.

Single colonies of cotransformed BL21-(DE3) cells were picked and incubated overnight at 37 °C for 16−18 h, and overnights were reinoculated into 1 L of LB culture containing 100 μg/mL ampicillin, 50 μg/mL chloramphenicol, and 1 mM arabinose (to induce the expression of GroEL/ES chaperone proteins). Once the OD600 of the culture reached 0.6–0.7, the LDH expression was induced with 1 mM IPTG for 3 h, and cells were harvested. Cells were resuspended in breaking buffer and lysed in French pressure cell. Cell debris and insoluble fractions were removed using ultracentrifuge, and soluble fractions were purified using HisPur Ni-NTA affinity column following the product protocols. Samples of each fraction from the affinity column were run on SDS-PAGE. The elution fractions with soluble LDH proteins were combined and exchanged into phosphate buffer using Zeba Desalting columns. The concentration of the purified LDH was obtained with a micro BCA Kit and stored at −80 °C.

Protein Characterization.

Characterization of LDH was based on prior protocols for thermophilic proteins derived from *B. stearothermophilus*.[47] In summary, purified LDH was run on 12% SDS-PAGE gel to examine the presence of impurities during and after purification. Mass spectroscopy was also performed (Waters Quattro Premier XE) to verify molecular weight of purified LDH. The secondary structure and thermostability of LDH were obtained following the protocol of Dalmau et al.[47] Jasco 810 spectropolarimeter equipped with Jasco Peltier temperature controller (Jasco, Easton, MD) were used to measure the far-UV circular dichroism (CD). LDH proteins were examined at a concentration of 0.06 mg/mL in 50 mM potassium phosphate and 100 mM NaCl. Samples were scanned between 200 and 260 nm at 25 °C at scanning speed of 10 nm/min in 0.1 cm path length quartz cells.

LDH Kinetics.

Protocols for determining K_{cat} and K_m of LDH were based on previous studies by Clarke et al.[48] Enzyme kinetics were measured by absorbance increases at 340 nm in the generation of NADH. All assays were done at 25 °C and in 100 mM triethanolamine hydrochloride buffer. Enzyme at 100 nM was mixed with 10 mM NAD+ and 20 mM FBP with varying lactate concentrations. The initial slope of the absorbance versus time was obtained for a range of lactate concentrations. This initial slope versus concentration of lactate was plotted in GraphPad Prism and kinetic parameters (K_m and K_{cat}) were determined using a nonlinear curve fit to the Michaelis−Menten equation.

Quantification of LDH Uptake.

A 1 mL sample of NP (0.4 mg/mL), FBP (1 mM), NAD+ (1 mM), and LDH (0.35 mg/mL) was prepared in nanopure water. Control samples consisted of NIPAm NPs (0.4 mg/mL) with LDH (0.35 mg/mL) and FBP (1 mM). After LDH was incubated with its coenzymes in water (1 min), NP was added. After incubating at rt for 30 min, the samples were heated in a water bath at 37 °C for 10 min, followed by centrifugation for 10 min at 14000 rpm. For samples that were not incubated at 37 °C, they incubated at room temperature for an additional 10 min before centrifugation. A white pellet formed at the bottom of the centrifuge tube and the supernatant was collected for fluorescence measurements. Measurements were taken in quartz cuvettes (Starna Cells, 3 mm) on a Cary Eclipse Spectrometer. Excitation was set to 280 nm and emission was measured from 290 to 400 nm, RFU measurements were recorded at 342 nm. A calibration curve of LDH was created starting at 0.01 mg/mL ending at 0.35 mg/mL.

The number of proteins bound to OxNPs was calculated using the wt/wt ratio of proteins bound to NPs. Using the respective molecular weights (Mn for the OxNPs), the mole to mole ratio was calculated. Using Avogadro’s number, we were then able to calculate the exact number of LDH proteins per OxNP. Determining density of OxNPs required the molar mass of OxNPs and the Z-average value to determine the volume. The molar mass of one OxNP was calculated as stated above using M_n and Avogadro's number, this value was then divided by the volume of an OxNP. To determine the percent volume of OxNP taken up by LDH, we divided the volume of 1000 LDH proteins by the volume of OxNP. The volume of LDH was calculated using the mass of one LDH protein divided by its density. The mass of one LDH protein was calculated using the molecular weight of LDH divided by Avogadro's number.

Circular Dichroism of NPs with LDH.

Measurements were carried out on a Jasco J-380 spectrometer. Continuous scanning was used with a speed of 20 nm/min at increments of 1 nm from 200 to 260 nm. Baseline correction was used with a 2 nm bandwidth. All data are an average of three scans. Phosphate buffer (150 mM) was used for baseline correction. Samples (200 μL) consisted of FBP (1 mM), NAD^+ (0.5 mM), LDH (0.6 mg/mL), and OxNPs (0.1 mg/mL) in phosphate buffer (150 mM). Measurements were carried out at room temperature and 37 °C. For measurements performed at elevated temperatures, samples were incubated for 10 min before measuring. Controls were taken of LDH and OxNPs individually. OxNP controls did not include any coenzymes and were taken in phosphate buffer (150 mM). LDH controls were performed with necessary coenzymes in phosphate buffer (150 mM).

Response of OxNPs to Small Molecules.

Solutions (1 mL) were made consisting of OxNP (0.4 mg/mL) and small molecules (10 mM) in nanopure water. Samples incubated for 5−10 min at rt before being measured. DLS measurements at 25 °C were performed in triplicate and the average was taken to determine the hydrodynamic diameter. Samples were then incubated for 2 min at 37 °C before repeating measurements in triplicate. It was visually apparent that particles were above LCST as the solution became turbid with turbidity increasing with the size of the particles. The size change was converted to percent change in volume using the size of OxNP as the standard. This was determined by calculating the volume of OxNPs with small molecules based on their Z-average. This was subtracted from the volume of OxNP and divided by the volume of OxNP using eq 1. OxNP percent change in volume was set as 0.

Equation 1. $$\%\ Change\ in\ volume = \frac{(Volume\ of\ OxNP\ with\ Small\ Molecule - Volume\ of\ OxNP)}{Volume\ of\ OxNP}$$

Response of OxNP−LDH Complexes to Small Molecules.

Solutions (1 mL) were made consisting of OxNP, FBP (1 mM), NAD$^+$ (1 mM), and LDH (0.175 mg/mL). The control sample consisted of NIPAm NPs (0.4 mg/mL) in water. NAD$^+$, FBP, and LDH were incubated together in water for 1 min before adding NP. Samples were incubated at rt for 10 min before taking DLS measurements at 25 °C. Measurements were performed in triplicate and the average was taken to determine the hydrodynamic diameter. Samples were then incubated for 2 min at 37 °C before repeating measurements in triplicate. It was visually apparent that particles were above LCST as the solution became turbid. OxNP−LDH complexes containing small molecules (10 mM) were prepared in a similar manner as above except small molecules were added at rt before measuring. The same procedure was also followed for their DLS measurements. To test whether the addition of lactic acid was temperature-dependent, a separate set of experiments were performed in which lactic acid was added at 37 °C to premixed OxNP−LDH samples. The same procedure as above was performed except OxNP−LDH solutions were not allowed to come to rt before lactic acid was added. Measurements were taken immediately at 37 °C.

The hydrodynamic diameter of NP was the same, regardless of whether lactic acid was added at 25 or 37 °C. The percent change in volume is detailed by eq 2.

Equation 2. $$\%\ Change\ in\ volume = \frac{(Volume\ \ OxNP\ LDH\ with\ Small\ Molecule - Volume\ OxNP\ LDH)}{Volume\ OxNP\ LDH}$$

SEM of Inhibitor-Functionalized NPs.

A stock solution of OxNP (0.4 mg/mL) containing LDH (0.175 mg/mL), FBP (10 mM), and NAD$^+$ (5 mM) was diluted 10-fold to a final concentration of 0.04 mg/mL OxNP and 0.0175 mg/mL LDH. OxNP samples were prepared by drop casting a solution of OxNP in water (0.04 mg/mL, 10 μL) onto glass slides, which were then heated in the oven at 150 °C until dry (1 min). OxNP−LDH complexes were prepared by combining OxNP with LDH and coenzymes before diluting to concentrations previously mentioned. The solution was heated to 37 ˚C, followed by drop casting onto glass slides and drying in the oven. Samples of OxNP with LDH and lactic acid were prepared similarly, but a stock solution of OxNP with LDH was treated with lactic acid before dilution and drop casting. The samples were sputter coated with a thin conductive layer (5 nm) of gold/palladium alloy (Polaron SC7620) to render the surface of the NP electrically conductive for SEM imaging. Morphological characterization from the SEM (FEI Quanta 3D) was conducted using an electron voltage of 5 kV and a current of 53 pA.

CryoTEM of OxNP−LDH Complexes.

Cryo-TEM samples were prepared by depositing 3 μL sample on a 200 mesh Cu grids with lacey carbon films (Electron Microscopy Sciences). All TEM grids were surface plasma treated for 20 s using a Gatan Solarus Advanced Plasma Cleaning System 950 prior to use. An automated vitrification robot (Leica EM GP) was used for plunge vitrification in liquid propane. Cryo-TEM studies were performed on the JEOL JEM 2100F operated at 200 kV, 2k × 2k Gatan CCD camera. Gatan Digital Micrograph. ImageJ was used for TEM image analysis.

Results and Discussion

Synthesis of Polymerizable Oxamate Derivative

To impart NPs with affinity for LDH, we chose an oxamate derivative as a noncovalent inhibitor. Oxamate is a competitive inhibitor of pyruvate for LDH with a similar K_m as pyruvate for LDH (0.6 mM).[48] Since attachment of the inhibitor to a polymer backbone can restrict access to the LDH active site, we chose a six carbon atom tether for the oxamate inhibitor. Our choice was based on the successful use of a solid-phase tethered oxamate derivative to purify LDH by affinity chromatography.[49,50] In the chromatographic application, the oxamate moiety was coupled to a 1,6-hexanediamine spacer bound to a Sepharose bead. Drawing from these results, an α,ω-1,6-diamine was functionalized with the oxamate group at the α position and an acrylamide at the omega position. In this design, the α position can bind to LDH, while the omega position can be covalently incorporated into the polymer backbone.

The synthesis of the oxamate derivative **6** (Scheme 1.1) begins with monoprotection of 1,6 -hexanediamine with Boc-anhydride. After purifying the mono-Boc diamine **2** via flash column chromatography, initial efforts to couple oxalic acid to the mono-Boc protected diamine **2** proved challenging, most likely due to the low electrophilicity of oxalic acid. The synthesis was simplified by switching to a more reactive, electrophilic acid chloride ethyl chlorooxoacetate. The free amine was coupled to ethyl chlorooxoacetate in the presence of Hünig's base. The resulting mono-Boc oxamide **3** was then deprotected with TFA in DCM. Following deprotection, acryloylation of the free amine **4** was performed and ester **5** was purified via flash column chromatography. The resulting ethyl ester **5** was then hydrolyzed using KOH in MeOH to produce the oxamate-derived monomer **6**.

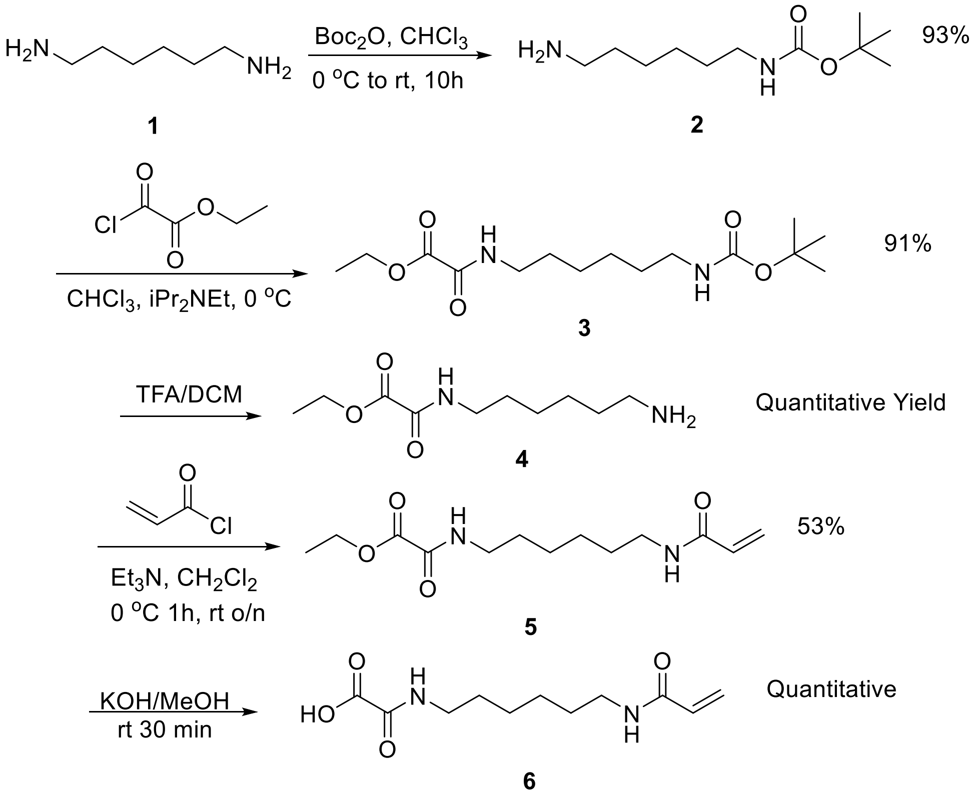

Scheme 1.1: Synthetic Pathway to Polymerizable Oxamate Derivative **6**

OxNP Synthesis

The next step was incorporation of **6** into a NIPAm based polymer (Scheme 1.2). The oxamate functionalized NP (OxNP) formulation consisted of 2 mol % polymerizable oxamate inhibitor **6**, 2 mol % *N,N'*-methylenebis(acrylamide) (Bis) as cross-linker, and 96 mol % NIPAm. We assumed equal reactivity of NIPAm and the oxamate derivative since both are N-substituted acrylamides.[51] Under these conditions, the feed ratios should reflect the actual incorporation of the monomers in the polymer with random distribution of the oxamate derivative. This is further supported by the high yield of the polymerization (90%). The OxNPs contain an additional permanent cross-linker, 2 mol % Bis. This low-level of covalent cross-linking was included to ensure uniformly sized NPs form but low enough to remain responsive to changes in noncovalent cross-linking between the oxamate and LDH.[52] Using a high concentration of Bis would restrict the polymer chains due to high cross-linking density, making it difficult to observe swelling.

OxNPs were synthesized via precipitation polymerization in water and were purified by dialysis for 4 days to remove low molecular weight polymerization byproducts.

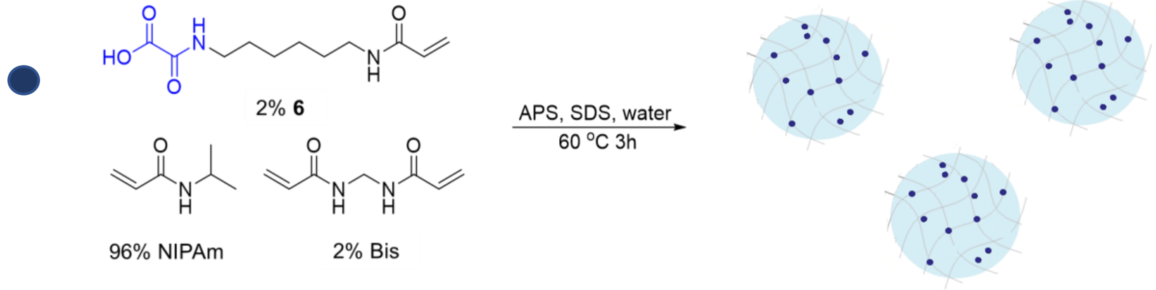

Scheme 1.2: Synthesis utilizing 2 mol % Polymerizable Oxamate Inhibitor, 96 mol % NIPAm, and 2 mol % Bis

Following dialysis, the yield of polymers was determined by weighing a lyophilized aliquot of NP solution (90% yield). Dynamic light scattering (DLS) was used to determine the hydrodynamic diameter of the particles and their polydispersity (Experimental Section). Because NIPAm polymers exhibit an LCST ~ 32 °C,[30] particle size was measured at both 25 °C and 37 °C. Below the LCST at 25 °C, the hydrodynamic diameter of OxNPs was 403±7 nm. At 37 °C, OxNP diameter decreased to 183±1 nm. Since these particles have intended applications under physiological conditions, 37 °C was chosen for all measurements and experimental conditions. Particle size was designed to be at or below 200 nm at body temperature to take advantage of the enhanced permeability and retention effect which promotes accumulation of nanoparticles in tumor tissues and to prevent encumbered circulation.[53]

Quantification of LDH Uptake

Following OxNPs synthesis the next step was to study LDH uptake by OxNPs. The K_m of oxamate for *Bacillus stearothermophillus* LDH is 0.6 mM.[48] For LDH to serve as a cross-link, it must bind to two or more oxamate groups. This is realized under conditions where LDH is present as a homomeric tetramer with four discrete binding sites for oxamate groups. These conditions are realized in the presence of NAD^+ and fructose bisphosphate (FBP)[49,50] which were present in all binding and uptake studies.

OxNPs were incubated with LDH and its coenzymes FBP and NAD^+ at room temperature to allow LDH to diffuse into the solvent swollen OxNPs and bind to the polymer bound oxamate groups. After 30 min at room temperature, samples were heated to 37 °C for 10 min. Protein uptake was followed by centrifugation of OxNP–LDH complexes, which pelleted at the bottom, leaving unbound LDH in the supernatant. Protein concentration in the supernatant was determined using tryptophan fluorescence (Ex 280 nm, Em 342 nm) standardized against known concentrations of LDH. The results are summarized in Figure 1.2. Control experiments with unfunctionalized (no oxamate ligands) NIPAm NPs (98 mol % NIPAm and 2 mol % Bis) were included for comparison. OxNPs (0.4 mg/mL) were calculated to bind 0.24 mg/mL of LDH in solution. Control NPs showed negligible LDH uptake. The wt/wt ratio of LDH to OxNPs was calculated to be 0.6 to 1.0. Using size exclusion multiangle light scattering (SEC- MALS), OxNP molecular weight was determined to be M_n of 2.276×10^8, M_w of 2.863×10^8, with a PDI of 1.26. Using the known molecular weight of LDH (140 kDa for the tetramer) and OxNP (M_n of 2.276×10^8), one calculates approximately 1000 proteins per OxNP. Despite this seemingly large number, less than 1% of the OxNP volume is taken up by LDH. This was derived after determining the density of OxNPs (0.01 g/mL assuming the OxNPs are spherical) and using an assumed density of 1.3 g/mL for LDH.[54] The density calculated for OxNPs does not include the water hydrating the polymer.

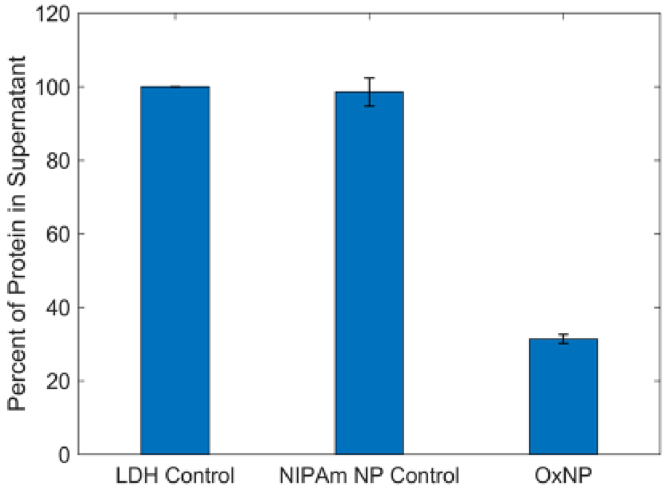

Figure 1.2: Quantification of LDH uptake by NPs. Centrifugation was performed to pull down NP–LDH complexes leaving the unbound protein free in supernatant. Bars represent amount of LDH leftover in supernatant. LDH Control corresponds to the maximum amount of LDH added to solutions. NIPAm NP Control represents NIPAm NPs without oxamate inhibitor incubated with LDH. OxNP represents NIPAm NPs containing the oxamate inhibitor. The NIPAm NP Control showed no affinity for LDH while the OxNP demonstrated affinity for LDH.

Circular Dichroism (CD) Measurements

Noncovalent complexation of LDH with OxNPs and subsequent thermal cycling of the copolymer–protein complex could subject the protein to structural deformation and denaturation. To evaluate this, we used CD spectroscopy to interrogate the OxNP–LDH complex. Samples containing OxNPs alone, LDH alone (both at room temperature and 37°C), OxNP–LDH complexes prepared at room temperature, and OxNP–LDH complexes prepared at room temperature followed by heating to 37 °C and cooling to room temperature were evaluated. In all cases, the α-helical motifs in LDH were maintained (Figure 1.3). OxNPs do not disrupt the secondary structure of LDH. These results also indicate that the mechanical distortions from the polymer network's contraction at 37 °C and expansion at room temperature are insufficient to produce detectable distortions in the noncovalently bound protein.

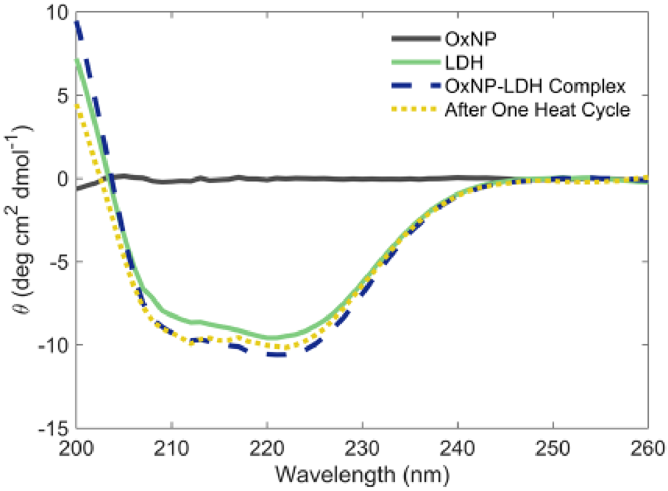

Figure 1.3: CD Measurements of OxNPs and LDH. CD was performed on OxNP alone and showed no signal. LDH was measured alone as a baseline. OxNP – LDH complexes showed no significant difference from the baseline LDH. After one heat cycle corresponds to measurements of OxNP – LDH complexes after being heated at 37 °C for 10 min followed by cooling and measurement. Each set of conditions demonstrated no denaturation occurring.

Response of OxNP to Small Molecules

To establish that the OxNP–LDH complexes are metabolite (lactate) responsive, several controls with OxNPs were performed. DLS was used to monitor the change in size upon exposure of OxNPs to 10 mM solutions of lactic acid and several small molecules containing three or four carbons with either mono- or difunctional carboxylic acid and alcohol moieities at 25 and 37 °C. We found at 37 °C, pyruvic acid and oxalic acid caused aggregation (not swelling) of OxNPs, a conclusion supported by the high polydispersity

alcohol moieities at 25 and 37 °C. We found at 37 °C, pyruvic acid and oxalic acid caused alcohol moieities at 25 and 37 °C. We found at 37 °C, pyruvic acid and oxalic acid caused aggregation (not swelling) of OxNPs, a conclusion supported by the high polydispersity

(0.23±0.2 for pyruvic acid and 0.096±0.02 for oxalic acid). Because these two molecules cause aggregation of OxNPs, they were not included in tests on OxNP-LDH complexes. The

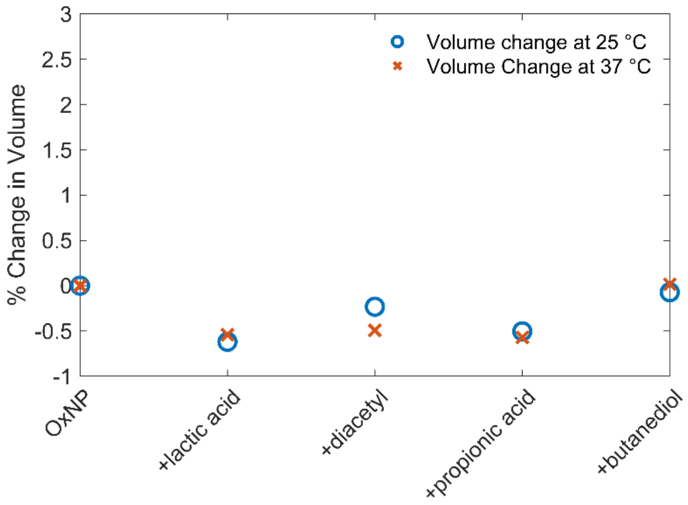

Figure 1.4: Change in volume of OxNP exposed to small molecules at 25 °C and 37 °C. All small molecules had a concentration of 10 mM. Pyruvic acid and oxalic acid not shown.

response of OxNPs to lactic acid, diacetyl, propionic acid, and 2,3-butanediol are shown in Figure 1.4. None of the small molecules significantly affected the size of OxNPs at 25 °C or 37 °C.

Response of OxNP–LDH Complexes to Small Molecules

A similar set of experiments was used to evaluate the response of the NP-protein complexes (OxNP–LDH complexes) to lactic acid and related small molecules. To establish a baseline for the OxNP–LDH complexes, DLS measurements were run in water at 25 ^{o}C and 37 °C. At 25 °C, the complexes had an average size of 308±3 nm and 180±1 nm at 37 °C. One important observation is the change in size of OxNP at 25 °C when LDH is added, the resulting complex is about 100 nm smaller than OxNP by itself (403±7 nm). In contrast, NIPAm NPs do not experience a significant change in size when exposed to LDH at 25 °C (337±8 nm without LDH to 338±5 nm with LDH). The decrease in size of OxNP after exposure to LDH at 25 °C is consistent with the uptake of tetrameric LDH and cross-linking the polymer backbone by binding at least two polymer-bound oxamate moieties. It is reasonable that this shrinkage upon LDH cross-linking would be more apparent when performed in the solvent swollen state (25 °C).

With the preceding benchmarks, the response of OxNP–LDH to small molecules was examined. The conditions were similar to the previous experiment but an additional trial using 1 mM of lactic acid was used to establish if OxNP–LDH complexes exhibit a concentration dependent response to lactic acid. The results, shown in Figure 1.5, reveal there were no significant changes in volume of OxNP–LDH at 25 °C in the presence of any small molecules at 10 mM concentration.

At 37 °C the volume of OxNP–LDH complexes remained constant with one exception, lactic acid. OxNP–LDH samples treated with 10 mM lactic acid at 37 °C experienced a significant increase in volume. In contrast, 1 mM of lactic acid did not influence the volume of OxNP–LDH complexes. We suggest the increase in OxNP–LDH complex volume upon exposure to 10 mM lactic acid arises from a combination of effects that include lactate displacement of the polymer bound oxamate moieties resulting in reduced cross-linking, electrostatic interactions, solvation, and possibly the catalytic activity of LDH. Importantly, we note that 10 mM lactate was the only condition that

induced a response.

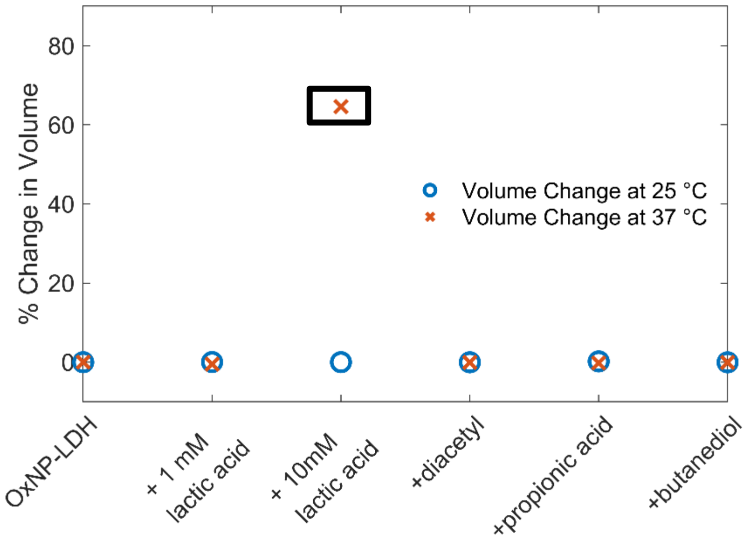

Figure 1.5: Change in volume of OxNP – LDH complexes exposed to small molecules at 25 °C and 37 °C. Low lactic acid concentrations mirroring those found in healthy tissues (1 mM) do not cause a change in volume. High lactic acid concentrations (10 mM) cause a significant change in volume of OxNP – LDH complexes. The box highlights the data point correlated to a large change in volume at 37 °C. Other small molecules (10 mM) elicited no effect on OxNP-LDH complex volume.

Due to the sensitivity of NIPAm systems to a variety of external factors, it is important to consider alternative explanations. Although NIPAm is sensitive to changes in temperature,[55] pH,[56] and solvent ionic strength,[56,57] our observed increase in size is not accounted for by these factors. However, we considered that pH may partially or indirectly contribute to the observed swelling. Kratz et al.[56] demonstrated a size increase of NIPAm NPs containing low loadings (1.25 mol % and 12.5 mol %) of acrylic acid (AAc) at low pH above their LCST. Because the oxamate derivative incorporated into the polymer also has a carboxylic moiety, comparisons may be drawn between the 1.25 mol % loaded AAc NIPAm polymer and our system (OxNP). Kratz attributed this observation to an expected collapse (desolvation) above LCST, but the collapsed NPs were prone to form somewhat uniform aggregates at low pH.[56] This behavior was attributed to weak interparticle interactions. They also observed that this was completely reversible.

The pH of OxNP solutions drops significantly upon addition of lactic acid. If the observed swelling of OxNP–LDH complexes in 10 mM lactic acid was solely pH-dependent, one would have expected OxNPs to have exhibited the same response when exposed to lactic acid at 37 °C. This, however, was not observed. Furthermore, at lactic acid concentrations similar to those found in healthy tissues in the body (1 mM), there is no response of OxNP–LDH complexes. Once lactic acid concentrations exceed the normal range, only NP–protein complexes (OxNP–LDH) responded. We conclude, therefore, that the increase in size is due to a reduction in cross-linking brought about by competitive displacement of the polymer-bound oxamate moiety by lactic acid.

Our main hypothesis is that lactic acid competitively displaces the polymer bound oxamate moiety, decreasing the cross-linking of the OxNP. However, due to the complexity of this system, it is not unreasonable to think that other factors might also contribute. For example, under 10 mM lactate conditions there could be “open” active binding sites on the homomeric tetramer LDH.[48] The generation of pyruvic acid within the OxNP could potentially contribute to swelling of particles since the K_d of pyruvate is similar to that of oxamate, this could displace more oxamate moieties and further increase swelling. Although this potential exists, this is not likely the most significant reason for swelling. Experiments involving OxNP and OxNP–LDH complexes with pyruvic acid led to irreversible aggregation of particles, unlike what was observed with lactic acid. This suggests there is something specific about lactic acid that does not lead to aggregation of particles but, instead, leads to swelling.

Scanning Electron Microscopy Imaging of NPs

Scanning electron microscopy (SEM) was performed on OxNPs and lactic acid exposed OxNP–LDH complexes (Figure 1.6) to observe the size change of OxNP–LDH complexes in the presence of 10 mM lactic acid. Samples were prepared by drop-casting a solution of OxNP in water onto glass slides then heated at 150 °C until dry. To establish a

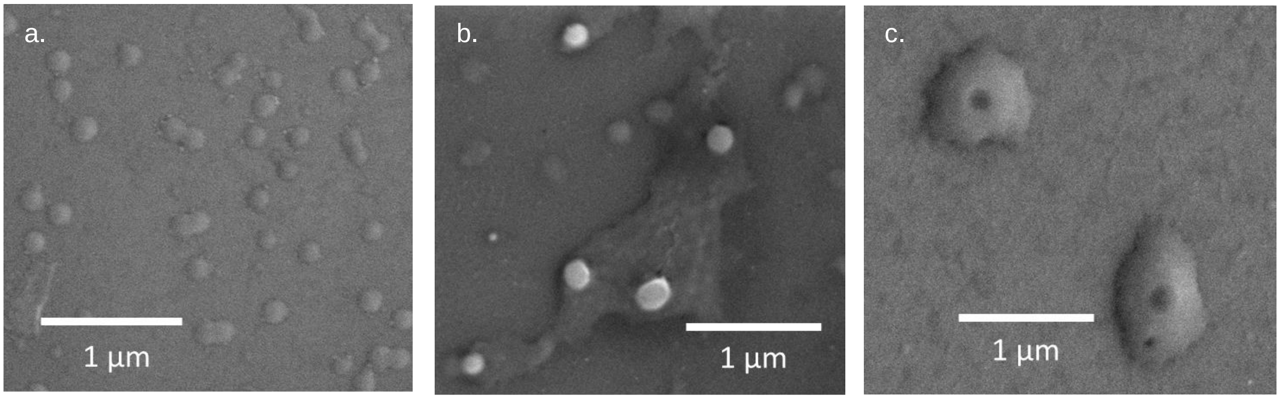

Figure 1.6: SEM images of OxNPs. OxNPs alone (a); OxNPs with LDH (b); OxNPs with LDH and lactic acid (c).

point of reference, SEM images were taken of OxNPs (Figure 1.6a). The sizes of OxNPs in Figure 1.6a, b (~ 160 nm) are roughly the same as those measured by DLS at 37 °C (183±1 nm). These images are consistent with the experimental results obtained by DLS for lactic acid responsiveness.

Cryo-Transmission Electron Microscope Images

To further characterize OxNP–LDH complexes, we employed cryo-transmission electron microscopy (cryoTEM) which enables the native state of the OxNPs to be imaged at high resolution (Figure 1.7).[58] Due to the 100-fold difference in density between OxNPs (0.01 g/mL) and LDH (1.3 g/mL), the contrast will be dominated by the LDH particles. At high defocus values (~10-20 µm), the OxNP-LDH complexes are easily identifiable and appear as homogeneous spheres with a 200 nm diameter (Figure 1.7a, highlighted with the dashed blue circles). This is consistent with the DLS measurements. At lower defocus values (~0.5 - 1 µm) the OxNP–LDH complexes display extremely low contrast (Figure 7b, highlighted by the dashed blue circles), but the resolution is sufficient to identify individual LDH particles (Figure 1.7c). Due to the superposition of the LDH particles it is only possible to measure their individual diameter (~ 8 nm) close to the edge of the structures[59], however, this is consistent with their previously measured R_H values (~ 4.3 nm).[60]

If LDH bound selectively to the surface, there would be a distinct and visible ring around the OxNPs; consequently, it was inferred that LDH distributed through the 3D volume of the OxNPs. This is consistent with our observation that OxNPs contract when exposed to LDH by 100 nm, and OxNP-LDH complexes swell when exposed to lactate. If LDH were confined to the surface of the OxNPs, cross-linking and subsequent swelling would be minimized.

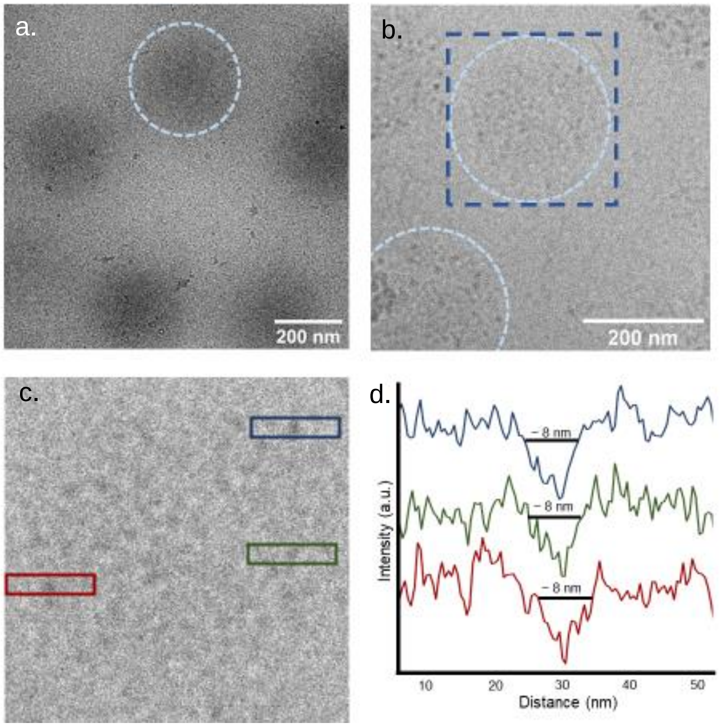

Figure 1.7: CryoTEM images of OxNPs and OxNP – LDH complexes. Image of OxNPs cluster (a); Image of OxNPs with protein bound (b); Magnification of blue box from (b.), showing discrete LDH particles (c); Plot profile of selected protein particles (d).

Conclusions

In summary, a polymerizable oxamate LDH inhibitor **6** was synthesized and incorporated into lightly cross-linked NIPAm NPs, producing OxNPs. LDH was efficiently taken up into OxNPs in the solvent-swollen state through incubation and noncovalent binding to the polymer bound oxamate moieties in the polymer backbone. Protein loading was estimated to be 0.6 mg LDH/1 mg OxNP. CD was used to demonstrate that OxNPs do not lead to distortion or denaturation of LDH's secondary structure after being exposed to OxNPs below and above LCST as well as after one full heating cycle, which is important for cross-linking. OxNP–LDH complexes showed a large swelling response in the presence of high lactic acid concentrations (10 mM), but none at low lactic acid concentrations (1 mM). OxNP–LDH complexes exposed to lactic acid below LCST behave normally and remain the same size as without lactic acid. Above the LCST, lactic acid treated OxNP–LDH complexes swell almost double their size at room temperature. We have also used SEM to visualize OxNP–LDH complex's response to lactic acid. Through TEM, we have imaged OxNP–LDH complexes to further validate uptake. We conclude that we have developed a metabolite-responsive system. OxNP–LDH complexes swell in the presence of high lactic acid concentrations that mirror those found in tumors. The influence of temperature and lactic on particle swelling only influences OxNPs when they are complexed with LDH. This supports our hypothesis that LDH acts as a cross-linker within the polymer and is displaced in the presence of lactic acid. This system provides a platform for metabolite responsive NPs.

Prior work in our lab[61] recognized the formation of hydrophobic domains when monomers containing aliphatic chains were incorporated into similar hydrogel polymers. We envisioned that the metabolite responsive system reported here could be used in combination with a nanoparticle containing discrete hydrophobic domains. These hydrophobic domains may be the ideal method of encapsulating nonpolar drug molecules such as Taxol®. This drug has high efficacy as a chemotherapeutic agent but is limited by low solubility in the body thus leading to poor bioavailability. In addition, Taxol® is not highly specific in terms of therapeutic affect and can damage healthy cells. If hydrophobic monomers were incorporated into this lactate responsive nanoparticle, we believe it would then be possible to load Taxol® into the nanoparticle. Once the system is exposed to high lactic acid concentrations within the tumor microenvironment, the hydrophobic domains would be disrupted by the swelling of these nanoparticles and allow for release and diffusion of drug molecules. In this way, we believe a selective drug delivery vehicle can be developed.

References

(1) Xu, R.; Zhang, G.; Mai, J.; Deng, X.; Segura-Ibarra, V.; Wu, S.; Shen, J.; Liu, H.; Hu, Z.; Chen, L.; Huang, Y.; Koay, E.; Huang, Y.; Liu, J.; Ensor, J. E.; Blanco, E.; Liu, X.; Ferrari, M.; Shen, H. An injectable nanoparticle generator enhances delivery of cancer therapeutics. *Nat. Biotechnol*. **2016**, *34*, 414–418.

(2) Kabanov, A. V.; Bronich, T. K.; Kabanov, V. A.; Yu, K.; Eisenberg, A. Soluble stoichiometric complexes from poly(N-ethyl-4-vinylpyridinium) cations and poly(ethylene oxide)-block-polymethacrylate anions. *Macromolecules* **1996**, *29*, 6797–6802.

(3) Harada, A.; Kataoka, K. Formation of polyion complex micelles in an aqueous milieu from a pair of oppositely-charged block copolymers with poly(ethylene glycol) segments. *Macromolecules* **1995**, *28*, 5294–5299.

(4) Bae, Y.; Fukushima, S.; Harada, A.; Kataoka, K. Design of environment-sensitive Supramolecular assemblies for intracellular drug delivery: polymeric micelles that are responsive to intracellular pH change. *Angew. Chem., Int. Ed*. **2003**, *42*, 4640–4643.

(5) Lee, Y.; Fukushima, S.; Bae, Y.; Hiki, S.; Ishii, T.; Kataoka, K. A protein nanocarrier from chargeconversion polymer in response to endosomal pH. *J. Am. Chem. Soc*. **2007**, *129*, 5362–5363.

(6) Hartgerink, J. D.; Beniash, E.; Stupp, S. I. Self-assembly and mineralization of peptide-amphiphile nanofibers. *Science* **2001**, *294*, 1684–1688.

(7) Sun, W.; Jiang, T.; Lu, Y.; Reiff, M.; Mo, R.; Gu, Z. Cocoon-like self-degradable DNA nanoclew for anticancer drug delivery. *J. Am. Chem. Soc*. **2014**, *136*, 14722−14725.

(8) Garbern, J. C.; Minami, E.; Stayton, P. S.; Murry, C. E. Delivery of basic fibroblast growth factor with a pH-responsive, injectable hydrogel to improve angiogenesis in infarcted myocardium. *Biomaterials* **2011**, *32*, 2407−2416.

(9) Pacardo, D. B.; Ligler, F. S.; Gu, Z. Programmable nanomedicine: synergistic and sequential drug delivery systems. *Nanoscale* **2015**, *7*, 3381−3391.

(10) Ling, D.; Park, W.; Park, S. J.; Lu, Y.; Kim, K. S.; Hackett, M. J.; Kim, B. H.; Yim, H.; Jeon, Y. S.; Na, K.; Hyeon, T. Multifunctional tumor pH-Sensitive self-assembled nanoparticles for bimodal imaging and treatment of resistant heterogeneous tumors. *J. Am. Chem. Soc*. **2014**, *136*, 5647−5655.

(11) Chung, M.-F.; Chia, W.-T.; Wan, W.-L.; Lin, Y.-J.; Sung, H.-W. Controlled release of an anti-inflammatory drug using an ultrasensitive ROS-responsive gas-generating carrier for localized inflammation inhibition. *J. Am. Chem. Soc*. **2015**, *137*, 12462−12465.

(12) Callmann, C. E.; Barback, C. V.; Thompson, M. P.; Hall, D. J.; Mattrey, R. F.; Gianneschi, N. C. Therapeutic enzyme-responsive nanoparticles for targeted delivery and accumulation in tumors. *Adv. Mater*. **2015**, *27*, 4611−4615.

(13) Zhang, S.; Ermann, J.; Succi, M. D.; Zhou, A.; Hamilton, M. J.; Cao, B.; Korzenik, J. R.; Glickman, J. N.; Vemula, P. K.; Glimcher, L. H.; Traverso, G.; Langer, R.; Karp, J. M. An inflammation-targeting hydrogel for local drug delivery in inflammatory bowel disease. *Sci. Transl. Med*. **2015**, *7*, 300ra128.

(14) Kim, H.-J.; Zhang, K.; Moore, L.; Ho, D. Diamond nanogel-embedded contact lenses mediate lysozyme-dependent therapeutic release. *ACS Nano* **2014**, *8*, 2998−3005.

(15) Jiang, T.; Mo, R.; Bellotti, A.; Zhou, J.; Gu, Z. Gel− liposome-mediated co-delivery of anticancer membrane-associated proteins and small-molecule drugs for enhanced therapeutic efficacy. *Adv. Funct. Mater*. **2014**, *24*, 2295−2304.

(16) Hu, Q.; Sun, W.; Lu, Y.; Bomba, H. N.; Ye, Y.; Jiang, T.; Isaacson, A. J.; Gu, Z. Tumor microenvironment-mediated construction and deconstruction of extracellular drug-delivery depots. *Nano Lett*. **2016**, *16*, 1118−1126.

(17) Mo, R.; Jiang, T.; DiSanto, R.; Tai, W.; Gu, Z. ATP-triggered anticancer drug delivery. *Nat. Commun.* **2014**, *5*, 3364−3373.

(18) Wilson, W. R.; Hay, M. P. Targeting hypoxia in cancer therapy. *Nat. Rev. Cancer* **2011**, *11*, 393−410.

(19) Holme, M. N.; Fedotenko, I. A.; Abegg, D.; Althaus, J.; Babel, L.; Favarger, F.; Reiter, R.; Tanasescu, R.; Zaffalon, P. L.; Ziegler, A.; Muller, B.; Saxer, T.; Zumbuehl, A. Shear-stress sensitive lenticular vesicles for targeted drug delivery. *Nat. Nanotechnol*. **2012**, *7*, 536−543.

(20) Korin, N.; Kanapathipillai, M.; Matthews, B. D.; Crescente, M.; Brill, A.; Mammoto, T.; Ghosh, K.; Jurek, S.; Bencherif, S. A.; Bhatta, D.; Coskun, A. U.; Feldman, C. L.; Wagner, D. D.; Ingber, D. E. Shear-activated nanotherapeutics for drug targeting to obstructed blood vessels. *Science* **2012**, *337*, 738−742.

(21) McDaniel, J. R.; Callahan, D. J.; Chilkoti, A. Drug delivery to solid tumors by elastin-like polypeptides. *Adv. Drug Delivery Rev*. **2010**, *62*, 1456−1467.

(22) Bae, Y. H.; Okano, T.; Hsu, R.; Kim, S. W. Thermo-sensitive polymers as on−off switches for drug release. *Makromol. Chem., Rapid Commun*. **1987**, *8*, 481−485.

(23) Youn, Y. S.; Bae, Y. H. Perspectives on the past, present and future of cancer nanomedicine. *Adv. Drug Delivery Rev*. **2018**, *130*, 3−11.

(24) Duncan, R. Polymer therapeutics at a crossroads? Finding the path for improved translation in the twenty-first century. *J. Drug Targeting* **2017**, *25*, 759−780.

(25) Wang, T.; Ng, D. Y. W.; Wu, Y.; Thomas, J.; Tam Tran, T.; Weil, T. Bis-sulfide bioconjugates for glutathione triggered tumor responsive drug release. *Chem. Commun*. **2014**, *50*, 1116−1118.

(26) Stayton, P. S.; Shimoboji, T.; Long, C.; Chilkoti, A.; Ghen, G.; Harris, J. M.; Hoffman, A. S. Control of protein-ligand recognition using a stimuli-responsive polymer. *Nature* **1995**, *378*, 472−474.

(27) Huang, X.; Li, M.; Green, D. C.; Williams, D. S.; Patil, A. J.; Mann, S. Interfacial assembly of protein-polymer nano-conjugates into stimulus-responsive biomimetic protocells. *Nat. Commun*. **2013**, *4*, 2239−2247.

(28) Ge, J.; Neofytou, E.; Lei, J.; Beygui, R. E.; Zare, R. N. Protein-polymer hybrid nanoparticles for drug delivery. *Small* **2012**, *8*, 3573−3578.

(29) Zhang, L.; Lu, Z.; Li, X.; Deng, Y.; Zhang, F.; Ma, C.; He, N. Methoxy poly(ethylene glycol) conjugated denatured bovine serum albumin micelles for effective delivery of camptothecin. *Polym. Chem*. **2012**, *3*, 1958−1961.

(30) Wu, Y.; Ihme, S.; Feuring-Buske, M.; Kuan, S. L.; Eisele, K.; Lamla, M.; Wang, Y.; Buske, C.; Weil, T. A core-shell albumin copolymer nanotransporter for high capacity loading and two-step release of doxorubicin with enhanced anti-leukemia activity. *Adv. Healthcare Mater*. **2013**, *2*, 884−894.

(31) Flenniken, M. L.; Liepold, L. O.; Crowley, B. E.; Willits, D. A.; Young, M. J.; Douglas, T. Selective attachment and release of a chemotherapeutic agent from the interior of a protein cage architecture. *Chem. Commun*. **2005**, 447–449.

(32) Ren, D.; Kratz, F.; Wang, S. W. Protein nanocapsules containing doxorubicin as a pH-responsive delivery system. *Small* **2011**, *7*, 1051−1060.

(33) Lu, Y.; Aimetti, A. A.; Langer, R.; Gu, Z. Bioresponsive materials. *Nature Reviews Materials* **2017**, *2*, 1−17.

(34) Vander Heiden, M. G.; Cantley, L. C.; Thompson, C. B. Understanding the Warburg effect: the metabolic requirements of cell proliferation. *Science* **2009**, *324*, 1029–1033.

(35) Romero-Garcia, S.; Moreno-Altamirano, M. M. B.; Prado-Garcia, H.; Sanchez-Garcia, F. J. Lactate contribution to the tumor microenvironment: mechanisms, effects on immune cells and therapeutic relevance. *Front. Immunol*. **2016**, *7*, 1−11.

(36) Ward, P. S.; Thompson, C. B. Metabolic reprogramming: a cancer hallmark even Warburg did not anticipate. *Cancer Cell* **2012**, *21*, 297–308.

(37) Brooks, G. A. Lactate production under fully aerobic conditions− the lactate shuttle during rest and exercise. *Faseb J.* **1986**, *45*, 2924–2929.

(38) West, J. B. Lactate during exercise at extreme altitude. *Faseb J*. **1986**, *45*, 2953–2957.

(39) Schumer, W. Cell metabolism and lactate. *Lactate in Acute Conditions International Symposium* **1979**, 1−9.

(40) Walenta, S.; Wetterling, M.; Lehrke, M.; Schwickert, G.; Sundfor, K.; Rofstad, E. K.; Mueller-Klieser, W. High lactate levels predict likelihood of metastases, tumor recurrence, and restricted patient survival in human cervical cancers. *Cancer Res*. **2000**, *60*, 916–921.

(41) Roland, C. L.; Arumugam, T.; Deng, D. F.; Liu, S. H.; Philip, B.; Gomez, S.; Burns, W. R.; Ramachandran, V.; Wang, H. M.; Cruz-Monserrate, Z.; Logsdon, C. D. Cell surface lactate receptor Gpr81 is crucial for cancer cell survival. *Cancer Res.* **2014**, *74*, 5301−5310.

(42) Walenta, S.; Salameh, A.; Lyng, H.; Evensen, J. F.; Mitze, M.; Rofstad, E. K.; Meuller-Klieser, W. Correlation of high lactate levels in head and neck tumors with incidence of metastasis. *Am. J. Pathol*. **1997**, *150*, 409−415.

(43) Brizel, D. M.; Schroeder, T.; Scher, R. L.; Walenta, S.; Clough, R. W.; Dewhirst, M. W.; Mueller-Klieser, W. Elevated tumor lactate concentrations predict for an increased risk of metastases in head-and neck cancer. *Int. J. Radiat. Oncol., Biol., Phys*. **2001**, *51*, 349−353.

(44) Yamagata, M.; Hasuda, K.; Stamato, T.; Tannock, I. F. The contribution of lactic acid to acidification of tumours: studies of variant cells lacking lactate dehydrogenase. *Br. J. Cancer* **1998**, *77*, 1726−1731.

(45) O'Brien, J.; Shea, K. Tuning the Protein Corona of Hydrogel Nanoparticles: The Synthesis of Abiotic Protein and Peptide Affinity Reagents. *Acc. Chem. Res*. **2016**, *49*, 1200−1210.

(46) Dardonville, C.; Fernandez-Fernandez, C.; Gibbons, S. L.; Ryan, G. J.; Jagerovic, N.; Gabilondo, A. M.; Meana, J. J.; Callado, L. F. Synthesis and pharmacological studies of new hybrid derivatives of fentanyl active at the μ-opioid receptor and I2−imidazoline binding sites. *Bioorg. Med. Chem*. **2006**, *14*, 6570−6580.

(47) Dalmau, M.; Lim, S.; Chen, H. C.; Ruiz, C.; Wang, S. W. Thermostability and molecular encapsulation within an engineered caged protein scaffold. *Biotechnol. Bioeng*. **2008**, *101*, 654−664.

(48) Clarke, A. R.; Wilks, H. M.; Barstow, D. A.; Atkinson, T.; Chia, W. N.; Holbrook, J. J. An investigation of the contribution made by the carboxylate group of an active site histidine-aspartate couple to binding and catalysis in lactate dehydrogenase. *Biochemistry* **1988**, *27*, 1617–1622.

(49) O'Carra, P.; Barry, S. Affinity Chromatography of Lactate Dehydrogenase. *FEBS Lett.* **1972**, *21*, 281–285.

(50) Roop-ngam, P.; Thongboonkerd, V. Development of an oxalate affinity chromatographic column to isolate oxalate-binding proteins. *Anal. Methods* **2010**, *2*, 1051–1055.

(51) Otsu, T.; Inoue, M.; Yamada, B.; Mori, T. Structure and reactivity of vinyl monomers: Radical reactivities of N-substituted acrylamides and methacrylamides. J. Polym. Sci., *Polym. Lett. Ed*. **1975**, *13*, 505–510.

(52) Senff, H.; Richtering, W. Influence of cross-link density on rheological properties of temperature-sensitive microgel suspensions. *Colloid Polym. Sci*. **2000**, *278*, 830–840.

(53) Hoshyar, N.; Gray, S.; Han, H.; Bao, G. The effect of nanoparticle size on in vivo pharmacokinetics and cellular interaction. *Nanomedicine (London, U. K.)* **2016**, *11*, 673–692.

(54) Beardsley, D. S.; Kauzmann, W. J. Local densities orthogonal to β-sheet amide planes: Patterns of packing in globular proteins. *Proc. Natl. Acad. Sci. U. S. A*. **1996**, *93*, 4448–4453.

(55) Huffman, A. S.; Afrassiabi, A.; Dong, L. C. Thermally reversible hydrogels: II. Delivery and selective removal of substances from aqueous solutions. *J. Controlled Release* **1986**, *4*, 213–222.

(56) Kratz, K.; Hellweg, T.; Eimer, W. Influence of charge density on the swelling of colloidal poly(N-isopropylacrylamide-co-acrylic acid) microgels. *Colloids Surf., A* **2000**, *170*, 137−149.

(57) Du, H.; Wickramasinghe, R.; Qian, X. Effects of salt on the lower critical solution temperature of Poly (N-Isopropylacrylamide). *J. Phys. Chem. B* **2010**, *114*, 16594−16604.

(58) Patterson, J. P.; Xu, Y.; Moradi, M. A.; Sommerdijk, N.; Friedrich, H. CryoTEM as an Advanced Analytical Tool for Materials Chemists. *Acc. Chem. Res*. **2017**, *50*, 1495−1501.

(59) van de Put, M. W.; Patterson, J. P.; Bomans, P. H.; Wilson, N. R.; Friedrich, H.; van Benthem, R. A.; de With, G.; O'Reilly, R. K.; Sommerdijk, N. A. Graphene oxide single sheets as substrates for high resolution cryoTEM. *Soft Matter* **2015**, *11*, 1265−70.

(60) Andersson, M. M.; Hatti-Kaul, R.; Brown, W. Dynamic and Static Light Scattering and Fluorescence Studies of the Interactions between Lactate Dehydrogenase and Poly(ethyleneimine). *J. Phys. Chem. B* **2000**, *104*, 3660−3667.

(61) Chou, B.; Mirau, P.; Jiang, T.; Wang, S.W.; Shea, K.J. "Tuning hydrophobicity in abiotic affinity reagents: Polymer hydrogel affinity reagents for molecules with lipid-like domains" *Biomacromolecules* **2016**, *17*, 1860-1868.

Chapter 2: Polymers of Intrinsic Microporosity for Water Purification

Introduction

Access to clean water is a global health issue. The WHO estimated that globally, about 1.1 billion people do not have access to safe potable water[1] and that at least 2 billion people use a drinking water source that has been contaminated with faeces.[2] Contaminated water can transmit a wide variety of parasites, viruses, and bacteria which in turn can lead to major outbreaks. There also remains a lack water safety standards in rural and low-income communities. This in combination with a shortage of potable water is a significant motivator to develop water purification systems which can be used in less developed areas.

Currently, there are a variety of methods to remove soluble and insoluble contaminants from water. The process for removing pathogens includes pre-treatment followed by coagulation, flocculation, sedimentation, and lastly filtration. However, there are various classes of water treatment – household/small-scale, drinking water, and wastewater treatment. A common method relies on chemical treatment of water in combination with UV light exposure. The most commonly used chemicals are free chlorine and monochloramine.[3] Overall, filtration is utilized in every water treatment class and can be characterized into four methods listed here in order of decreasing pore size – microfiltration, ultrafiltration, nanofiltration, and reverse osmosis. All of them remove microbes (algae, protozoa, and bacteria) and all but microfiltration removes viruses.

Many of these membranes are made from polymers or inorganic ceramics. Synthetic methods of creating membranes consist of block copolymer self-assembly, inorganic materials grown onto porous polymer substrates, interfacial polymerization with and without nanoparticles, phase inversion, track-etching,[4,5] thin-film composites[6,7] and other methods incorporating biomacromolecules, such as aquaporins.[8-10] Extensive reviews have been published which examine these topics in more detail and may be found elsewhere.[11,12] Considerable emphasis has been placed on the importance of pore size uniformity and the ability to perform under a variety of conditions such as a wide pH range and in the presence of chemical additives. One class of materials that may fulfill these requirements are polymers of intrinsic microporosity (PIM).

PIMs are an especially interesting class of porous organic polymers. Their polymer backbone prevents close packing of polymer chains in the solid state, thereby leading to a uniform pore structure and high surface area. They have been employed in various areas including, but not limited to, gas separations and storage,[13] catalysis,[13] small molecule capture,[14] chiral separations,[15] sensors,[16,17] and electrochemical applications.[18,19] However, various post polymerization modifications of PIM-1 have been made in an effort to improve its properties[20-32] or extend its usefulness to other applications, such as desalination.[33,34] Previously, our lab synthesized the first chiral PIM-1 and a chiral carboxylic derivative (PIM COOH) for membrane separation of enantiomers.[15] We wanted expand applications of this material by broadening it to aqueous filtration. Despite the attractive qualities of PIM-1 (high surface area, uniform pore structure, and processability), the membranes are extremely hydrophobic. The inability for PIM-1 membranes to wet in water renders them useless in terms of aqueous applications. Our goal was to develop a membrane which could be used under aqueous conditions that can filter out virus particles, which range from 20 to 100 nm, by size exclusion. The challenge is to modify the internal surface of a complex pore structure with pore sizes around 3 nm.

In this report, we present a method to modify PIM-1, which will be referred to as PIM CN, as a filtration membrane under hydrophilic conditions. Chemical, surface, and membrane modifications were made with marginal or inconsistent success. However, we were able to utilize a wetting non-solvent, methanol, to allow permeation of small dye molecules. We proceeded to use methanol to wet the membrane and open the pores. Methanol was also able to lower the overall surface tension of water, allowing the fluid to infiltrate the membrane channels. We demonstrated that various particles such as bovine serum albumin and silver nanoparticles would not pass through the membrane. We envisioned using other smaller biomacromolecules such as peptides and proteins but were unable due to time constraints.

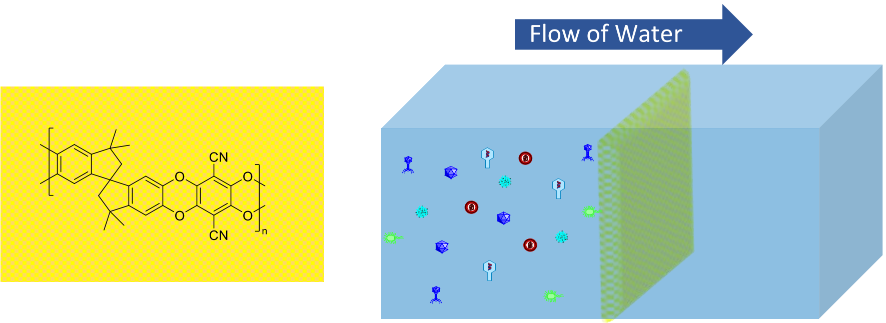

Figure 2.1: PIM CN filtering virus particles in aqueous conditions.

Experimental Section

Synthesis and Fabrication of Polymer Membranes

PIM CN

3,3,3’,3’-Tetramethyl-1,1’-spirobisindane-5,5’,6,6’-tetrol (TTSBI) (270 mg, 0.871 mmol) was dissolved in dry DMF (5 mL) followed by addition of 2,3,5,6-tetrafluorphthalonitrile (TFPT) (174 mg, 0.872 mmol). Once the mixture was homogenous, excess anhydrous K_2CO_3 (1 g, 7.2 mmol) was added and the heterogenous mixture was heated to 70 °C for 72 h. After about 30 min the reaction mixture turned from brown to bright yellow. Once cooled, the mixture was precipitated into water (50 mL), filtered, rinsed with water, and dried in a vacuum oven o/n at 70 °C. The crude powder was then suspended in methanol (10 mL) and heated to reflux for 3 h. The mixture was filtered hot and rinsed with hot methanol before drying in a vacuum oven o/n at 70 °C. The product was a fine, fluorescent yellow powder (86% yield).

Polymer Membranes

PIM CN (80 mg) was dissolved in THF (2 mL) at 60 °C over 1 h. Once cooled, the solution was poured into a glass petri dish of either 2 cm or 5 cm in diameter to cast two different thicknesses. Once the solution was carefully placed in the glass petri dishes, they were covered with a watch glass and the solvent evaporated at rt until the membranes were dry. Thicknesses were either 25 μm or 170 μm depending on the desired thickness. The same procedure detailed above was used when casting PIM COOH membranes.

Chemical Modifications

PIM NH_2

A PIM CN membrane (78 mg, 0.19 mmol CN) was treated with borane dimethyl sulfide complex (5.0 M in Et_2O, 3.8 mL, 19 mmol) and heated to 40 °C. The membrane became more orange throughout the reaction and bubbles formed on the membrane. After 6 h, the reaction was quenched with EtOH (15 mL) at 0 °C until the reaction stopped bubbling. The membrane was removed and was noticeably more yellow. The membrane was rinsed with EtOH before suspending in methanolic HCL (1.25 M, 12 mL) under N_2 over night. The color of the membrane became more orange and was rinsed with water before submerging in 5% NaOH (10 mL) for 3 h. The membrane became lighter in color and more brittle. FTIR showed full conversion of the nitrile to the primary amine.

PIM COOH

The acid catalyzed hydrolysis experimental methods were the same as used in our previous work.[15] (PIM CN (200 mg) was treated with a solution of H_2SO_4 (3 mL), H_2O (3 mL), and glacial acetic acid (1 mL). The suspension was heated to 110 °C for 48 h. The powder slowly turned from fluorescent yellow into a light brown color. Once cooled, the mixture was diluted into water (50 mL), filtered, rinsed with saturated aqueous $NaHCO_3$, rinsed with copious amounts of water, then dried in a vacuum oven at 70 °C o/n. The product appeared as a light brown powder (86 % yield). FTIR showed full conversion. Incomplete conversion was apparent when temperatures were at 105 °C.

Surface Modification

Membranes were placed in an oxygen plasma device (WS-400A-6NPP/LITE). Treatment times varied from 210 sec, 240 sec, and 300 sec in total. One side of the membrane was exposed for half that time before flipping over to expose the other side of the membrane for the remaining time.

Composite Membranes

Linear pNIPAm Synthesis

NIPAm (1 g, 8.8 mmol) was dissolved in water (20 mL) before adding ammonium persulfate (10 mg, 0.033 mmol). The solution was purged with N_2 for 30 min then heated to 65 °C. After 1 h, the reaction solution was cooled to rt and opened to air before diluting into MeOH. Solvent removed to produce a white solid.

Membrane Casting

pNIPAm was dissolved in THF before being added to a solution of PIM CN in THF. Once the solutions were mixed well, they were drop cast following the same procedure as listed above for PIM CN membrane casting.

Fluorescence Lifetime Imaging Microscopy Measurements

The optical measurements were performed using a National Institute of Standards and Technology-built two-photon fluorescence microscope utilizing a Ti:Sapphire laser centered at 810 nm, generating ≈140 fs pulses, at a repetition rate of ≈76 MHz, with an average power of 1.0 mW. The sample was excited through an air objective with a numerical aperture (NA) of 0.75. The sample was raster scanned through the laser focus using an X-Y piezo scan stage to build up images. The lifetime decay curves were analyzed using a multiexponential model and a measured instrument response function from the second harmonic generation signal of gold nanoparticles.

Water and Dye Transport

Equilibrium dialysis experiments were performed with PIM CN, PIM COOH, and PIM NH_2 membranes that were cut to fit the Teflon blocks. Each membrane was placed in the apparatus so that there were three wells present. Once the membranes were put in place, water (100 μL) was placed on the receiver side and a solution of bromophenol blue (bromophenol blue) in water (100 μL, 0.6 mg/mL) was placed on the feed side. The apparatus was sealed with tape and covered with aluminum foil. After 24 h, the feed side was removed and tested by UV-Vis (λ_{max} 591 nm).

The U-tube apparatus was custom built. PIM CN and PIM-NIPAm membranes were cut to about 1 cm diameter. PIM-NIPAm membranes were soaked in water for 20 min before being placed in the apparatus. Then, water was placed on one side (receiver) with a solution of bromophenol blue in water (0.6 mg/mL) on the other (feed). The level of the receiver side was always equal to or lower than the level of the feed side. Samples (100 μL) were taken from the receiver side at various time points before being measured by UV-Vis (λ_{max} 591). PIM CN membranes that were pre-treated with MeOH followed a similar procedure. After soaking in MeOH for 2 min, they were placed in the apparatus and the feed side was immediately filled with an aqueous solution of MeOH. The volume percent of MeOH in aqueous solutions varied from 20%, 30%, 50%, and 75%. A solution of bromophenol blue in methanol (0.3 mg/mL) was placed in the feed side quickly after. Samples (100 μL) were removed from the receiver side at set time points and measured by UV-Vis (λ_{max} 591 nm). The experiment was performed in triplicate. Water transport studies were performed similarly to what is reported above, however the solution of bromophenol blue was replaced with water.

Bovine Serum Albumin Filtration

Bovine serum albumin (BSA) was dissolved in 20% methanol (0.9 mg/mL). PIM CN membranes were soaked in methanol for 2 minutes before placing in U-tube apparatus. Quickly, the BSA solution and 20% methanol were added to the feed and receiver side, respectively. Time points (100 μL) were taken every 10 min until 1 h, then every hour until 5 h, and the last time point was taken at 24 h. The samples were measured by UV-Vis at 280 nm to determine the concentration of BSA that passed through the membrane. The experiment was performed in triplicate.

Silver Nanoparticle Filtration

Silver nanoparticles (Sigma Aldrich, 20 nm, stabilized, 0.2 mg/mL) were diluted into methanol to achieve a final concentration of 0.16 mg/mL in 20% methanol. The same general procedure was performed for silver nanoparticles as is described above for BSA. Samples were measured by UV-Vis at 390 nm to determine the concentration of silver nanoparticles that passed through the membrane.

Results and Discussion

Synthesis of PIM CN and Fabrication of Polymer Membranes

PIM CN was synthesized via step growth polymerization between 3,3,3',3'-tetramethyl-1,1'-spirobisindane-5,5',6,6'-tetrol and 2,3,5,6-tetrafluorphthalonitrile (Scheme 2.1). Due to time constraints, we were unable to characterize the molecular weight and polydispersity of the PIM CN. However, we followed the same protocol as previously established in our lab and anticipate the M_n, M_w, and PDI to be about 62,000 g mol^{-1}, 73,000 g mol^{-1}, and $M_w/M_n = 1.2$ respectively.[15] Membranes were drop cast by first dissolving the polymer powder of PIM CN in hot THF over 30 min. Then, after cooling to room temperature, the solution was placed in petri dishes and covered with watch glasses before slowly evaporating at room temperature overnight on an even surface in the chemical fume hood. Two thicknesses of membranes were made using petri dishes with different diameters. The same volume (2 mL) and concentration (40 mg/mL) of polymer in THF was used to cast both thicknesses. Thin membranes (~25 μm) were cast in dishes with an internal diameter of 5 cm while thick membranes (~170 μm) were made in dishes with an internal diameter of 2 cm.

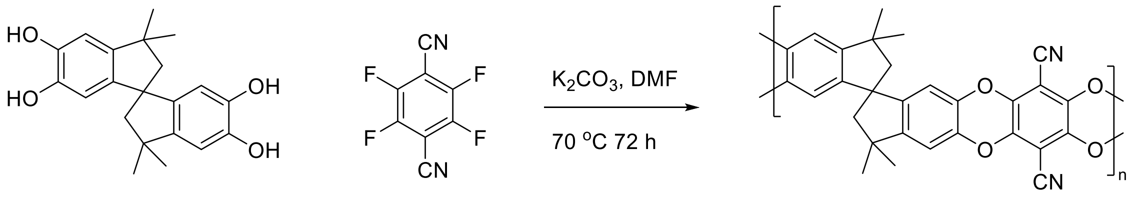

Scheme 2.1: Synthesis of PIM CN.

Chemical Modifications

PIM CN membranes are amenable to different chemical modifications post synthesis.[15,20-32] We hypothesized the presence of primary amine or carboxylic acid groups would increase the hydrophilicity of the overall polymer by increasing the number of hydrogen bond donor and acceptor sites. We pursued a borane reduction of PIM CN to produce a primary amine PIM (PIM NH_2) (Scheme 2.2) and acid catalyzed hydrolysis to produce a carboxylic acid PIM (PIM COOH) (Scheme 2.3). A previous study by Mason et. al.[30] reported PIM NH_2 is insoluble in almost all commonly used organic solvents. This was corroborated by our own experience when PIM NH_2 could not be dissolved for drop casting and thus PIM CN had to be reduced in its membrane form. It was noted that the PIM NH_2 experienced some color changes and became more brittle. Thin membranes were too fragile to be handled after borane reduction, so we moved forward with reduced thick membranes. Thick membranes also underwent a color change and were more brittle but were robust enough for easy handling. FTIR showed a full conversion of the nitrile to a primary amine and was indicated by the absence of the nitrile peak around 2200 cm^{-1} and a larger signal around 3000 cm^{-1} indicating appearance of the -NH group (Figure 2.2).

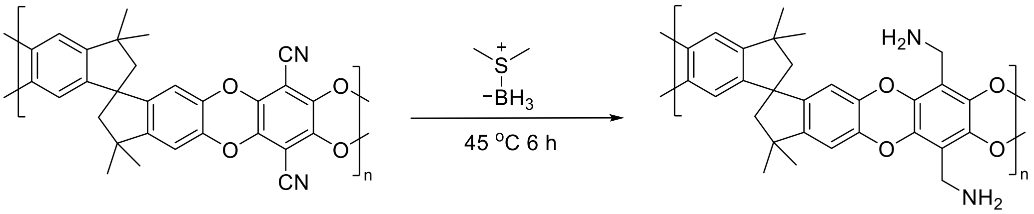

Scheme 2.2: Borane reduction of PIM CN into PIM NH_2.

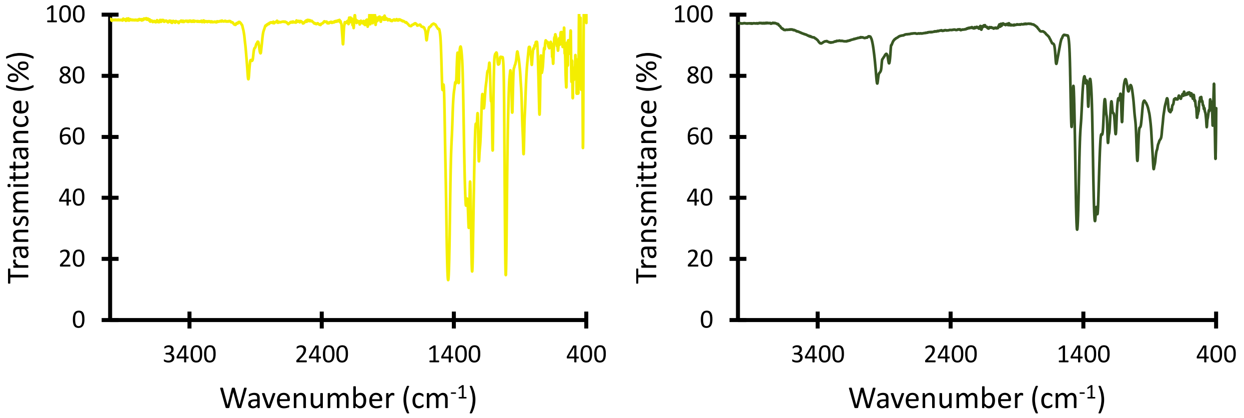

Figure 2.2: FTIR of PIM CN and PIM NH_2. Right: PIM CN. Left: PIM NH_2. The peak around 2200 cm^{-1} corresponding to the -CN functionality disappears. There is an increase in the signal around 1700 cm^{-1} and 3000 cm^{-1} corresponding to the $-NH_2$ functionality.

PIM COOH membranes were prepared by hydrolyzing the PIM CN at elevated temperatures with sulfuric and acetic acid (Scheme 2.3). The reaction is heterogenous and as it proceeds, the polymer powder color darkens from fluorescent yellow to light brown. The temperature must be 110 °C because incomplete hydrolysis was observed at lower temperatures and THF-insoluble products formed at 115 °C. If the sulfuric acid has a high water content, then partial hydrolysis will occur. Complete hydrolysis was determined by FTIR (Figure 2.3). The nitrile peak around 2200 cm^{-1} disappeared and a new carbonyl stretch appeared around 1750 cm^{-1} as well as a hydroxyl signal at 3300 cm^{-1}.

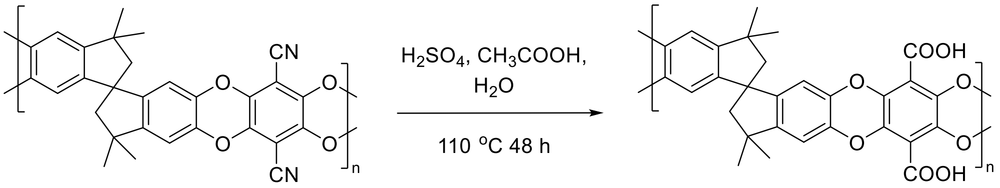

Scheme 2.3: Acid catalyzed hydrolysis of PIM CN into PIM COOH.

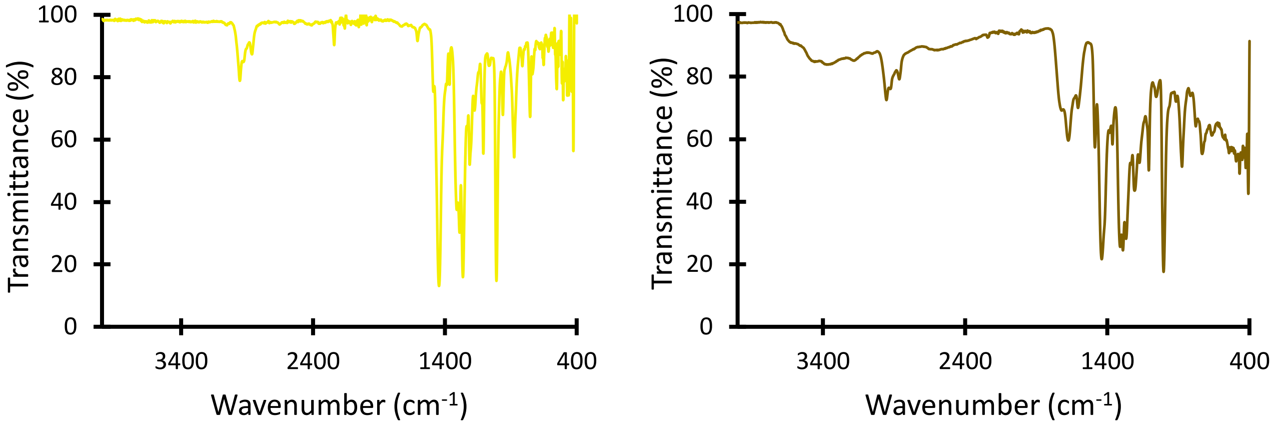

Figure 2.3: FTIR measurements of PIM CN and PIM COOH membranes. Right: PIM CN. Left: PIM COOH. PIM CN contains the -CN peak around 2200 cm^{-1}, but this disappears after hydrolysis and instead the presence of the carbonyl stretch around 1750 cm^{-1} appears as well as the -OH signal around 3300 cm^{-1}.

Both the PIM NH_2 and PIM COOH appeared to be more hydrophilic than their PIM CN precursor based upon water contact angle experiments. The water contact angle decreased from low wettability (θ = 100°) for PIM CN to high wettability for PIM COOH (θ = 30°) and PIM NH_2 (θ = 66°), which closely matched previously reported values.[15,30] Despite the change in water contact angle measurements, neither membrane submerged when placed in water. Both membranes floated when placed in a petri dish with water and exhibited the "lotus effect". When pushed under the water and released, both membranes floated to the top and the water slid off leaving the membrane dry. We determined that a decrease in water contact angle was not sufficient evidence to support a conclusion that borane reduction and acid hydrolysis would allow us to use PIM membranes for water purification applications. To explain this, we examined various wetting models. The high surface tension of water in addition to the interaction between the water droplet and the PIM membranes topology were of particular interest. The "lotus effect" explains why water beads before falling off the polymer membranes. Water assumes a near spherical shape due to its high surface tension and minimizes the solid-liquid surface energy. The Cassie-Baxter to Wenzel transition may explain why the water droplet sits at the top of the PIM membrane, which can be considered a rough surface, but does not flatten on the surface. Air could be trapped underneath the droplet in some of the membrane pores, leading to a mushrooming and apparent decrease in water contact angle. Then hemiwicking at the surface of the PIM membrane may occur as some of the membrane allows some water to penetrate the surface pores. The inability to fully submerge the membranes in water despite the decreases in water contact angle support the idea that the overall hydrophobicity of the internal pore structure was too high to allow water to penetrate the pores. However, we still wanted to evaluate the PIM NH_2 and PIM COOH membranes' capacity for water and dye transport, results of which will be discussed in a later section. However, we felt it necessary to pursue additional methods of increasing the water wetting ability of the PIM membrane due to the lack of success with the chemical modifications.

Surface Modification

Oxygen plasma treatment is commonly used for increasing hydrophilicity of microscopy grids and surfaces, presumably by creating oxidized and charged functional groups within the pore structure surfaces which can participate in hydrogen bonding. We hypothesized oxygen plasma treatment could also significantly increase the wettability of PIM CN membranes.[33] PIM CN membranes were treated on both sides for a determined amount of time. As little as 30 seconds managed to increase the hydrophilicity of the membrane surface, as evidenced by a decreased water contact angle ($\theta = 35°$). The water contact angle of PIM CN after oxygen plasma treatment on both sides was similar to that of

PIM COOH (θ = 30°). However, oxygen plasma treated PIM CN membranes completely submerged in water, unlike PIM NH_2 and PIM COOH membranes. It was noted that small bubbles formed on the surface of the membranes after being placed in water. These were thought to arise from displaced air from the interior of the pores as water moved through the inner channels of the membranes. Another observation was that as the oxygen plasma treatment time increased, the membranes began to stick more to the glass petri dish upon which they were resting and had to be carefully peeled off. However, the results from oxygen plasma treatment were not consistent. The dye transport studies, which will be described later, produced inconsistent results. We determined that oxygen plasma treatment is not a reliable technique for internal modification of PIM pore surfaces, therefore we pursued another method, making composite membranes.

Composite Membranes

Commercial products usually contain additives such as plasticizers to produce materials which better suit their applications. Therefore we doped PIM CN membranes with linear poly(*N*-isopropylacrylamide) (NIPAm). NIPAm was chosen due to its hydrophilic nature and thermal response. It was our hypothesis that the linear NIPAm would be incompatible with the PIM CN chains, leading to phase separation during solvent evaporation. It was hoped that phase separation would force NIPAm into the free volume of the open channels and voids within the PIM CN membrane, thereby acting as a conduit

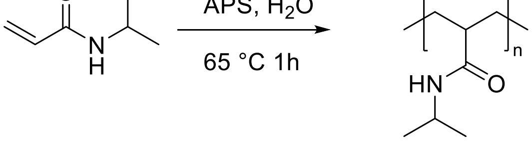

Scheme 2.4: Synthesis of linear poly(*N*-isopropylacrlyamide).

for water to pass through. The amount of dopant would be critical since we wished to retain the high surface area and internal pore volume by coating the interface of the pores without filling them. An advantage of using NIPAm would be a membrane that could selectively control permeation of water-soluble analytes based upon temperature.[35] The NIPAm polymer was synthesized via free radical polymerization (Scheme 2.4). Due to time constraints and facility closures, we were unable to obtain molecular weight data. Based on results from similar polymerizations, I anticipate a high molecular weight of NIPAm and a PDI of 2.0. Linear NIPAm was dissolved in THF and mixed with a solution of PIM CN in THF before drop casting in the same fashion as previously mentioned. Solutions were homogenous before drop casting and allowed to evaporate slowly at room temperature. The weight percent compositions of NIPAm in the composite membranes ranged from 2%, 5%, 7%, and 10%. The composite membranes are notated as PIM-NIPAm followed by the percentage of NIPAm (for example: a PIM CN membrane with 2% NIPAm will be written as PIM-NIPAm 2%).

As the weight percent of linear NIPAm increased, the appearance of the membranes began to change (Figure 2.4). PIM-NIPAM 2% was similar in appearance to PIM CN membranes but slightly cloudier. PIM-NIPAm 5% contained striations in the membrane. However, they were not evenly distributed and caused a slight puckering of the membrane. PIM-NIPAm 7% had the most evenly distributed striations throughout and seemed to be less puckered than PIM-NIPAm 5%. Lastly, PIM-NIPAm 10% was the most fragile with thick, uneven striations and puckering. It was then decided that the maximum weight percent of NIPAm to continue with would be 7%.

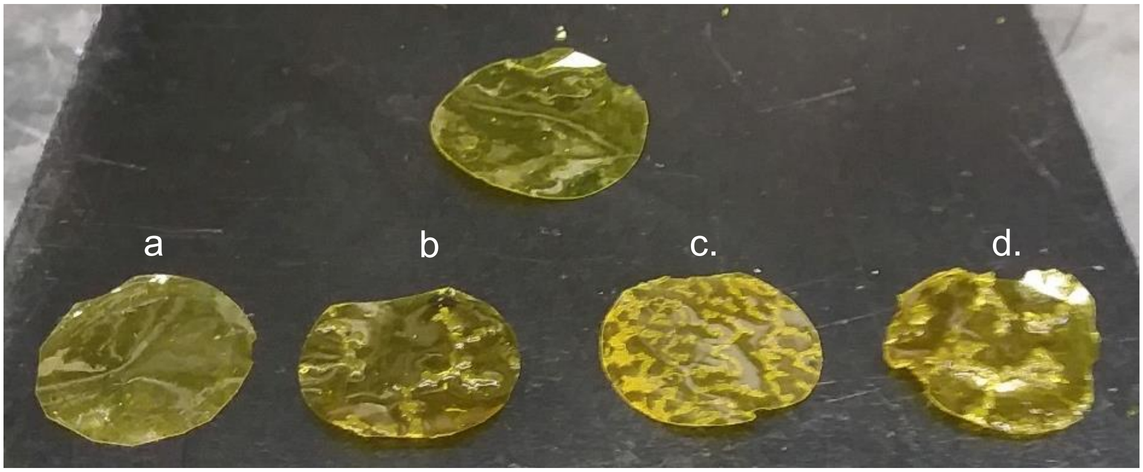

Figure 2.4: Composite PIM NIPAm membranes. Top: PIM CN shown for comparison. PIM-NIPAM 2% (a); PIM-NIPAM 5% (b); PIM-NIPAM 7% (c); and PIM-NIPAM 10% (d). Moving from left to right the striations and patterns in the membranes begin to change as do the physical properties of the membranes.

Characterizing the composite membranes was of great interest. In collaboration with NIST, we decided to employ fluorescence lifetime imaging microscopy (FLIM) to better understand the polymer-polymer interactions and interfaces between PIM CN and NIPAm. PIM CN is intrinsically fluorescent and possesses a λ_{max} at 480 nm in THF.[15] Therefore, we wanted to investigate how adding NIPAm may influence the fluorescence lifetime of PIM CN. This would give us an indication if NIPAm was filling the free volume of the PIM CN after co-dissolving the polymers and drop casting. The FLIM images of PIM-NIPAm membranes were compared to those of PIM CN (Figure 2.5). The fluorescent lifetimes give an indication of the polymer dynamics. PIM CN exhibits two lifetimes (T1 and T2). T1 represents the polymer-air interface while T2 represents the bulk polymer environment of PIM CN membranes. The bulk polymer environment has a longer lifetime because the solid matrix restricts molecular movement, delaying their return to the lowest energy state. It was notable that adding NIPAm leads to the presence of a third lifetime, which can be attributed to the PIM-NIPAm interface. T1 and T2 very likely arise from the PIM CN membrane interface with air and in bulk, but T3 is thought to arise from the interaction of NIPAm and PIM CN polymer chains. As the amount of NIPAm increases in the composite membranes, there is a change in the shape of these decay curves as well as the rate of decay. The third lifetime in PIM-NIPAm 2% exhibits some tailing, which may arise from two separate decay distributions which are overlapping. PIM-NIPAm 5% exhibits a much sharper T3, but a broader T2. These may reflect the decreasing degrees of freedom as the amount of NIPAm increases and fills more pores. PIM-NIPAm 7% seems to exhibit a combination of the effects seen in the 2% and 5% NIPAm samples, but best demonstrates a phase separation due to the differences in lifetimes. These preliminary results supported our hypothesis that adding NIPAm would lead to phase separation and force NIPAm into the open, free volume within PIM CN channels. Unfortunately, due to time constraints, we were unable to further explore the interactions between PIM CN and NIPAm in composite membranes. It was our hope to further use FLIM to better understand various changes in the PIM CN membrane when exposed to methanol, which is discussed in the next section.

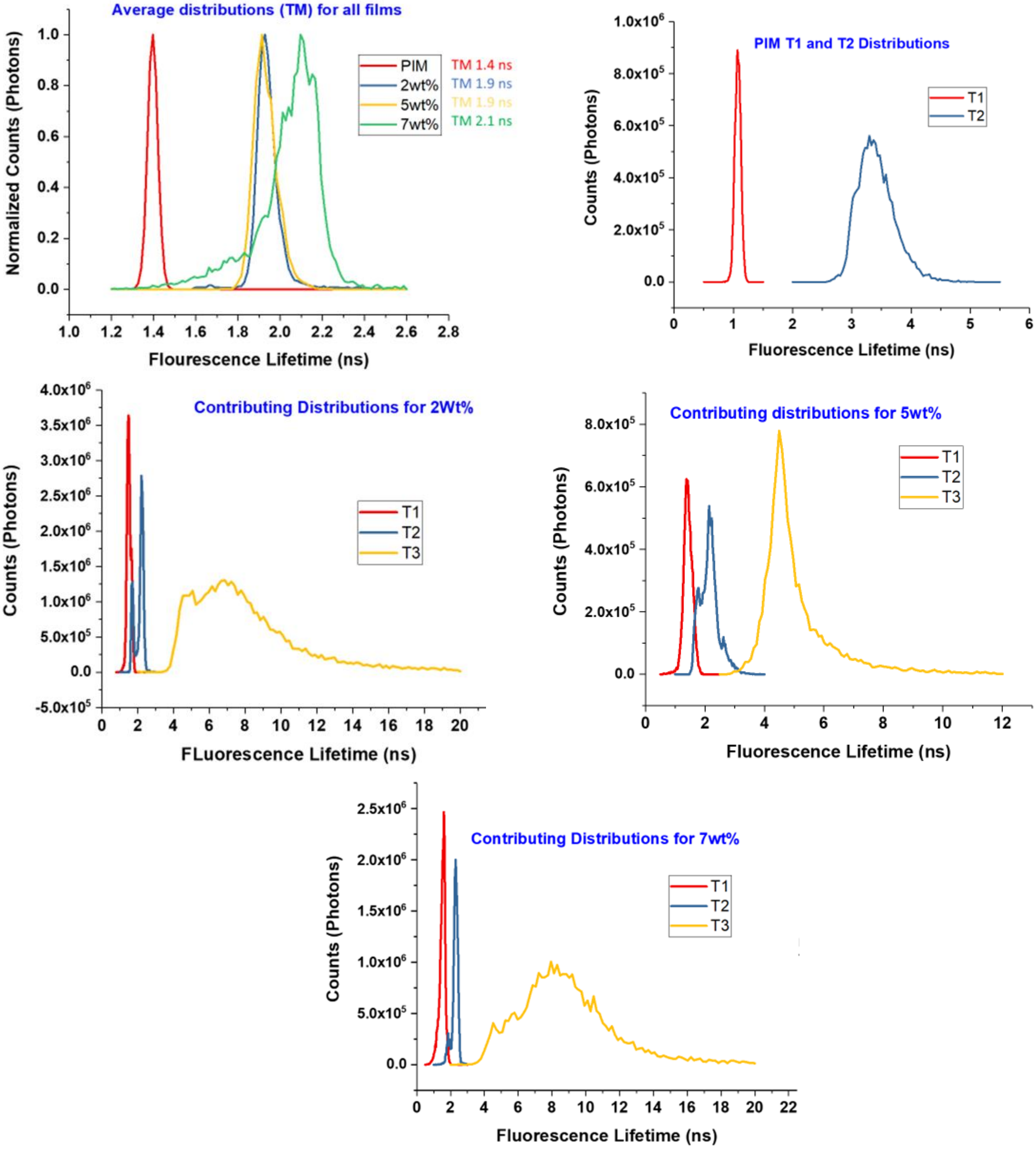

Figure 2.5: Fluorescence lifetime imaging microscopy (FLIM) images of PIM CN and PIM-NIPAm composite membranes. Top left: overlay of the average of each sample lifetime. Top right: contributing distributions of PIM CN. Middle left: contributing distributions of PIM-NIPAm 2%. Middle right: contributing distributions of PIM-NIPAm 5%. Bottom: contributing distributions of PIM-NIPAm 7%.

Treatment with Methanol

The last method examined for improving water wettability of PIM CN membranes was treatment with methanol. Methanol is a known wetting nonsolvent of PIM CN that has been reported to remove processing history from PIM CN membranes and can help restore some of the lost free volume of pores after membranes are cast.[36] Therefore, we rationalized that briefly soaking PIM CN membranes in methanol before placing the membrane in water could aid us in our goals in two ways. First, methanol would help re-open any pores that potentially collapsed during membrane casting. During membrane formation, polymer chains reach equilibrium packing and lose some of the excess free volume. Methanol conditioning for PIM membranes is a common method to increase free volume in the microstructure, thus reversing the packing.[36] Secondly, methanol left in the membrane's pores would act as a medium for water to penetrate the membrane's channels. This second hypothesis was based on lowering the overall surface tension of water when mixed with methanol. The surface tension of water would be high at the water-polymer interface due to the high hydrophobicity of PIM CN, as previously mentioned. Combining methanol with water decreases the overall surface tension of pure water.[37] Methanol decreases the energy of hydrogen bonding within bulk water by competing for hydrogen donating and accepting sites. The energetically unfavorable interactions of bulk water with the polymer are thereby decreased. The aqueous methanol mix lowers the liquid-membrane surface tension allowing water to access the pores.[37]

When a thin membrane was first placed in a shallow dish of methanol, the membrane wrinkled before actively folding and unfolding. However, as the pores filled with methanol, the membrane smoothed out and small bubbles formed on the membrane surface. This was used as an indication that methanol displaced air within the pores. The membrane was then removed from methanol and immediately placed into water. The membrane submerged completely and remained submerged even after being left to sit for hours, presumably because water filled the pores of the membrane. It was noted that if the membrane was removed from the water and placed back in after having some time to dry, the wettability significantly decreased. Additionally, if the methanol on the membrane evaporated before the membrane came in contact with water, the membrane did not wet. It became clear that the time it took to place the membrane in water after methanol treatment significantly impacted membrane wettability in water. If the methanol evaporated from within the pores of the membrane, water would be unable to access the pores. This supports the hypothesis that methanol both opens the pores and decreases the surface tension after mixing with water, allowing water to enter.

Water and Dye Transport Studies

Increasing the hydrophilicity of the membranes was an important goal, however it was not sufficient to simply decrease water contact angle measurements without any indication that water and water-soluble analytes pass through the pores. Surface measurements do not establish if the entire pore network is modified adequately to allow for water transport through the pores. Therefore, we examined how well water and dye solutions flow through the membranes. We examined dye permeation using equilibrium dialysis (Figure 2.6) before moving on to a U-tube set up to monitor water and dye solution permeation through membranes.

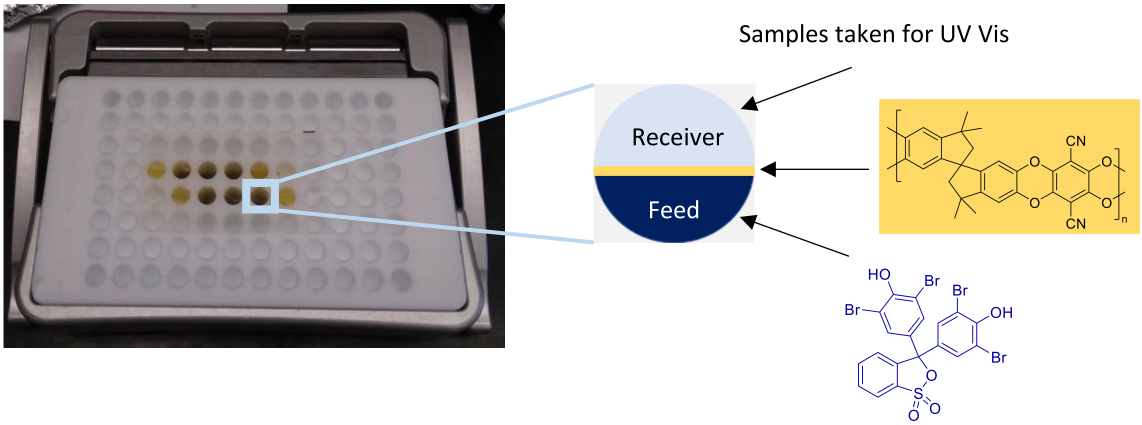

Figure 2.6: Equilibrium dialysis apparatus for dye transport using PIM CN membranes and bromophenol blue.

Equilibrium dialysis is an easy and efficient method of examining transport of small molecules through membranes. It allows for many replicates to be performed at once and is easily carried out. The dye used was bromophenol blue (Scheme 2.5), a water-soluble dye that lacks affinity for PIM CN membranes. Bromophenol blue is a pH sensitive dye which exhibits a yellow color at pH ≤ 3 and is blue at pH ≥ 4.6. The experiments were performed between pH 5.5 and 6, as measured by pH strips. After each experiment, bromophenol blue was easily rinsed off demonstrating the absence of fouling and non-specific binding between the dye and the membrane. Membranes were placed between the equilibrium dialysis blocks with a dye solution (0.6 mg/mL) on one side and pure water on the other. After 24 h, we examined the amount of dye that passed through the membrane.

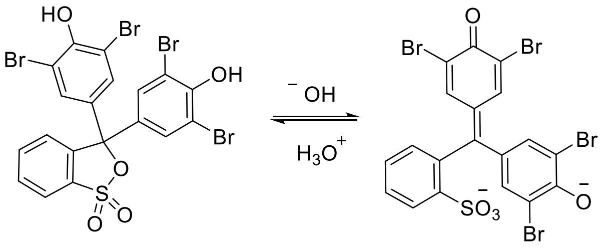

Scheme 2.5: Equilibrium of bromophenol blue under basic and acidic conditions.

Although acid hydrolysis decreased the water contact angle of membranes, thin PIM COOH membranes showed little to no permeation of dye solutions using equilibrium dialysis. Thick PIM NH_2 membranes also exhibited no permeation of water or dye. However, the thick PIM NH_2 membrane changed the color of the dye solution from a dark blue to an almost violet purple. Because of the unexpected color change exhibited by bromophenol blue solutions exposed to PIM NH_2 membranes, we measured the pH of the dye solutions to determine what pH the PIM NH_2 may have induced. It was determined separately that bromophenol blue exhibited the same violet color as was observed in the equilibrium dialysis experiment at pH 9. Although there was no evidence that dye passed through the PIM NH_2 membrane, we believe the dye may have adsorbed to the PIM NH_2 membrane. We hypothesize that once immersed in water, the primary amine of PIM NH_2 deprotonates water leading to generation of hydroxide ions. These hydroxide ions then act as a Brønsted-Lowry base and deprotonate the phenolic hydroxide on bromophenol blue. In turn, the protonated amine on PIM NH_2 can then coordinate with the negatively charged phenolic oxide on bromophenol blue. In a previous report, it was determined that the open anionic state of bromophenol blue dominates at basic pH values (Scheme 2.4).[38] We believe the anionic sulfonate group can also coordinate with the cationic protonated amine, thus leading to dye adsorption on the membrane. The dye molecule therefore acts as the counterion to the protonated amine on the membrane. Adsorption of the charged dye molecules and primary amines on the membrane would explain why there was no observable diffusion of dye, but instead produced a discernible change to the color and pH of the solution.

We then tested oxygen plasma treated membranes. These membranes appeared to be the most promising because they immediately submerged in water, unlike PIM COOH and PIM NH_2 membranes. However, the dye experiment results were inconsistent (Figure 2.7). The wells gave different values when testing different areas of the same piece of membrane. The membranes used for the study were cut from a single piece of film and subjected to identical oxygen plasma treatment conditions. While some wells showed no dye permeation, others had much higher concentrations of dye (1 μM) passing through. For example, samples exposed to oxygen plasma for 240, 330, and 360 seconds demonstrated no dye permeation, despite the fact that lower exposure times did. There was also no indication that a specific oxygen plasma treatment time gave optimal results.

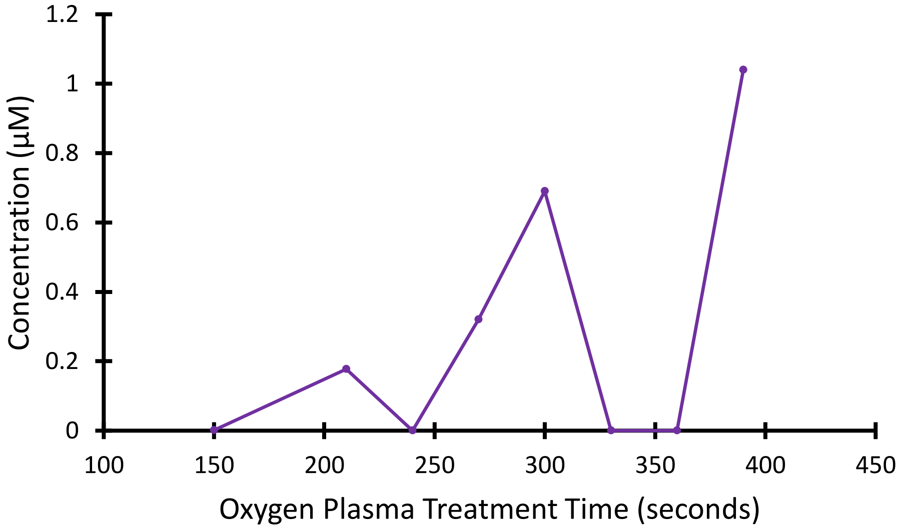

Figure 2.7: Dye transport through oxygen plasma treated PIM CN membranes as a function of oxygen plasma exposure time. All samples were measured after 24 hours using UV-Vis at a wavelength of 591 nm.

Plasma is a fluid, therefore it can penetrate the pores of the membranes. However, the depth of penetration is most important. As plasma filled the pores, it should immediately react with available functional groups on the membrane. Using FTIR, we examined if oxygen plasma treatment up to 210 seconds incurred any chemical changes (Figure 2.8). However, the data shows there were no major changes to the chemical functionalities of the membrane.

The poor reproducibility of the dye transport studies confirms this was a process that could not be relied upon to give consistent results. Our results led us to the conclusion that oxygen plasma treatment is unable to functionalize the entire pore network uniformly throughout the membrane. We also recognized that it was not feasible to expose our membranes to plasma for extended periods of time for fear of degrading the material and its properties. Although this method significantly increased the water wettability of membranes and showed some dye transport, we decided it was too irreproducible to further pursue. We shifted our efforts elsewhere.

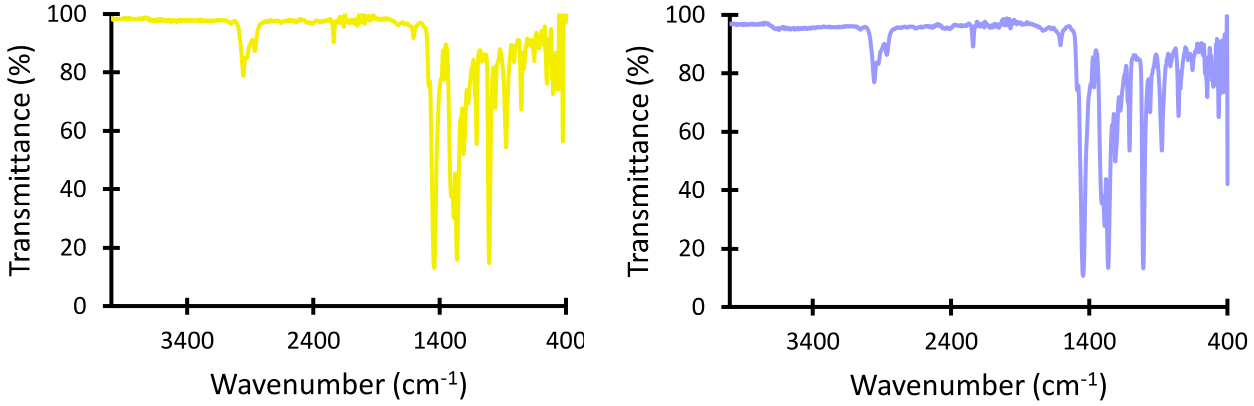

Figure 2.8: FTIR of PIM CN after oxygen plasma treatment. PIM CN before (left) and after (right) exposure to oxygen plasma for 210 seconds.

We began using a U-tube set up (Figure 2.9) for the remaining experiments. Although there were many positive aspects to using the equilibrium dialysis apparatus, we thought there might be some issues. Equilibrium dialysis does not fully submerge the membrane in the dye solution because there is membrane head space at the top of the well. We thought it feasible that capillary action may influence some of the results of the studies. If the membrane was wicking the dye solution or water in the well up into the headspace, this would create an alternate pathway for the fluid to move through. This is similar to what occurs during the Cassie-Baxter to Wendel transition model mentioned earlier. This hemiwicking may have diverted the path of the dye solution so instead of passing through the membrane to the other side, some of it moved into the head space of the membrane. The first membranes we studied using the U-tube apparatus were the composite membranes. PIM-NIPAm composite membranes were cut to about 1 cm diameter circles and mounted in the apparatus. A solution of bromophenol blue was placed on one side

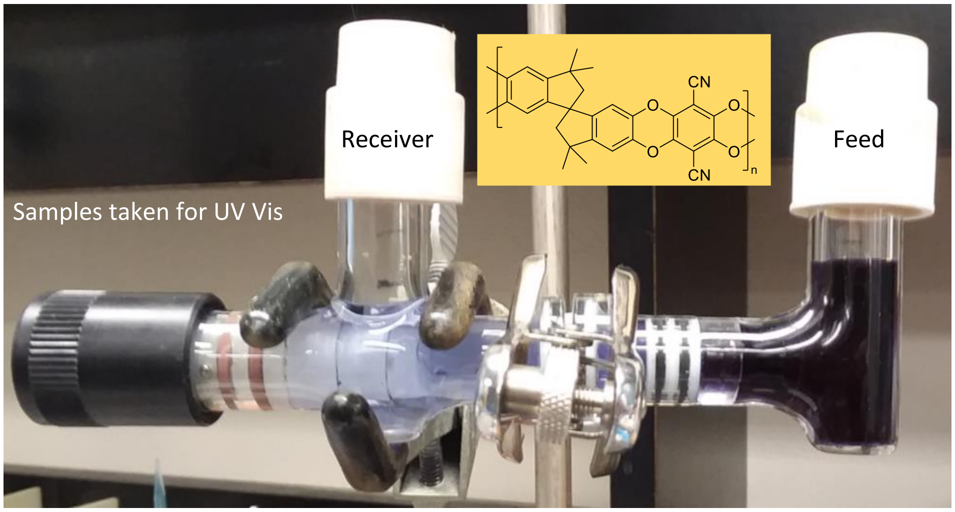

Figure 2.9: U-tube set-up for dye transport through PIM CN membranes.

(feed) and water on the other (receiver). Time point samples were taken from the receiver side and measured by UV-Vis. The data was compared to a bromophenol blue calibration curve. Only PIM-NIPAm 2% and PIM-NIPAm 7% were used because they were robust enough to be handled without cracking. There was some dye transport (Figure 2.10), however dye permeation was extremely slow. After 2 or 3 days, the amount of dye that did permeate was insignificant. The data points obtained demonstrated extremely low concentrations of dye passing through, most values were below the limit of detection of the instrument (0.02 abs for the Nanodrop2000c). Therefore, confidence in the data for dye transport is rather low. The results led us to conclude that the PIM-NIPAm composites were not an effective method to increase the hydrophilicity of PIM membranes to allow water transport, despite the increased hydrophilicity as evidenced by their ability to be submerged in water. Filling the open free volume of the PIM CN membranes with a hydrophilic polymer was not sufficient to allow for water to pass through the membrane. Thus, we decided to pursue treatment with methanol, a wetting non-solvent.

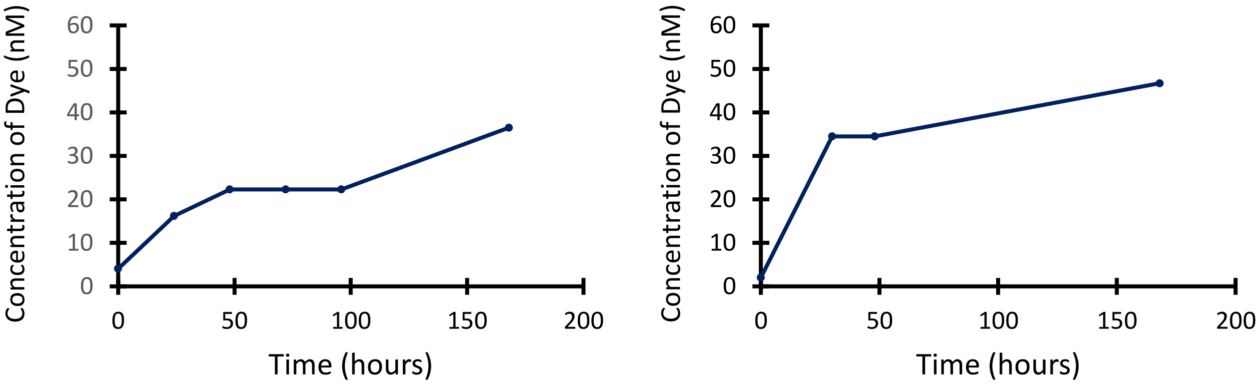

Figure 2.10: Dye transport through PIM-NIPAm composite membranes. Left: PIM-NIPAm 2% Right: PIM-NIPAm 7%. Both membranes allowed some dye to pass through, however it was over a long period of time, exceeding practical timelines.

As mentioned previously, methanol is commonly used to remove variability in membranes caused by casting solvent, thermal treatment, and age. In fact, methanol treatment can be especially helpful in treating highly porous polymers by removing residual solvent trapped in the membrane structure and to erase any changes to the microstructure that processing may have caused. PIM CN is a high free volume glassy polymer and can naturally lose its excess volume due to polymer chains relaxing into their equilibrium packing. Previous studies have shown that methanol treatment can help increase the surface area and pore-volume of PIM CN.[36] With this in mind, we ventured to refresh PIM CN membranes with methanol and evaluate how a wetting nonsolvent may help improve water transport through the membranes.

First, we examined if simply wetting PIM CN membranes with methanol before placing in the apparatus was sufficient to allow for water to pass through the membrane. To examine this, we briefly soaked PIM CN in methanol for about 1 minute before placing it in the U-tube and testing with a solution of bromophenol blue in water (0.6 mg/mL). After PIM CN membranes stopped forming bubbles while submerged in methanol, we determined they were ready for testing. We measured dye permeation on the receiver side at various time points using UV-Vis. Little to no dye crossed the membrane. These results suggest that although methanol wets the membrane, the surface tension of water alone may be too high to pass through these 2 nm pores at atmospheric pressure. We concluded that it would be necessary to lower the surface tension of water to decrease the surface tension of the overall liquid. We then decided to examine if a dilute solution of methanol in water would allow water and a water-soluble analyte to permeate the PIM CN membrane.

To determine the optimum conditions for wettability and transport, we investigated 20%, 30%, 50%, and 75% methanol solutions. We hypothesized that increasing the percent volume of methanol would also improve dye and water transport. However, the results obtained from methanol concentrations of 50% and 75% rejected this hypothesis. During these experiments, water (receiver side) moved to the feed side instead of the dye (feed side) moving to the receiver side, causing a decrease in the receiver volume and an increase in the feed volume. This can be explained by a difference in the osmotic pressure between the feed and receiver side. Solvent will naturally move from a low concentration of analyte to a higher concentration, which is why we observed the changes in solvent volume that we did. We also wanted to avoid high concentrations of organic solvent in our system, so we continued our experiments with 20% methanol. This concentration was determined earlier to be the lowest content of methanol we could use to achieve our goal of utilizing PIM CN as a size selective membrane under aqueous conditions. The results from bromophenol blue in 20% methanol (0.3 mg/mL) are shown in Figure 2.11. These results demonstrate higher levels of dye transport under a shorter amount of time than exhibited by composite membranes. The flux started to decrease after 2 hours and plateaued after 3 hours. Although the dye transport using methanol was lower than what some of the oxygen plasma treatment membranes achieved, the results are significantly more consistent. After optimizing experimental conditions, we tested larger particulates such as bovine serum albumin and silver nanoparticles.

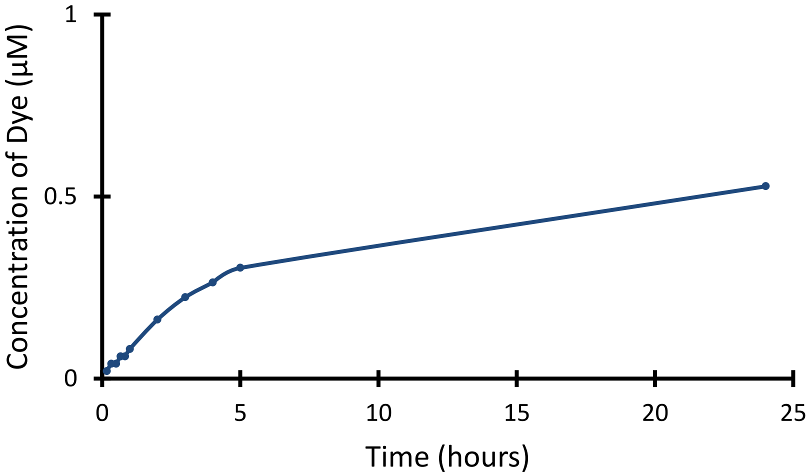

Figure 2.11: Bromophenol blue transport through PIM CN membranes wet with methanol. The feed side contained bromophenol blue dissolved in 20% methanol (0.03 mg/mL) and the receiver side contained 20% methanol. UV-Vis measurements were taken at 591 nm.

Bovine Serum Albumin Filtration

Our goal is to use these membranes for aqueous filtration of particles around the size of the smallest viruses, which is around 20 nm. Therefore, to further validate the size selectivity of our PIM CN membranes, we moved to protein filtration studies as a way to investigate how a biological macromolecule or particulate would behave in our system. We chose bovine serum albumin (BSA) due to its availability and solubility in aqueous methanol. Previous reports suggest that BSA does not undergo secondary structure changes in 30% ethanol and below.[38] BSA is about 7 nm in diameter in buffer by dynamic light scattering (DLS) and previous studies examining BSA's size in 30% ethanol reflect a similar size.[38] The pore size of PIM was measured to be around 2 nm by BET analysis (data not shown) and has been confirmed by our previous work.[15] Based upon these size differences, we predicted BSA would not be able to pass through PIM CN.

We dissolved BSA in 20% methanol (0.9 mg/mL) and placed it on one side of the membrane while the other side contained 20% methanol. The membrane was pre-soaked in methanol before the experiment. The data (Figure 2.12) revealed that protein did not pass through the membrane in a span of 24 hours. The absorbance data was well below the limit of detection of the instrument (0.02 abs for the Nanodrop2000c), therefore the confidence that these values are anything more than noise is rather low. After three trials, the data strongly supports that a biological material ~7 nm in diameter would not be able to pass through the membrane. Due to time constraints, we were unable to test other candidates such as smaller proteins and peptides to see if other biomacromolecules would also be excluded, or, depending on their size pass through PIM CN membranes. However, we were able to use 20 nm silver nanoparticles which match the size of the smallest viruses to obtain additional size exclusion data.[12]

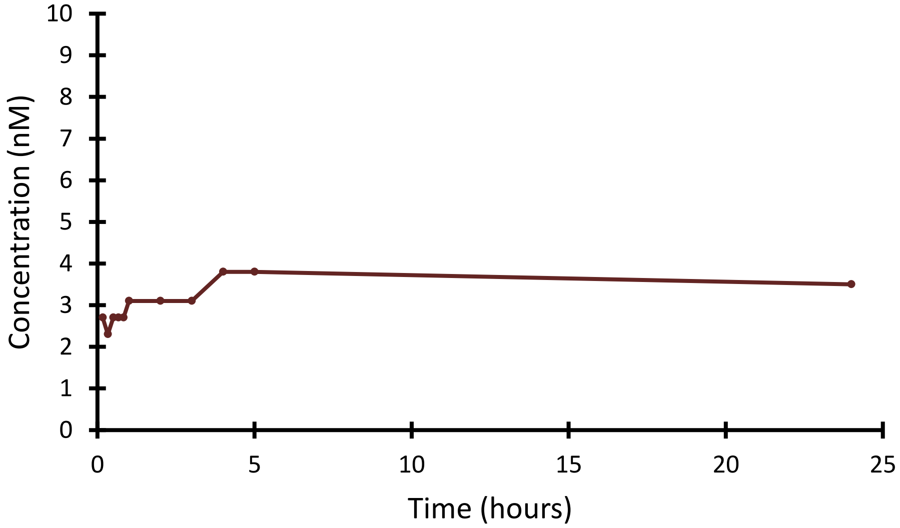

Figure 2.12: BSA transport through PIM CN membranes wet with methanol. The feed side contained BSA dissolved in 20% methanol (0.9 mg/mL) and the receiver side contained 20% methanol. UV-Vis measurements were taken at 280 nm.

Silver Nanoparticle Filtration

Our next goal was to ascertain that the PIM CN membrane was capable of filtering small, virus sized particles. Before using them in our experiments, the silver nanoparticles were measured by UV-Vis at a λ_{max} of 390 nm. The silver nanoparticles were diluted into 20% methanol (0.016 mg/mL) on the feed side with 20% methanol on the receiver side. Silver nanoparticles are hard spheres and cannot pass through the small channels and pores in the PIM CN. The data (Figure 2.13) demonstrates that there was little to no absorbance observed. Most of the measurements can be attributed to noise as their absorption values were all below the limit of detection of the instrument (0.02 abs for the Nanodrop2000c).

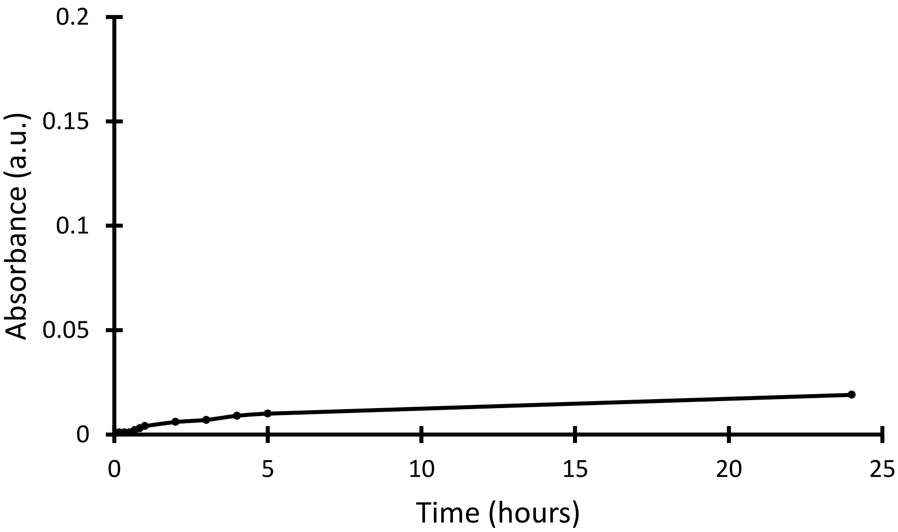

Figure 2.13: Silver nanoparticle transport through PIM CN membranes wet with methanol. The feed side contained 20 nm silver nanoparticles in 20% methanol (0.016 mg/mL) and the receiver side contained 20% methanol. UV-Vis measurements were taken at 390 nm.

We recognize that 20% methanol is not considered aqueous conditions and would be impractical to implement in commercial and industrial applications. However, we consider this work as the first steps in modifying the internal pore structure of these fascinating materials and developing analytical diagnostics that may be used to evaluate ways to improve PIM CN materials for water filtration applications. Though our conditions are less than ideal, we feel we have made steps towards better understanding how to modify PIM CN materials to function in an aqueous environment for applications such as viral particle filtration. Due to the unforeseen time constraints, we were unable to move forwards in our study. We would have continued our collaboration with NIST to learn more about the interfaces of these composite materials and to study how methanol mixed with water affects the microstructure of PIM CN.

Conclusion

In this report we detailed efforts to increase the hydrophilicity and water wetting of PIM CN. Chemical modifications such as reducing the nitrile to a primary amine and hydrolyzing the nitrile to a carboxylic acid had minimal effect on aqueous dye solution transport through the membrane. We had marginal success using oxygen plasma treatment and composite membranes with NIPAm. We learned that methanol, a wetting non-solvent, helps not only open the pores of the membrane, but enables transport of a water-soluble dye through the membrane. We also demonstrated that under these conditions, larger particulates within the size range of viruses were unable to permeate the membrane. Both BSA and silver nanoparticles were unable to pass through the membrane. This system takes the first steps to a viable small-scale method to filter aqueous solutions of virus particles. We envision that this could be used as a low cost, accessible water filter of viruses and microplastics for underdeveloped and low-income regions. We also foresee an application on an industrial scale given the correct engineering parameters.

References

(1) WHO/, U.N.I.C.E.F., 2017. Progress on drinking water, sanitation and hygiene 2017 update and SDG baseline.

(2) WHO, 2019, Drinking Water, https://www.who.int/en/news-room/fact-sheets/detail/drinking-water.

(3) Gall, A.M.; Mariñas, B.J.; Lu, Y.; Shisler, J.L. "Waterborne viruses: A barrier to safe drinking water" *PLoS Pathog,* **2015**, *11*, e1004867.

(4) Elimelech, M.; Philip, W.A. "The future of seawaterdesalination: energy, technology, and the environment" *Science*, **2011**, *333*, 712-717.

(5) Baker, R.W. *Membrane technology and applications* (John Wiley & Sons, 2012).

(6) Lu, X.; Nejati, Siamak, Choo, Y.; Osuji, C.O.; Ma, J.; Elimelech M. "Elements provide a clue: nanoscale characterization of thin film composite polyamide membranes" *ACS Appl. Mater. Interfaces*, **2015**, *31*, 16917-16922.

(7) Karan, S.; Jiang, Z.; Livingston, A.G. "Sub-10 nm polyamide nanofilms with ultrafast solvent transport for molecular separation" *Science*, **2015**, *348*, 1347-1351.

(8) Wang, M.; Wang, Z.; Wang, X.; Wang, S. Ding, W.; Gao, C. "Layer-by-layer assembly of aquaporin Z-incorporated biomimetic membranes for water purification" *Environ. Sci. Technol.*, **2015**, *49*, 3761-3768.

(9) Wang, H.; Chung, T.S.; Tong, Y.W.; Jeyaseelan, K.; Armugam, A.; Chen, Z.; Hong, M.; Meier, W. "Highly permeable and selective pore-spanning biomimetic membrane embedded with aquaporin Z" *Small*, **2012**, *8*, 1185-1190.

(10) Kumar, M.; Grzelakowski, M.; Zilles, J.; Clark, M.; Meier, W. "Highly permeable polymeric membranes based on the incorporation of the functional water channel protein aquaporin Z" *Proc. Natl Acad. Sci. USA*, **2007**, *104,* 20719-20724.

(11) Fane, A.G.; Wang, R.; Hu, M.X. "Synthetic membranes for water purification: Status and future" *Angew. Chem. Int. Ed.*, **2015**, *54*, 3368-3386.

(12) Werber, J.R.; Osuji, C.O.; Elimelech, M. "Materials for next-generation desalination and water purification membranes" *Nature Reviews*, **2016**, *1*, 16018.

(13) McKeown, N.B.; Budd, P.M. "Polymers of intrinsic microporosity (PIMs): organic materials for membrane separations, heterogeneous catalysis and hydrogen storage" *Chem. Soc. Rev.*, **2006**, *35*, 675-683.

(14) Pan, Y.; Zhang, L.; Li, Z.; Ma, L.; Zhang, Y.; Wang, J.; Meng, J. "Hierarchical porous membrane via electrospinning PIM-1 for micropollutants removal" *Applied Surface Science*, **2018**, *443*, 441-451.

(16) Weng, X.; Baez, J.E.; Khiterer, M.; Hoe, M.Y.; Bao, Z.; Shea, K.J. "Chiral polymers of intrinsic microporosity: Selective membrane permeation of enantiomers" *Angew. Chem. Int. Ed.*, **2015**, *54*, 11214-11218.

(16) Wang, Y.; McKeown, N.B.; Msayib, K.J.; Turnbull, G.A.; Samuel, I.D. "Laser chemosensor with rapid responsivity and inherent memory based on a polymer of intrinsic microporosity" *Sensors*, **2011**, 2478-2487.

(17) Rakow, N.A.; Wendland, M.S.; Trend, J.E.; Poirier, R.J.; Paolucci, D.M.; Maki, S.P.; Lyons, C.S.; Swierczek, M.J. "Visual indicator for trace organic volatiles" *Langmuir*, **2010**, *26*, 3767-3770.

(18) Yang, Z.; Guo, r. Malpass-Evans, R.; Carta, M.; McKeown, N.B.; Guiver, M.D.; Wu, L.; Xu, T. “Highly conductive anion-exchange membranes from microporous Tröger’s Base polymers” *Angew. Chem. Int. Ed.,* **2016**, *55*, 11499-11502.

(19) Madrid, E.; Rong, Y.; Carta, M.; McKeown, N.B.; Malpass-Evans, R.; Attard, G.A.; Clarke, T.J.; Taylor, S.H.; Long, Y.T.; Marken, F. “Metastable ionic diodes derived from an amine-based polymer of intrinsic microporosity” *Ange. Chem. Int. Ed.*, **2014**, *53*, 10751-10754.

(20) Du, N.; Park, H.B.; Robertson, G.P.; Dal-Cin, M.m.; Visser, T.; Scoles, L.; Guiver, M.D. “Polymer nanosieve membranes for CO_2-capture applications” *Nat. Mater.* **2011**, *10*, 372-375.

(21) Du, N.; Roberston, G.P.; Dal-Cin, M.M.; Scoles, L.; Guiver, M.D. “Polymers of intrinsic microporosity (PIMs) substituted with methyl tetrazole” *Polymer* **2012**, *53*, 4367-4372.

(22) Patel, H.A.; Yavuz, C.T. “Noninvasive functionalization of polymers of intrinsic microporosity for enhanced CO_2 capture” *Chem. Commun.* **2012**, *48*, 9989-9991.

(23) Swaidan, R.; Ghanem, B.S.; Litwiller, E.; Pinnau, I. “Pure- and mixed-gas CO_2/CH_4 separation properties of PIM-1 and an amidoxime-functionalized PIM-1” *J. Membr. Sci.* **2014**, *457*, 95-102.

(24) Mason, C.R.; Maynard-Atem, L.; Al-Harbi, N.M.; Budd, P.M.; Bernardo, P.; Bazzarelli, F.; Clarizia, G.; Jansen, J.C. “Polymer of intrinsic microporosity incorporating thioamide functionality: preparation and gas transport properties” *Macromolecules*, **2011**, *44*, 6471-6479.

(25) Satilmis, B.; Alnajrani, M.N.; Budd, P.M. “Hydroxyalkylaminoalkylamide PIMs: selective absorption by ethanolamine- and diethanolamine-modified PIM-1” *Macromolecules*, **2015**, *48*, 5663-5669.

(26) Du, N.; Robertson, G.P.; Song, J.; Pinnau, I.; Guiver, M.D. “High-performance carboxylated polymers of intrinsic microporosity (PIMs) with tunable gas transport properties” *Macromolecules*, **2009**, *42*, 6038-6043.

(27) Du, N.; Dal-Cin, M.M.; Pinnau, I.; Nicalek, A.; Robertson, G.P.; Guiver, M.D. “Azide-based cross-linking of polymers of intrinsic microporosity (PIMs) for condensable gas separation” *Macromol. Rapid Commun.,* **2011**, *32*, 631-636.

(28) Du, N.; Dal-Cin, M.M.; Robertson, G.P.; Guiver, M.D. “Decarboxylation-induced cross-linking of polymers of intrinsic microporosity (PIMs) for membrane gas separation” *Macromolecules*, **2012**, *45*, 5135-5139.

(29) Khan, M.M.; Bengtson, G.; Shishatskiy, S.; Gacal, B.N.; Rhaman, M.M.; Neumann, s.; Filiz, V.; Abetz, V. “Cross-linking of polymer of intrinsic microporosity (PIM-1) via nitrene reaction and its effect on gas transport property” *European Polymer Journal*, **2013**, *49*, 4157-4166.

(30) Mason, C.R.; Maynard-Atem, L.; Heard, K.W.J.; Satilmis, B.; Budd, P.M.; Friess, K.; Lanč, M.; Bernardo, P.; Clarizia, G.; Jansen, J.C. “Enhancement of CO_2 affinity in a polymer of intrinsic microporosity by amine modification” *Macromolecules*, **2014**, *47*, 1021-1029.

(31) Yanaranop, P.; Santoso, B.; Etzion, R.; Jin, J. “Facile conversion of nitrile to amide on polymers of intrinsic microporosity (PIM-1)” *Polymer*, **2016**, *98*, 244-251.

(32) Halder, K.; Neumann, S.; Bengtson, G.; Khan, M.M.; Filiz, V.; Abetz, V. “Polymers of intrinsic microporosity postmodified by vinyl groups for membrane applications” *Macromolecules*, **2018**, *51*, 7309-7319.

(33) Kim, H.J.; Kim, D.G.; Lee, K.; Baek, Y.; Yoo, Y.; Kim, Y.S.; Kim, B.G.; Lee, J.C. "A carbonaceous membrane based on a polymer of intrinsic microporosity (PIM-1) for water treatment" *Scientific Reports*, **2016**, *6*, 36078.

(34) Shi, Q.; Zhang, K.; Lu, R.; Jiang, J. "Water desalination and biofuel dehydration through a thin membrane of polymer of intrinsic microporosity: Atomistic simulation study" *Journal of Membrane Science*, **2018**, *545*, 49-56.

(35) Cetintas, M.; de Grooth, J.; Hofman, A.H.; van der Kooji, H.M.; Loos, K.; de Vos, W.M.; Kamperman, M. "Free-standing thermo-responsive nanoporous membranes from high molecular weight PS-NIPAM block copolymers synthesized via RAFT polymerization" *Polym. Chem.*, **2017**, *8*, 2235-2243.

(36) Jue, M.l.; McKay, C.S.; McCool, B.A.; Finn, M.G.; Lively, R.P. "Effect of Nonsolvent treatments on the microstructure of PIM-1" *Macromolecules*, **2015**, *48*, 5780-5790.

(37) Ghahremani, H.; Moraid, A.; Abedini-Torghabeh, J.; Hassani, S.M. "Measuring surface tension of binary mixtures of water + alcohols from the diffraction pattern of surface ripples" *Der Chemica Sinica*, **2011**, *2*, 212-221.

(38) Chattopadhyaya, M.; Murugan, N.A.; Rinkevicius, Z. "Origin of the absorption band of bromophenol blue in acidic and basic pH: Insight from a combined molecular dynamics and TD-DFT/MM study" *J. Phys. Chem. A* **2016**, *120*, 7175-7182.

(39) Yoshikawa, H.; Hirano, A.; Arakawa, T.; Shiraki, K. "Effects of alcohol on the solubility and structure of native and disulfide-modified bovine serum albumin" *International Journal of Biological Macromolecules*, **2012**, *50*, 1286-1291.

Chapter 3: Progress Towards Photodegradable Polymethylene

Introduction

Plastics are ubiquitous, much in part due to their low cost, usefulness, and durability. Some scientists have identified the current era as the *Plasticene* due to the widespread use of plastics.[1] Since 1950, about 8300 million metric tons (Mt) of resins and fibers have been manufactured, half of which was produced in the last 13 years.[2] These materials have enabled humans to sustain a lifestyle that can be considered advanced and convenient. However, this is not necessarily sustainable for the planet and its inhabitants. By 2015, 380 Mt of plastic were being produced per annum with none of these commercial plastics being biodegradable.[2] Once these plastics are made, they persist throughout the environment for up to five decades.[3] Although recycling and incineration are viable options, their current implementation makes a small impact in the amount of plastic in existence. Only 6-26% of plastics are recycled with 21-42% finding its way to landfills.[4-8] One study showed that of the 8300 Mt of plastic produced, 2500 Mt are in use, 4900 Mt were discarded to landfills or the environment, 800 Mt were incinerated, and 600 Mt were recycled.[2] Others have estimated that over 250 Mt of plastic will have accumulated in the ocean by 2025.[9,10] Although plastics can slowly degrade over time, there is an important distinction between the classifications degradable and biodegradable.

Degradable plastics seem to be a viable solution to the issues of litter and pollution. However, the term “degradable” does not necessarily entail that smaller byproducts of plastics are innocuous to the environment. Plastics slowly degrade by exposure to UV radiation and mechanical abrasion to form macroplastics (>25 mm), mesoplastics (5-25 mm), microplastics (0.1-5 mm), and nanoplastics (<100 nm).[11,12] These smaller particles are not biodegradable, so they persist and travel. The term biodegradable describes "a plastic in which the degradation results from the action of naturally-occurring micro-organisms such as bacteria, fungi, and algae".[13] Many misconceptions exist regarding the relationship of bioderived and biodegradable materials. A bioderived plastic contains "organic carbon of renewable origin" from "plant, animal, fungi, microorganisms, marine, or forestry" sources.[14] Therefore, a bioderived plastic is not necessarily biodegradable and a petroleum-based plastic could potentially be biodegradable. Examples of bioderived but not biodegradable plastics include bio-based polyethylene (PE) and bio-based poly(ethylene terephthalate) (PET). Examples of petrochemically-based plastics that are biodegradable are polybutylene adipate-*co*-terephthalate (PBAT) and polycaprolactone (PCL).[15] There are few examples of a bioderived and biodegradable material. Polylactic acid (PLA) is one such a polymer. However, the biodegradability of the L-isoform depends on microbial communities that are not widespread in soil[16] and the D-isoform is hydrolysable, but not biodegradable.[17-19] New alternatives to plastic feedstocks and disposal are necessary for preserving our environment.

Crude oil is the source of most plastics. In fact, 8% of the global crude oil and gas produced is used to make plastics.[20] As opposed to focusing on nonrenewable sources, the plastic industry has begun to focus on more renewable resources. The global production of biomass is estimated to be 1 billion tons per year, of which only 3% is grown, harvested, and used in both food and nonfood applications. To further classify this biomass, 75% consists of carbohydrates, 20% is lignin, with the remaining 5% a combination of terpenes, proteins, and triglycerides.[21] Carbohydrates can be used to derive important monomers such as succinic acid, furan derivatives, and diols. Lignin is of particular interest due to its natural abundance of various aromatic groups.

Current methods of chemical recycling are inefficient and costly. PE is the most common plastic and does not recycle well. As of 2017, over 100 Mt of PE were produced annually, this accounts for 34% of the total plastics market.[2] There is a clear need in developing materials that are more amenable to simpler recycling and breakdown processes. Extending this notion to oxygen containing carbohydrates, the structure and breakdown of lignin itself is complex. Various studies and reviews have examined catalytic, oxidative, and photocleavage of lignin model compounds.[22-30] Of note are β-1, β-O-4, and β-5 inter-unit linkages (Figure 3.1). Scission of C-O bonds in lignin, found in the β-O-4 linkage, has been a popular focus as it comprises up to two-thirds of the inter-unit linkages. However, this is only true for the raw plant biomass, referred to as native lignins. During lignin fractionation, or pulping, many C-C bonds form and it has been suggested that the β-O-4 content is very low after undergoing the kraft process, which is a common pulping method.[31] Pulping separates lignin from lignocellulose, these byproducts from processing and production are considered technical lignin. Currently, research is being done to minimize the chemical changes made to lignin during processing. However, most of the commercial lignin available undergoes the kraft process and will thus result in an increase in C-C bonds. This change in the ratio of C-O and C-C bonds alters the reactivity of lignin. Research on effectively targeting the C-C bonds in lignin has been studied to a lesser extent than the C-O bond scission in β-O-4 types. Lignin is also known to be susceptible to fungal and bacterial degradation, thus making it amenable to biodegradation. These characteristics support the utility of commercializing lignin-like plastics.

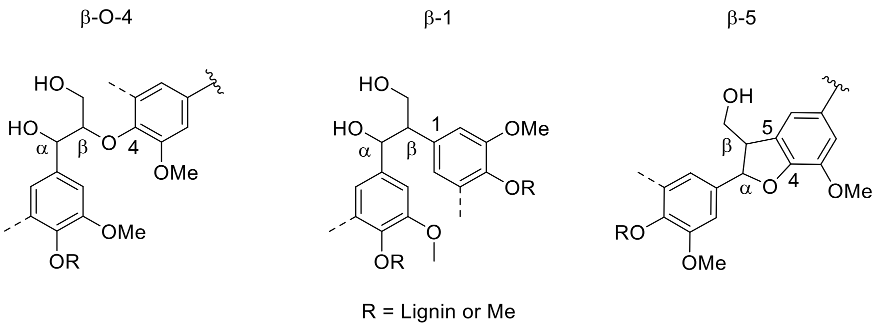

Figure 3.1: Structures of lignin linkages of interest.

We initiated a study to explore the potential utility of integrating lignin inspired molecules (LMs) into intractable synthetic polymers to enhance their photodegradability. This work is an exploratory step in a general approach to establish the feasibility of enhancing the intrinsic photodegradability of commodity synthetic polymers. We envision incorporating a chemical moiety that can undergo C-C cleavage under solar irradiation into commercial plastics will be a valuable contribution to reducing the plastic waste in the environment. Photolyzing polymer chains within plastics can accelerate the breakdown by lowering the molecular weight of the polymer and thus making it more amenable to biodegradation.[3] In this way, plastics accumulating in oceans, landfills, or other environments can be consumed by microbes faster, thereby preventing the formation of microplastics. Our broad goals included developing a LM with appropriate electron donating (EDG) and electron withdrawing groups (EWG) to increase the photoefficiency of C-C fragmentation of the LM (Figure 3.2). Incorporating these LMs into polymers used in commercial plastics would allow development of a material which can aid in preventing an accumulation of microplastics in the environment. Our intention was to collaborate with the Furche group to carry out electronic energy structure calculations to determine arene substituents that lower the activation energy of C-C bond cleavage. Unfortunately, due to time constraints these studies were not able to progress.

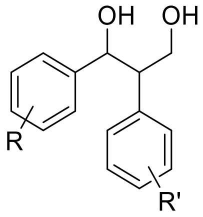

Figure 3.2: Structure of a lignin β-1 model compound with different substituents.

In this study, we pursued a photolabile molecule, LM, that can be incorporated into commodity plastics without compromising the physical properties of these materials. The physical properties of the polymer will be influenced by the level of dopant needed to produce significant breakdown. This was be important to consider for future studies. The modified polymer contains a mimic of a β-1 lignin molecule that undergoes C-C bond scission upon irradiation under a broad wavelength range similar to what is experienced on the Earth's surface (Figure 3.3). We inserted the LM into the center of a PE analogue, polymethylene (PM). We focused on cleaving the C_{α}-C_{β} inter-unit linkage of a β-1 analogue. We also examined how methoxy substitution influences photocleavage reactivity; this was to inform us of how EDG may influence C-C scission. The mimic lignin molecule was incorporated into the middle of a PM chain using polyhomologation. Polyhomologation is a living C1 polymerization that uses ylides as a monomer source and an organoborane initator/catalyst. By growing the polymer chain one carbon at a time, it provides precise control over molecular weight and a low polydispersity. Polyhomologation produces PM as opposed to PE because it grows the polymer one carbon at a time. The advantage to using polyhomologation is that it allows equal lengths of polymer to grow from either side of the difunctional mimic lignin molecule with narrow molecular weight distributions. In turn, carefully controlling molecular weight distributions allows us to accurately monitor any changes to the molecular weight of the polymer. The LM will cleave upon exposure to light, thereby cutting the polymer chain in half. This will reduce the molecular weight of the polymer to half its original weight. We can study the occurrence of photocleavage of the PM chain by gel permeation chromatography.

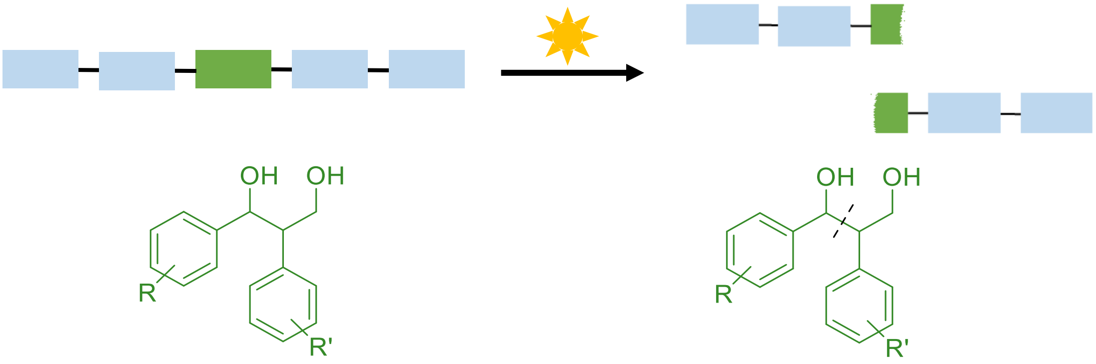

Figure 3.3: Irradiation of a polymer containing the lignin model compound leads to breakdown of the polymer backbone.

Experimental Section

General Procedures

Thin layer chromatography (TLC) was performed on 60G F_{254} plates from Sigma-Millipore. ^{1}H NMR spectra were recorded at 500 MHz, using a Bruker GN500 spectrometer. ^{13}C NMR spectra were recorded at 125 MHz, using a Bruker CRYO500 spectrometer. ^{1}H and ^{13}C NMR spectra for small molecules were run in $CDCl_3$ and polymers were run in deuterated tetrachloroethane (TCE) at 100 °C with shifts reported as δ values in ppm and referenced to residual solvent proton or carbon. Splitting patterns are abbreviated as follows: s = singlet, d = doublet, dd = doublet of doublets, t = triplet, q = quartet, quint = quintet, sext = sextet, sep = septet, m = multiplet, br = broad.

Differential Scanning Calorimetry (DSC) Experiments

DSC experiments were performed on a TA Instruments DSC 2500 at a heating/cooling rate of 10 °C/min. Samples were cooled from room temperature to -80 °C and equilibrated at this temperature for 10 min. Samples were then heated to 190 °C and kept at this temperature for 10 min to release any thermal history. Samples were then cooled to -80 °C again and kept at this temperature for 10 min before heating again to 190 °C. DSC traces of isolated polymer product were obtained on 3 to 7 mg of sample using aluminum pans. Crystallinity % data are reported from the second heating cycle. Polymer crystallinities were calculated based on the melt enthalpy of 281 J/g for 100% crystalline polyethylene.[40]

Gel Permeation Chromatography (GPC) Experiments

GPC analysis was performed with Agilent PL-GPC 220 at 110 °C using 1,2,4-trichlorobenzene as eluent in a flow rate of 1.0 mL/min. The GPC instrument was equipped with three sets of MesoPore 3 μm 300×7.5 mm columns calibrated with seven narrow PE standards (Mn = 326–5300) using the conventional method. Samples (~3 mg/mL) were dissolved at 100 °C in the same solvent used in the GPC reservoir then filtered hot using 0.45 μm PTFE membranes which were also preheated. Injections were performed using 100 μL of sample.

Synthesis of Lignin Inspired Molecules

LM1

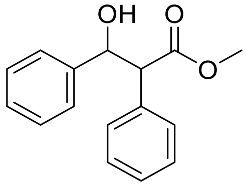

Methyl 3-hydroxy-2,3-diphenylpropanoate ***2***

To a solution of freshly distilled diisopropylamine (1.1 mL, 8 mmol) in dry THF (20 mL) at -78 °C was added n-butyl lithium (1.25 M in hexanes, 6 mL, 7.3 mmol). After 5 min, methyl phenylacetate (1 mL, 7.1 mmol) was added dropwise. The solution changed from clear to yellow. Reaction mixture was stirred for 20 min before dropwise addition of benzaldehyde (0.78 mL, 8.0 mmol) at -78 °C. Reaction mixture was stirred for an additional 15 min at -78 °C before coming to r.t. for 1 h. Reaction was quenched by addition of aqueous NH_4Cl then diluted with ethyl acetate (EtOAc). After partitioning, the organic layer was washed with H_2O (1×), aqueous NaCl (1×), then dried over $MgSO_4$ and filtered. Solvent removed affording white crystals in a yellow/brown oil which was purified via flash column chromatography eluting in 4:1 hexanes:EtOAc (R_f = 0.25). Product collected as an off-white solid (49% yield). ^{1}H NMR ($CDCl_3$-*d* 500 MHz): δ/ppm = 7.42-7.33 (m, 10H), 5.37-5.35 (d, 2H), 3.95-3.94 (d, 1H), 3.59 (s, 3H); ^{13}C NMR ($CDCl_3$-*d* 500 MHz): δ 173.95, 140.72, 135.22, 128.6, 128.54, 128.15, 127.87, 127.60, 126.66, 76.68, 59.90, 52.35; HRMS (ESI-TOF): m/z Calcd for $C_{16}H_{16}O_3$ [M + Na]$^+$, 279.0997; found, 279.1002.

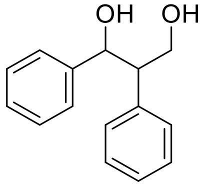

1,2-diphenypropane-1,3-diol ***LM1***

A solution of ethyl ester **2** (593 mg, 2.3 mmol) in dry Et_2O (5 mL) was added to a solution of $LiAlH_4$ (354 mg, 9.25 mmol) in dry Et_2O (2 mL) at 0 °C. Reaction allowed to come to r.t. and stirred for 3 h. After diluting with Et_2O, reaction quenched at 0 °C with H_2O (0.35 mL), then 15% NaOH (0.35 mL), followed by H_2O (1.05 mL). Solution stirred at rt for 15 min before drying over $MgSO_4$ and filtering. Solvent removed to afford a pure, white solid (86% yield). ^1H NMR ($CDCl_3$-*d* 500 MHz): δ/ppm = 7.23 (m, 8H), 7.09 (m, 2H), 5.10 (d, 1H), 4.27 (m, 1H), 4.06 (m, 1H), 3.23 (m, 1H), 2.9 (b, 1H). ^{13}C NMR ($CDCl_3$-*d* 500 MHz) δ 142.76, 139.22, 128.52, 18.47, 128.21, 127.72, 126.94, 126.57, 79.69, 66.42, 54.98; HRMS (ESI-TOF): m/z Calcd for $C_{16}H_{16}O_3$ $[M + Na]^+$, 251.1048; found, 251.1043.

LM2

Synthesis procedures were adopted from Kirk et. al.[32] and are summarized.

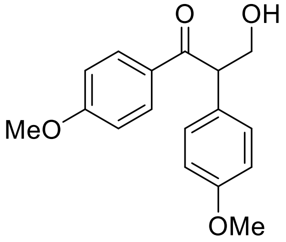

*3-hydroxy-1,2-bis(4-methoxyphenyl)propan-1-one **4***

Desoxyanisoin (500 mg, 1.95 mmol) and K_2CO_3 (40 mg, 0.29 mmol) were suspended in 96% ethanol (10 mL) and 1,4-dioxane (6 mL). The heterogenous mixture stirred for 5 min before treating dropwise with 37% formalin in water (150 μL, 2.0 mmol). Reaction stirred overnight at room temperature under atmospheric conditions during which time the reaction mixture became more homogenous. The mixture was filtered before removing solvent *in vacuo*. The residual desoxyanisoin was removed by flash column chromatography eluting with 2:1 hexanes:EtOAc (R_f = 0.3) to afford a pale, white oil that slowly crystallized (95% yield). ^{1}H NMR ($CDCl_3$-*d* 500 MHz): δ/ppm = 7.96 (d, 2H), 7.24 (d, 2H), 6.9 (dd, 4H), 4.73 (d, 1H), 4.27 (m, 1H), 3.89 (m, 1H), 3.87 (s, 3H), 3.81 (s, 3H); ^{13}C NMR ($CDCl_3$-*d* 500 MHz) δ 198.77, 163.56, 158.99, 131.29, 129.33, 128.70, 114.65, 113.78, 65.35, 55.47, 55.26, 55.22; HRMS (ESI-TOF): m/z Calcd for $C_{17}H_{18}O_4$ [M + Na]$^+$; 309.1103; found, 309.1107.

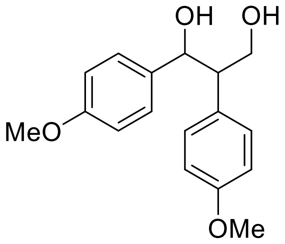

1,2-bis(4-methoxyphenyl)propane-1,3-diol ***LM2***

3-hydroxy-1,2-bis(4-methoxyphenyl)propan-1-one (530 mg, 1.85 mmol) was suspended in 50% aqueous ethanol (8 mL) and treated with $NaBH_4$ (280 mg, 7.4 mmol). After 3 h, the solids were filtered. The filtrate was diluted with aqueous NH_4Cl followed by extraction with diethyl ether (3×). The organic layers were combined, dried over $MgSO_4$, filtered, and the solvent removed *in vacuo*. The material was purified via flash column chromatography eluting with a gradient of 3:2 then 1:1 hexanes:EtOAc (R_f = 0.25) to afford a white solid (73% yield). ^{1}H NMR ($CDCl_3$-*d* 500 MHz): δ/ppm = 7.26-7.21 (q, 4H), 6.95-6.91 (q, 4H), 4.99-4.97 (d, 1H), 3.86 (s, 6H), 3.79 (b, 2H), 3.16 (q, 1H), 2.07 (b, 1H), 1.49 (b, 1H); ^{13}C NMR ($CDCl_3$-*d* 500 MHz) δ 159.33, 158.95, 134.17, 130.48, 130.09, 127.89, 114.25, 113.82, 75.60, 64.35, 55.33, 55.30, 55.12; HRMS (ESI-TOF): m/z Calcd for $C_{17}H_{20}O_4$ [M + Na]$^+$, 311.1259; found, 311.1251.

Photolysis of Lignin Inspired Molecules

LM1

Two solutions of LM1 were prepared, with photosensitizer 9,10-dicyanoanthracene (DCA) and without by the same general method. LM1 (24 mg) was dissolved in acetonitrile (5 mL) with and without DCA. The sample containing DCA was prepared by dissolving LM1 in a saturated solution of DCA in acetonitrile. Solutions were placed in quartz cuvettes and irradiated with a medium pressure Hg Arc lamp (228 nm - 420 nm) for 7h. TLC was performed in 3:2 EtOAc:hexanes and visualized using a compact UV lamp (254 nm).

LM2

Dissolved samples were prepared similarly as mentioned above for LM1, but with 2 mM of LM2. TLC conditions were the same as reported above. Solid samples of LM2 were also irradiated. LM2 (10 mg) was pressed into a thin layer between one quartz slide (ChemGlass) and one microscope slide (Fisher). The quartz slide was designated as the top and faced the lamp. The solid was a white powder before irradiation and after irradiation became yellow and sticky with a sweet odor. TLC was performed in 1:1 hexanes:EtOAc and visualized with p-anisaldehyde stain. GC-MS FID was performed in ethyl acetate at 1 mg/mL.

Model Polyhomologation Reaction

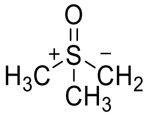

Dimethylsulfoxonium methylide

The ylide was prepared according to literature.[34] In summary, NaH (3.0 g, 89.3 mmol) was rinsed with dry hexanes (45 mL) then THF (15 mL) was added. After degassing the flask with nitrogen, oven dried trimethylsulfoxonium chloride (10.3 g, 81.2 mmol) was added hot using an oven dried spatula and funnel. The reaction flask was degassed again before adding the remaining THF (70 mL) to bring the volume of THF to a total of 85 mL. The mixture was slowly heated to 80 °C and refluxed for 4 h before filtering under N_2. The clear solution was then titrated using the following procedure. A sample of the reaction mixture (0.1 mL) was diluted into water (2 mL) followed by adding a couple drops of 0.5% phenolphthalein in ethanol. The solution became pink and was titrated with 0.1 M HCl until the color disappeared. The volume of HCl was used to determine the molarity of the ylide. This was repeated three times to obtain an average concentration of ylide.

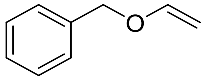

((vinyloxy)methyl)benzene

NaH (632 mg, 19 mmol) was rinsed with dry hexanes (5 mL, 3×) before suspending in THF (22 mL). The mixture was treated with benzyl alcohol (0.98 mL, 9.24 mmol) at room temperature. The reaction stirred under N_2 for 2 h before dropwise addition of allyl bromide (0.9 mL, 10.2 mmol). The reaction continued to stir at room temperature under N_2 for an additional 4 h before quenching with water. The mixture was extracted with ethyl acetate (3×), dried over $MgSO_4$, filtered through cotton, and solvent removed *in vacuo* to afford a light yellow liquid (95% yield). ^{1}H NMR ($CDCl_3$-*d* 500 MHz): δ/ppm = 7.41 (4H, m), 7.36 (1H, m), 6.01 (1H, m), 5.39-5.35 (1H, d), 5.28-5.26 (1H, d), 4.59 (2H, s), 4.09 (2H, d).

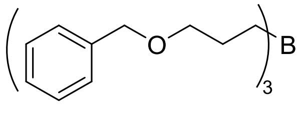

BnI

A dry, degassed flask was charged with a solution of ((vinyloxy)methyl) benzene (300 mg, 2.0 mmol) in dry, degassed THF or dichloromethane (0.67 mL). The solution was cooled to 0 °C before treating with borane dimethyl sulfide complex in THF 5M (0.13 mL, 0.67 mmol). The reaction became exothermic and darkened in color. The flask was allowed to come to room temperature slowly and stirred for an additional 2 h.

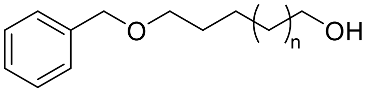

BnPM

Model Basic Aqueous Polyhomologation

A roundbottom flask was charged with trimethyl sulfoxonium iodide (19.8 g, 90 mmol) and tertbutyl ammonium iodide (997 mg, 2.8 mmol) then degassed three times with N_2. Then, degassed 50% NaOH (100 mL) and degassed dichloromethane (15 mL) were added and the reaction mixture was heated to 40 °C. After stirring vigorously for 24 h, the reaction mixture was treated with 30% H_2O_2 (3.1 mL) and stirred for an additional 24 h. The reaction mixture was allowed to cool to room temperature before being exposed to air. The mixture was then diluted into water (200 mL) and stirred for 30 min to allow the product to precipitate. The solution was filtered through Whatman filter paper 3 followed by rinsing with water then methanol. The white solid product was dried at 80 °C in a vacuum oven overnight to afford a quantitative yield. ^{1}H NMR (TCE-*d* 500 MHz): δ/ppm = 7.38-7.35 (5H, m), 4.54 (4H, s), 2.61 (2H, s), 1.48 (22H, b) 1.34 (276H, b).

Model Anhydrous Organic Polyhomologation

Dimethyl sulfoxonium methylide (1.3 M, 11.5 mL) was degassed for 30 min with N_2 before diluting into THF (25 mL), bringing the total volume to 36.5 mL. The solution was heated to 65 °C before fast injection of **BnI** (0.2 mL, 0.14 mmol). After 1 min, a large exothermic reaction was observed. After 35 min, the reaction was complete as confirmed by titration. Then, trimethylamine oxide dihydrate (333 mg, 3.0 mmol) was dissolved in DMSO (10 mL) and degassed with N_2 for 20 min before injecting into the reaction mixture. The reaction temperature was raised to 80 °C and allowed to stir for 24 h. The mixture was treated with aqueous NaOH (10 mL, 9 mmol) and allowed to stir for an additional 24 h. The reaction mixture became cloudy and light brown. The reaction mixture cooled to room temperature before diluting into water (200 mL) and stirring for 20 min. The mixture was filtered before rinsing the product with water then methanol. The product was dried at 80 °C in a vacuum oven over night (90% yield). ^{1}H NMR (TCE-*d* 500 MHz): δ/ppm = 7.38 (5H, m), 4.54 (2H, s), 3.67 (2H, t), 3.54 (2H, t), 1.35 (104H, s).

Synthesis of Organoborane Initiators

LM1 Initiator Synthesis

Initiators used in aqueous polyhomologation reactions were prepared in DCM. Initiators used in traditional polyhomologation reactions were prepared in THF.

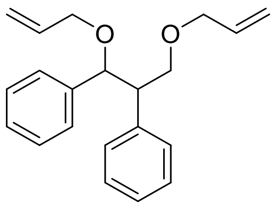

*(1,3-bis(allyloxy)propane-1,2-diyl)dibenzene **5***

A procedure adapted from literature[33] and is summarized as follows. Under a N_2 atmosphere, NaH (60% suspension in mineral oil, 258 mg, 7.5 mmol) was rinsed with dry hexanes (15 mL) then suspended in THF (15 mL). LM1 (428 mg, 1.87 mmol) was added as a solution in THF (5 mL). The reaction was slowly heated to 75 °C. After 30 min, allyl bromide (0.65 mL, 7.5 mmol) was added dropwise. After 3.5 h the reaction was complete by TLC (2% EtOAc in hexanes, $KMnO_4$ stain). The reaction was quenched with water (20 mL), extracted with EtO_2 (3×), the combined organic layers were dried over $MgSO_4$, filtered, and the solvent removed to produce a yellow liquid (89% yield). ^{1}H NMR ($CDCl_3$-*d* 500 MHz): δ/ppm = 7.26-7.10 (m, 10H), 5.91 (m, 2H), 5.31-5.17 (m, 4H), 4.87-4.66 (dd, 1H), 4.03 (m, 2H), 3.31 (m, 1H); ^{13}C NMR ($CDCl_3$-*d* 500 MHz) δ 140.24, 140.16, 135.14, 135.05, 129.17, 127.82, 127.78, 127.53, 127.30, 126.38, 116.49, 116.29, 82.54, 72.09,70.58, 69.76, 52.92; HRMS (ESI-TOF): m/z Calcd for $C_{21}H_{24}O_2$ [M + Na]$^+$, 331.1674; found, 331.1681.

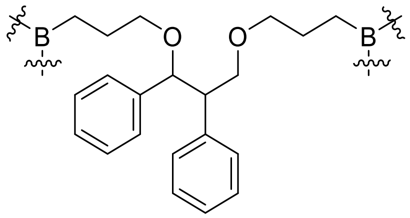

Organoborane initiator LM1

Under a N_2 atmosphere, LM1 (233 mg, 0.75 mmol) was dissolved in either THF or DCM (3 mL) then cooled to 0 °C before adding borane dimethylsulfide complex (5 M in Et_2O, 0.09 mL, 0.44 mmol). The reaction was allowed to warm to r.t. and then stirred for 2h. No further work up or purification was performed and the product was used as is.

LM2 Initiator Synthesis

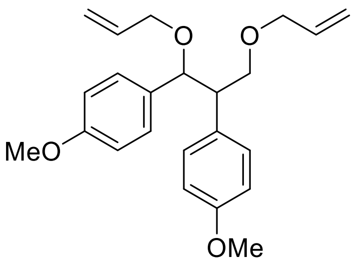

4,4'-(1,3-bis(allyloxy)propane-1,2-diyl)bis(methoxybenzene) ***6***

The same general procedure for **5** was used for **6**. In summary, NaH (60% dispersion in mineral oil, 178 mg, 5.3 mmol) was rinsed with dry hexanes (15 mL) then suspended in THF (5 mL). A solution of LM2 (381 mg, 1.32 mmol) in THF (8 mL) was added. The reaction was heated to 75 °C and after 30 min, allyl bromide (0.46 mL, 5.3 mmol) was added dropwise. After 3.5 h the reaction was complete by TLC (3:2 hexanes:EtOAc). The reaction was quenched with water (20 mL) then extracted with EtO_2 (3×), the combined organic layers were dried over $MgSO_4$, filtered, and the solvent removed producing a yellow oil (quantitative yield). ^{1}H NMR ($CDCl_3$-*d* 500 MHz): δ/ppm = 7.15-7.13 (d, 2H), 7.07-7.05 (d, 2H), 6.84-6.84 (dd, 4H), 5.95-5.83 (m, 2H), 5.29-5.25 (m, 1H), 5.21-5.20 (m, 1H), 5.17 (m, 1H), 5.14-5.12 (m, 1H), 4.77-4.76 (d, 1H), 3.96 (m, 2H), 3.84 (s, 6H), 3.81 (m, 2H), 3.76-3.72 (m, 1H), 3.52-3.49 (m, 1H), 3.08 (q, 1H); ^{13}C NMR ($CDCl_3$-*d* 500 MHz) δ 158.82, 158.20, 135.27, 135.05, 132.90, 131.76, 130.44, 128.42, 116.56, 115.95, 113.30, 113.12, 80.65, 72.05, 71.46, 69.55, 55.21, 55.18, 52.52; HRMS (ESI-TOF): m/z Calcd for $C_{23}H_{28}O_4$ $[M + Na]^+$, 391.1885; found, 391.1887.

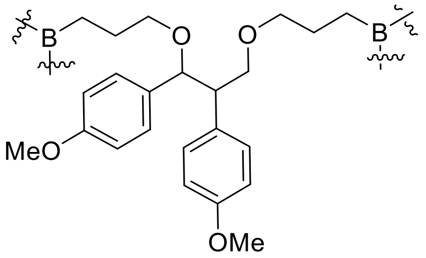

Organoborane initiator LM2

Under a N_2 atmosphere, a solution of LM2 (248 mg, 0.67 mmol) in either THF or DCM (3 mL) was treated at 0 °C dropwise with borane dimethylsulfide complex (5 M in Et_2O, 0.07 mL, 0.40 mmol). The reaction came to rt and stirred for 2h. No further work up or purification was performed and the product was used as is.

Synthesis of Polymers Containing Lignin Inspired Molecules

Polyhomologation with LM1

Basic Aqueous Polyhomologation of PMLM1

Trimethylsulfoxonium iodide (5.8 g, 26.4 mmol) and tetrabutylammonium iodide (220 mg, 0.59 mmol) were added to a flask then degassed. Degassed DCM (9 mL) was added followed by degassed 50% NaOH (17 mL). The mixture was stirred vigorously under N_2 and heated to 40 °C before fast addition of organoborane initiator LM1 (3 mL, 0.15 M). Reaction was stirred for 24 h before addition of 30% H_2O_2 (0.7 mL, 8.8 mmol) at r.t. Reaction was then heated to 40 °C and allowed to stir for another 24 h. Once cooled to rt the mixture was added into water and the precipitate filtered, rinsed with water and then methanol before drying under vacuum at 70 °C overnight to afford a white solid in quantitative yield. ^{1}H NMR (TCE-d_2 500 MHz): δ/ppm = 7.19-7.09 (m, 10H), 3.66 (t, 2H), 1.61 (m, 2H), 1.48 (s, 12H), 1.38 (s, 4H), 1.34 (s, 296H), 1.22 (b, 4H), 0.95 (t, 2H). Mw = 1897 g mol^{-1}, Mn = 1344 g mol^{-1}, PD = 1.41

Anhydrous Organic Polyhomologation of PMLM1

A solution of dimethylsulfoxonium methylide (20 mL, 28 mmol) was diluted with THF (60 mL) then heated to 65 °C followed by fast injection of organoborane initiator LM1 (3 mL, 0.44 mmol). After about 5 min, the reaction became exothermic and cloudy. After 1 h, the reaction was determined to be complete by titration of the reaction mixture. Then, a degassed solution of trimethylamine oxide (293 mg, 2.64 mmol) in DMSO (10 mL) was injected. The temperature of the reaction mixture was increased to 80 °C and allowed to reflux for 24 h. A degassed solution of aqueous NaOH (10 mL, 7.92 mmol) was added and a strong exothermic reaction was observed. The reaction mixture was stirred for an additional 24 hours before cooling to r.t. then precipitated into water. The solution was filtered, rinsed with water then methanol then dried in a vacuum oven at 70 °C to produce a white solid in quantitative yield. ^{1}H NMR (TCE-d_2 500 MHz): δ/ppm = 7.2-7.1 (m, 10H), 3.66 (t, 2H), 1.6 (m, 4H), 1.48 (s, 24H), 1.38 (s, 4H), 1.34 (s, 396H), 1.22 (b, 4H), 0.97-0.91 (m, 10H). Bimodal GPC trace, peak 1 Mw = 5784 g mol^{-1}, Mn = 5694 g mol^{-1}, PD = 1.10; peak 2 Mw = 3274 g mol^{-1}, Mn = 3205 g mol^{-1}, PD = 1.02

Polyhomologation with LM2

Basic Aqueous Polyhomologation of PMLM2

The same general procedure was used as reported for the aqueous polyhomologation of PMLM1. In summary, trimethylsulfoxonium iodide (3.96 g, 18.0 mmol) and tetrabutylammonium iodide (591 mg, 1.6 mmol) were added to a flask then degassed with nitrogen. Degassed DCM (3.5 mL) was added followed by degassed 50% NaOH (10.5 mL). The mixture was stirred vigorously and heated to 40 °C before fast addition of organoborane initiator **2**. Reaction stirred for 24 h and became milky white. The mixture was cooled to rt before addition of 30% H_2O_2 (0.7 mL, 8.8 mmol) which produced a large exothermic reaction. The reaction vessel was heated to 40 °C and allowed to stir for another 24 h. Once cooled to rt the mixture was precipitated into water, filtered, rinsed with water then methanol before being dried under vacuum at 70 °C to afford a white solid in quantitative yield. ^{1}H NMR (TCE-d_2 500 MHz): δ/ppm = 7.12-7.04 (m, 4H), 6.82-6.80 (m, 4H), 4.61 (d, 1H), 3.83 (s, 6H), 3.73 (b, 2H), 3.23 (b, 1H), 3.03 (b, 1H), 1.62-1.23 (b, 390H). Mw = 7648 g mol^{-1}, Mn = 7671 g mol^{-1}, PD = 1.003

Anhydrous Organic Polyhomologation of PMLM2

The same general procedure for dimethylsulfoxonium methylide and PMLM1 was used as described above.

In summary, a solution of dimethylsulfoxonium methylide (32 mL, 18 mmol) was diluted with THF (16 mL) then heated to 65 °C followed by fast injection of organoborane initiator LM2 (3 mL, 0.40 mmol). After about 5 min, the reaction became exothermic. After 1 h, the reaction was complete by titration of the reaction mixture. The reaction mixture was treated with a degassed solution of trimethylamine oxide (267 mg, 2.4 mmol) in DMSO (10 mL). The reaction then refluxed for 24 h. A degassed solution of aqueous NaOH (10 mL, 7.2 mmol) was added and a strong exothermic reaction was observed. The reaction mixture stirred for an additional 24 h before cooling to rt and precipitated into water. The solution was filtered, rinsed with water then methanol then dried in a vacuum oven at 70 °C to produce a white solid in quantitative yield. ^{1}H NMR (TCE-d_2 500 MHz): δ/ppm = 7.11-7.4 (m, 4H), 6.80 (m, 4H), 4.61 (d, 1H), 3.83 (s, 6H), 3.67 (t, 2H), 3.37 (m, 2H), 3.21 (b, 1H), 3.02 (b, 1H), 1.62 (m, 4H), 1.35 (s, 130H). Bimodal results; peak 1 Mw = 1692 g mol^{-1}, Mn = 1605 g mol^{-1}, PD = 1.01; peak 2 Mw = 863 g mol^{-1}, Mn = 836 g mol^{-1}, PD = 1.03

Photodegradation Studies of PMLM Films

Polymer samples (10 mg) were pressed between a quartz slide (ChemGlass) and a microscope slide (Fisher). One layer of labeling tape was attached to the microscope slide to set the thickness to about 25 μm. Once the polymer powder was crushed into a thin layer, the glass was heated to about 150 °C on a hot plate in order to quickly melt the polymer. The polymer was then cooled to r.t. and heated again to remove any thermal history. Samples were irradiated for 8 h using the same medium pressure Hg lamp as mentioned in the LM1 and LM2 photolysis experiments. After 8 h, the polymers were removed from the light source and shaved off with a razor blade for TLC and GPC experiments.

Samples were dissolved in hot toluene (~100 °C) for spotting. TLC was performed using a solution of toluene:hexanes:EtOAc in a 8:2:1 ratio at 60 °C. Spots were imaged using a compact UV lamp (254 nm). For staining, the TLC plates were treated with iodine followed by p-anisaldehyde stain.

Results and Discussion

Synthesis of Lignin Inspired Molecules

Drawing inspiration from studies that investigated the oxidation of lignin model compounds[22,32] as well as the photochemical and enzymatic cleavage of lignin β-1 model compounds[27] the molecular architecture of two lignin inspired molecules, LM1 and LM2 (Figure 3.4), were investigated. Our initial studies began by examining how methoxy substitution influences photoefficiency. These compounds were our first choice for our study of how arene substituents influence photocleavage. LM1 has no methoxy substitution while LM2 contains *para*-methoxy substituents. Based on a study of related molecules, it was hypothesized that LM1 would have lower photoefficiency for C-C bond cleavage compared to LM2.[27] Mariano et. al. previously determined the importance of methoxy substituents on arene rings of β-1 model compounds for photochemical C-C bond cleavage.

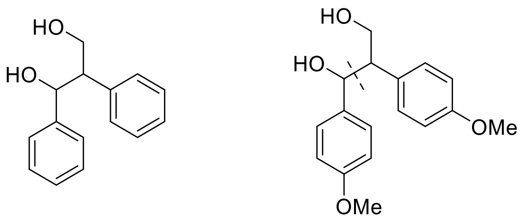

LM1 **LM2**

Figure 3.4: Structure of LM1 and LM2

LM1 was synthesized via an aldol addition followed by a lithium aluminum hydride reduction by procedure adapted from Mariano et al.[27] (Scheme 3.1). LM1 was obtained in 86% yield as a white solid. A similar method was originally used for LM2, but this afforded extremely low yields. Therefore, an alternative route was taken (Scheme 3.1).[32] The procedure adapted from Kirk et. al. provided LM2 in 73% yield as a white solid.

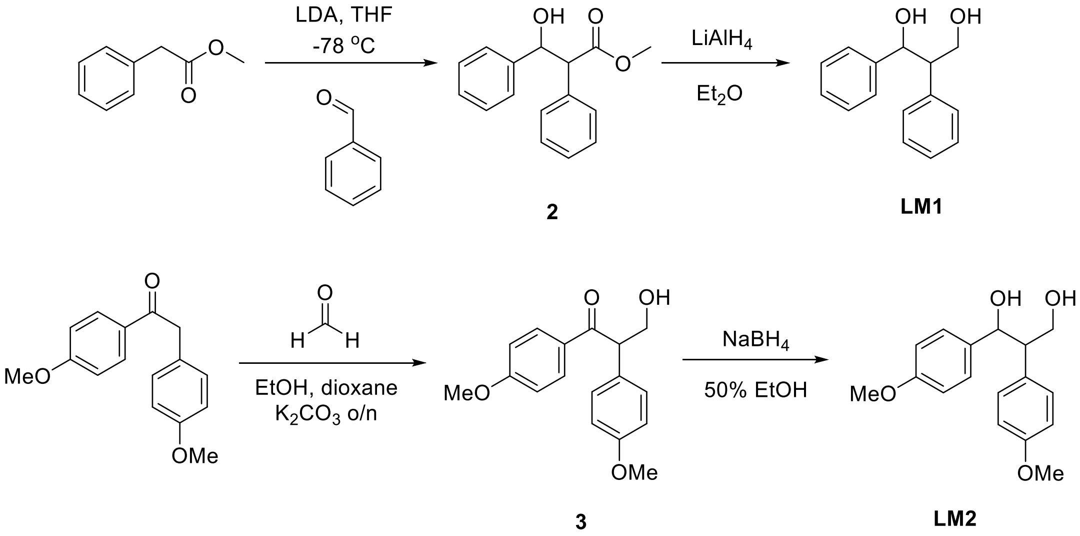

Scheme 3.1: Synthesis of LM1 and LM2.

Photolysis of Lignin Inspired Molecules

After synthesizing LM1 and LM2, we investigated the sensitivity of these molecules to irradiation with and without a photosensitizer, 9,10-dicyanoanthracene (DCA). DCA was chosen due to prior literature reports demonstrating photocleavage of similar compounds in the presence of DCA in aqueous acetonitrile.[27] It was expected that LM1 would show no sign of degradation, thereby acting as a control, while LM2 would experience C-C bond scission. Solutions of both compounds were prepared in acetonitrile (2 mM) with and without DCA. UV-Vis of each solution was obtained before irradiation to determine the λ_{max}. (Figure 3.5). The samples were then exposed to a medium pressure mercury lamp (450W, 280 – 420 nm) for up to 6 hours. After irradiation, UV-Vis, TLC, NMR, LCMS, and GC-MS were used to analyze the products.

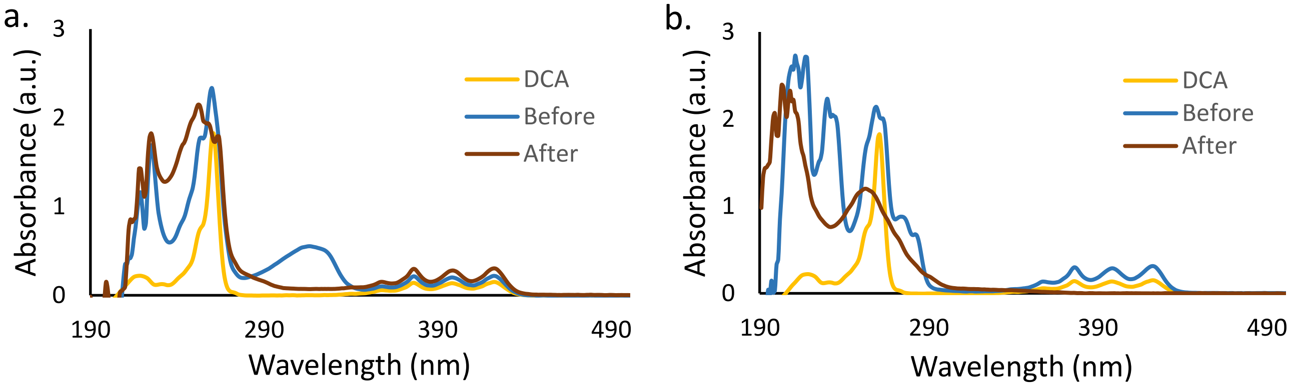

Figure 3.5: UV-Vis spectra of irradiation experiments with LM1 and LM2. DCA indicates the photosensitizer. Before indicates LM with DCA before irradiation. After indicates LM with DCA after irradiation. LM1 had a disappearance of its λ_{max} around 315 nm (a.). LM2 exhibited a shift and decrease of its λ_{max} around 275 nm (b).

The UV-Vis results were misleading. There was disappearance of a band at 304 nm in our LM1 samples. However, TLC and NMR data of LM1 suggested that LM1 was unchanged with no evidence of cleavage products. LCMS also supported the conclusion that LM1 did not undergo photolysis. We believe the band at 304 nm could be caused by an excimer between two LM1 molecules or an exciplex between LM1 and DCA. To further investigate the origin of this peak, we planned to alter concentrations of LM1 with and without DCA but did not have sufficient time to complete these experiments. After irradiation, the solution of LM2 exhibited a slight blue shift and decrease in intensity of the band at 261 nm. TLC and LCMS suggested that both LM2 and DCA were consumed. It should be noted that the DCA λ_{max} remained intact in the presence of LM1 but was consumed in the presence of LM2. The data supports our hypothesis that LM1 does not undergo photosensitized cleavage while LM2 does. The initial results of LM2 with DCA supports the idea that a photosensitizer and *para* methoxy substituted arene rings leads to C-C scission. We decided TLC, NMR, and MS data were the most reliable methods of understanding the photolabile nature of LMs.

In practical applications, the presence of a photosensitizer can interfere with the durability of plastic products. To examine if LM2 could undergo C-C scission without a photosensitizer, we performed photolysis experiments of LM2 as a solution in acetonitrile and as a solid, both in the absence of DCA. The data showed LM2 underwent complete cleavage after 4 hours in acetonitrile and up to 7 hours as a solid. There were several products on the TLC plate and in the NMR, but p-anisaldehyde was identified in both methods to be a major product based upon R_f values and comparing the NMR of an authentic p-anisaldehyde sample. This is in accordance to previous reports of similar compounds which favored formation of the aldehyde after undergoing sensitized photocleavage.[23-25,27] GC-MS with FID was performed and confirmed the presence of p-anisaldehyde as one of the major products with an *m/z* 135.0. Other products present in lower yield were not identified and starting material was also not present. From this data, we concluded that the C-C bond in LM2 could undergo C-C bond cleavage by direct irradiation in the absence of DCA.

Based upon previous reports, we believe the mechanism of scission involving DCA is through a SET leading to formation of a radical cation.[27] However, in the absence of DCA we suggest LM2 can undergo direct photoscission through a bimolecular mechanism. Instead of DCA acting as the single electron acceptor, a second molecule of LM2 may act as an electron acceptor. It is highly likely that based on the proximity of LM2 molecules in solution and as a neat solid, they would be able to form excimers through hydrogen bonding and π-π stacking. Therefore, excitation of one molecule can accept or donate an electron to its neighboring molecule. However, this would likely be diffusion controlled and the concentration of LM2 would be important. We were unable to perform concentration dependent experiments to further substantiate our hypothesis.

Model Polyhomologation Reactions

Our desire was to insert a photocleavable molecule in a PE-like polymer and evaluate the photodegradation of the polymer. Before continuing, we chose to run model reactions to ensure polyhomologation was compatible with our desired system. We explored benzyl alcohol as a model compound. The benzyl alcohol group is a substructural feature present in LM molecules and would give insight into properly running a polyhomologation reaction. To achieve a product with a narrow molecular weight distribution the polyhomologation reaction requires high analytical precision of monomer and catalyst. This living C1 polymerization method was developed in our lab and so we drew upon that expertise to pursue this reaction.[35-37]

Two polyhomologation protocols have been developed, a traditional organic anhydrous methodology (Scheme 3.2) and reactions run under basic aqueous conditions. The traditional method relies upon the prior formation of an “ate” complex between dimethylsulfoxonium methylide and an alkyl borane. The methylide acts as the monomer source while the alkyl borane is the initiator. Once the borane and ylide combine, a 1,2-migration results in insertion of a single carbon into the hydrocarbon polymer backbone and regenerates the borane initiator. This migration elongates the carbon chain by one carbon and repeats until the ylide is fully consumed. The last step is an oxidation-hydrolysis step, producing an α-hydroxypolymethylene. This occurs in the absence of termination or chain transfer events and produces a PM polymer with narrow molecular weight distribution.

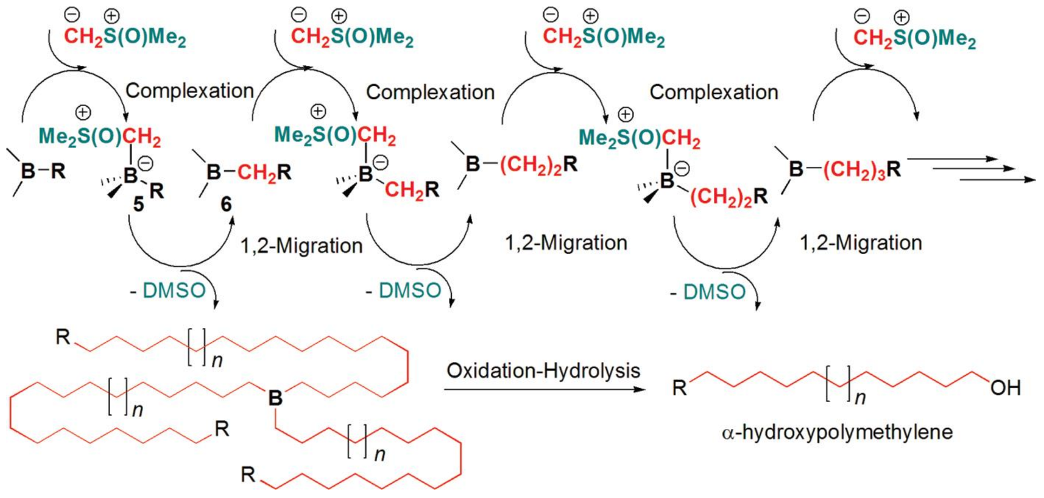

Scheme 3.2: Proposed mechanism for the polyhomologation reaction. Adapted with permission from reference 38. Copyright American Chemical Society 2010.

The basic aqueous method proceeds in a similar fashion, however instead of using dimethyl sulfoxonium methylide as the monomer source, the salt, trimethylsufloxonium iodide, is used as the monomer precursor.[39] Under strongly basic conditions, the ylide is generated *in situ* and hydroxide controls the rate of polymerization (Scheme 3.3).

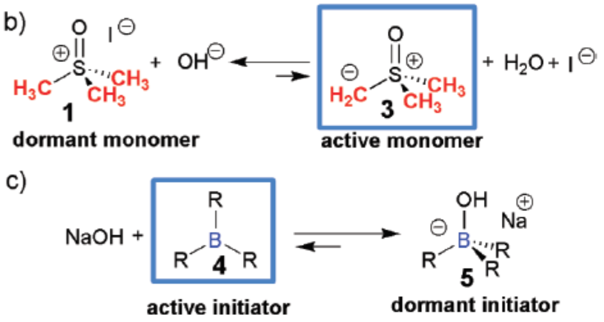

Scheme 3.3: Equilibrium for monomer production (b); equilibrium for initiator/catalyst production (c). Adapted with permission from reference 39. Copyright American Chemical Society 2012.

The borane initiator **BnI** was synthesized first. This was done by converting benzyl alcohol into an allyl benzyl ether followed by hydroboration. The same borane initiator was used in both the basic aqueous reaction and organic, anhydrous conditions. In both instances, **BnI** is injected into a solution containing the monomer source. Under basic aqueous conditions this includes trimethyl sulfoxonium iodide and tertbutyl ammonium iodide in an emulsion of 50% aqueous sodium hydroxide and dichloromethane. For anhydrous organic conditions, this involves a solution of dimethyl sulfoxonium methylide in THF. The polyhomologation reaction is then followed by oxidation and hydrolysis to produce the final polymer **BnPM** (Scheme 3.4).

Analysis by NMR suggested incorporation of an aromatic group into the polymer and end-group analysis of the methylene units suggested a degree of polymerization close to what was estimated based on the ratio of ylide to initiator used. GPC data showed a single, sharp peak. The molecular weight data from the organic anhydrous method (M_w of 1055, M_n of 974, and PD = 1.08) matched well with our calculated degree of polymerization and NMR data. It was noted that the molecular weight for the basic aqueous protocol (M_w of 7787, M_n of 7563, and PD = 1.03) was higher than calculated and expected. We felt confident in using the organic anhydrous protocol for polyhomologation to produce polymers with controlled molecular weights and narrow molecular weight distributions. This propelled us to incorporate LM1 and LM2 into a polyhomologation initiator/catalyst to produce polymethylene.

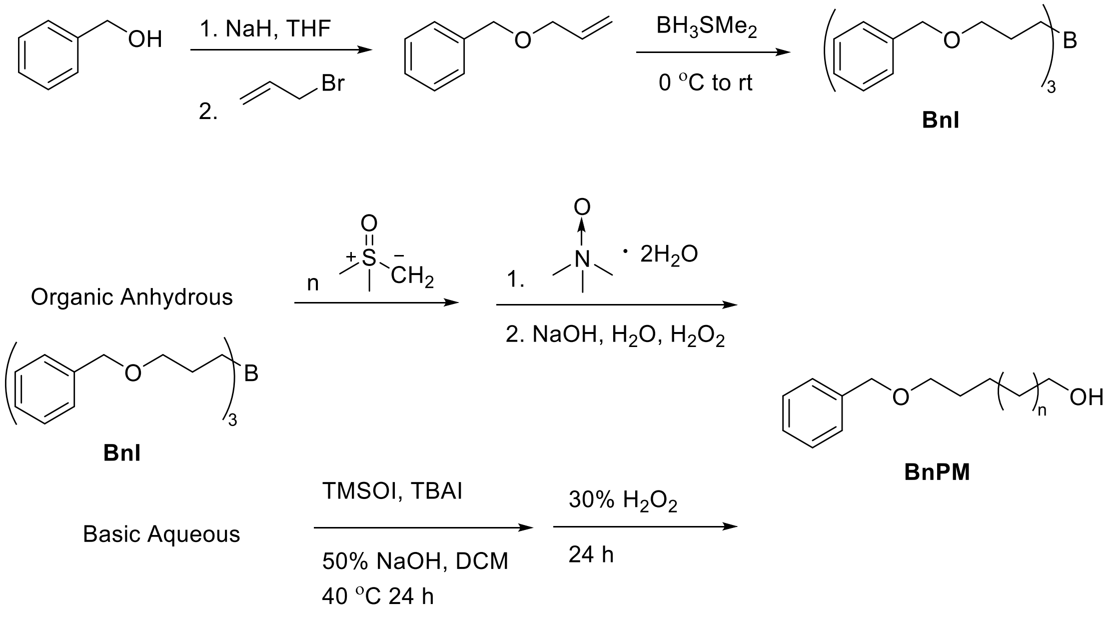

Scheme 3.4: Model polyhomologation reaction with benzyl alcohol.

Synthesis of Polymers Containing Lignin Inspired Molecules

To insert LM1 and LM2 into the middle of polymethylene polymers (PMLM1 and PMLM2 respectively), it was necessary to convert them into hexafunctional organoborane initiators. The 1,3 diol functionalities of LM1 and LM2 were converted into bis allyl ethers which were then subjected to hydroboration (Scheme 3.5). These initiator/catalysts were then exposed to the ylides, allowing polymer to growing from each end as described below. This, in theory, would allow us to place the LMs in the middle of the polymer. Obtaining very narrow molecular weight distributions would facilitate evaluation of chain scission by GPC. If the PMLMs were cleaved, the molecular weight would be reduced by half. PMLM1 was used as a control polymer (Figure 3.6) and was not expected to undergo chain scission.

The initiator/catalyst was used immediately after hydroboration to prevent oxidation of the borane which could result in formation of boronic esters. Boronic esters propagate at a lower rate than alkyl boranes which can lead to multiple products and a broader molecular weight distribution.[37] In both basic aqueous and organic anhydrous polyhomologation reactions, the organoborane initiator is injected quickly into hot solutions of the monomer or monomer precursor. Reactions are generally fast and exothermic, especially under traditional polyhomologation conditions. Caution should be exercised to control the reaction temperature to 65 °C since cooling of the reaction mixture can cause precipitation of the growing polymer, broadening the molecular weight distribution.

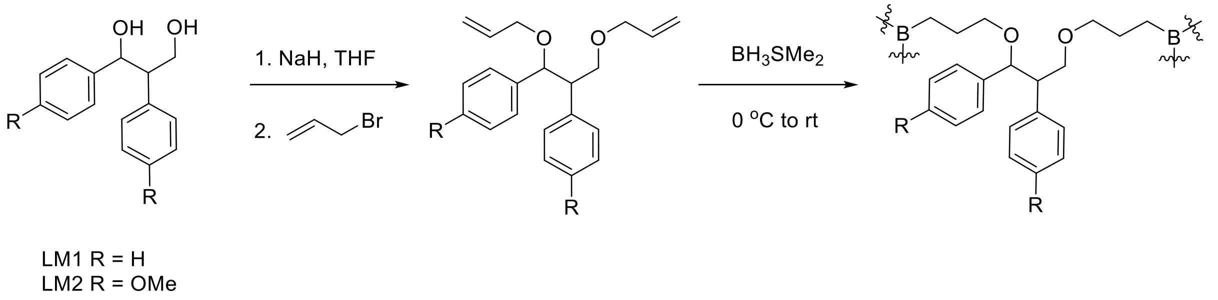

Scheme 3.5: Synthesis of organoborane initiators derived from LM1 and LM2.

Organic anhydrous polyhomologation reactions were titrated to confirm consumption of ylide prior to oxidation with trimethylamine oxide in DMSO. After about 30 min, all the ylide was consumed. Then, hydrolysis was performed with aqueous NaOH for an additional 24 hours under reflux. Once the reaction was cooled and precipitated into water, a white powder was obtained by filtration. Proposed PMLM1 and PMLM2 structures are shown in Figure 3.5. The organic anhydrous method afforded a 43% yield of PMLM1 and a 45% yield of PMLM2. Under basic aqueous conditions, after 24 hours oxidation is performed with 30% H_2O_2 and allowed to react for an additional 24 hours before cooling and diluting into water to collect the precipitated product. PMLM1 had a 43% yield and PMLM2 had a 60% yield.

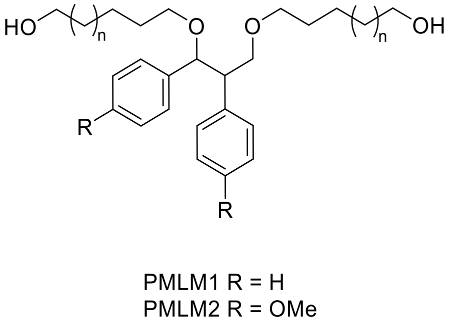

Figure 3.6: Structure of PMLM1 and PMLM2.

Polymers were then characterized by ^{1}H NMR, DSC, and GPC. We determined the organic anhydrous method of polyhomologation better suited our study and chose to focus on the results of those materials. The ^{1}H NMR analysis showed there were aromatic groups present from the LMs and a strong signal around 1.35 ppm indicating the presence of methylene units. From the DSC data (Figure S3.1), it was determined that these polymers were polycrystalline. The organic anhydrous polyhomologation afforded PMLM1 with 72% crystallinity and PMLM2 with 57%.[40] The basic structure of the polymer was confirmed, but end group analysis showed a higher DP than estimated based on the ratio of ylide to organoborane initiator. This may be in part due to the organoborane initiator synthesis from LMs (Scheme 3.4). Borane is a trifunctional molecule while the LMs are difunctional. If the analytical precision of each reagent is not high, the hydroboration might not have gone to completion, resulting in the presence of B-H bonds. The remaining B-H bonds would then react with the ylide at a faster rate than the B-R bonds leading to a separate population of polymers. Alternatively, if there was any oxidation leading to boronic esters from either the borane source or from the initiator/catalyst due to adventitious O_2, that would also contribute to another polymer population. In this case, it is more likely the hydroboration did not go to completion and for a reaction that requires high analytical precision to control molecular weight, this may have led contamination of our intended product by other side products. These side products may contribute an additional signal in the methylene region explaining why the DP appeared to be higher than predicted. To better understand the distribution of polymers, GPC was used to determine molecular weights.

GPC was performed at 110 °C using 1,2,4-trichlorobenzene as the solvent; the relative molecular weights are reported in the Experimental Section. It was intriguing to note that PMLM2 synthesized from the traditional polyhomologation conditions contained two polymer populations. The GPC showed one population that was half the molecular weight of the other. We believe this may be caused by an incomplete hydroboration reaction with LMs leading to B-H bonds that reacted with the ylide. After oxidation and hydrolysis, these single polymer chains would very likely have a lower molecular weight. This would explain the reason for two peaks in the GPC trace.

Photodegradation Studies of Polymers

Despite having less than perfect PMLM samples for the experiments, we felt it would be possible to analyze polymer fragmentation upon photolysis with the samples in hand. We therefore set out to test their susceptibility to photodegradation. This was accomplished by melting thin polymer films to about 130 °C between a quartz slide and a microscope slide. Quartz slides were used instead of glass to prevent short wavelength (190 – 340 nm) cutoff during irradiation. The film thickness was set to about 25 μm using labeling tape which prevented the slides from pressing completely together.

The same Hg lamp used in the LM photolysis experiments was used for polymer photodegradation studies. After irradiation, no change to the molecular weights of the PMLMs was detected. The GPC traces overlapped and no additional peaks indicating a lower molecular weight population of polymers appeared. These results led us to the conclusion that although LM2 is photosensitive, once incorporated into PMLM2, the system resists photocleavage.

There are a few plausible explanations as to why PMLM2 is not as photolabile as LM2. One may be that the population of LM2 is rather low in PMLM2, just as these linkages are in relatively low abundance in natural lignin. The absence of polymer cleavage suggests that the unsensitized photocleavage of LM2 may be a bimolecular process. This would be consistent with our earlier suggestion regarding our observation during the LM2 studies. Natural lignin does not easily photodegrade and this may in part be due to the abundance of aromatic moieties that can compete for absorption of photons. Another explanation is the crystalline nature of PMLM2. Highly crystalline polymers have many scattering centers. It is possible that the photoefficiency or quantum yield in these heterogenous highly scattering systems is extremely inefficient.

Due to time constraints, we were unable to move the project further. However, next steps include collaborating with the Furche group to determine the best combination of EDG and EWG on the arene rings to realize a molecule that undergoes C-C photofragmaentation more efficiently and at longer wavelengths. Based upon our understanding of the mechanism of cleavage, the bimolecular system is incompatible with our goals of achieving photolysis in a polymer system. Therefore, we would like to tune the functional groups on the arene rings to allow for a unimolecular excitation and cleavage. C-C bond cleavage could arise by promotion of electrons from the $C\text{-}C_{HOMO}$ into a C-C antibonding orbital. In this way, we would be able to develop a family of molecules which can then be incorporated into different commercially relevant polymers. Although in this study we focused on a PE analogue, we would like to develop a myriad of molecules that can be incorporated into various polymers through various polymerization methods to better suit industrial applications.

Conclusion

In this study, we synthesized two lignin model compounds to evaluate how methoxy substitution influences photosensitivity. After confirming LM2 is photolabile and successfully breaks down into smaller aromatic molecules in the absence of a photosensitizer, we incorporated both LMs into polymethylene to produce PMLM1 and PMLM2. Although we were unable to demonstrate PMLM2 was able to undergo C-C scission upon unsensitized UV irradiation, we believe that further studies may prove successful. To realize this suggestion, we propose converting the LMs into RAFT or ATRP initiators. Time permitted, there might have been optimal conditions to successfully convert the diol into an appropriate organoborane initiator for the polyhomologation reactions. Future studies would include computational work in collaboration with the Furche group to determine an appropriate match of EWG and EDG on the aromatic rings to optimize unimolecular photocleavage. Additionally, calculating the quantum efficiency of these substrates would be of particular interest.

References

(1) Reed, C., "Dawn of the Plasticene age" *New Sci.*, **2015**, *225*, 28-32.

(2) Geyer, R.; Jambeck, J.; Law, K.L., "Production, use, and fate of all plastics ever made" *Sci. Adv.*, **2017**, *3*, e1700782.

(3) Klemchuk, P.P., "Degradable plastics: a critical review" *Polym. Degrad. Stab.*, **1990**, *27*, 183-202.

(4) MacArthur, D.E.; Waughray, D.; Stuchtey, R.M., *The New Plastics Economy: Rethinking the Future of Plastics;* World Economic Forum, 2016.

(5) Nizzetto, L.; Futter, M.; Langaas, S., "Are agricultural soils dumps for microplastics of urban origin?" *Environ. Sci. Technol.*, **2016**, *50,* 10777-10779.

(6) O'Connor, I.A.; Golsteijn, L.; Hendriks, A.J., "Review of the partitioning of chemicals into different plastics: consequences for the risk assessment of marine plastic debris" *Mar. Pollut. Bull.,* **2016**, *113*, 17.

(7) Barnes, D.K.; Galgani, F.; Thompson, R.C.; Barlaz, M., "Accumulation and fragmentation of plastic debris in global environments" *Philos. Trans. R. Soc. B*, **2009**, *364*, 1985-98.

(8) Dris, R.; Imhof, H.; Sanchez, W.; Gasperi, J.; Galgani, F.; Tassin, B.; Laforsch, C., "Beyond the ocean: contamination of freshwater ecosystems with (micro-) plastic particles" *Environ. Chem.* **2015**, *12*, 539.

(9) Wright, S.L.; Kelly, F.J., "Plastic and human health: a micro issue?" *Environ. Sci. Technol.,* **2017**, *51*, 6634-6647.

(10) Jambeck, J.R.; Geyer, R.; Wilcox, C.; Siegler, T.R.; Perryman, M.; Andrady, A.; Narayan, R.; Law, K.L., "Plastic waste inputs from land into the ocean" *Science (Washington, DC, U.S.)*, **2015**, *347*, 768-771.

(11) Arthur, C.; Baker, J.; Bamford, H. Technical Memorandum NOS-OR&R-30; NOAA Marine Debris Program: Silver Spring, MD, 2009.

(12) Jahnke, A.; Arp, H.P.H.; Escher, B.I.; Gewert, B.; Gorokhova, E.; Kuhnel, D.; Ogonowski, M.; Potthoff, A.; Rummel, C.; Schmitt-Jansen, M.; Toorman, E.; Macleod, M., "Reducing uncertainty and confronting ignorance about the possible impacts of weathering plastic in the marine environment" *Environ. Sci. Technol. Lett.*, **2017**, *4,* 85-90.

(13) ASTM-D883, https://compass.astm.org/EDIT/html_annot.cgi?D88s, 2012.

(14) ASTM-D6866-16, https://www.astm.org/Standards/D6866.htm, 2016.

(15) Reddy, M.M.; Vivekandandhan, S.; Misra, M.; Bhatia, S.K.; Mohanty, A.K., "Biobased plastics and bionanocomposites: Current status and future opportunities" *Prog. Polym. Sci.*, **2013**, *38*, 1653-1689.

(16) Suyama, T.; Tokiwa, Y.; Ouichanpagdee, P.; Kanagawa, T.; Kamagata, Y., "Phylogenetic affiliation of soil bacteria that degrade aliphatic polyesters available commercially as biodegradable plastics" *Appl. Environ. Microbiol.*, **1998**, *64*, 5008-5011.

(17) Shogren, R.L.; doane, W.M.; Garlotta, D.; Lawton, J.W.; Willett, J.L., "Biodegradation of starch/polylactic acid/poly (hydroxyester-ether) composite bars in soil" *Polym. Degrad. Stab.*, **2003**, *79*, 405-411.

(18) Tokiwa, Y.; Calabia, B.P., "Biodegradability and biodegradation of poly (lactide)" *Appl. Microbiol. Biotechnol.*, **2006**, *72*, 244-251.

(19) Kim, E.Y; Lee, J.K.; Lee, W.K., "Hydrolytic kinetics of Langmuir monolayers of enantiomeric poly (lactide) s" *Curr. Appl. Phys.*, **2006**, *6*, 735-738.

(20) Hopewell, J.; Dvorak, R.; Kosior, E., "Plastics recycling: challenges and opportunities" *Philos. Trans. R. Soc. B*, 2009, **364**, 2115-2126.

(21) Sheldon, R.A.; Arends, I.W.C.E.; Hanefeld, U., Green Chemistry and Catalysis, Wiley-VCH, Weinheim, 2007.

(22) DiCosimo R.; Szabo, H.C., "Oxidation of Lignin Model Compounds Using Single-Electron transfer Catalysts" *J. Org. Chem.* **1988**, *53*, 1673-1679.

(23) Cho, D. W.; Parthasarathi, R.; Pimentel, A. S.; Maestas, G. D.; Park, H. J.; Yoon, U. C.; Dunaway-Mariano, D.; Gnanakaran, S.; Langa, P.; Mariano, P. S. "Nature and kinetic analysis of carbon-carbon bond fragmentation reactions of cation radicals derived from SET-oxidation of lignin model compounds" *J. Org. Chem.* **2010**, *75*, 6549-6562.

(24) Mitchell, L. J.; Moody, C. J.; "Solar photochemical oxidation of alcohols using catalytic hydroquinone and copper nanoparticles under oxygen: oxidative cleavage of lignin models" *J. Org. Chem.* **2014**, *79*, 11091-11100.

(25) Cho, D. W.; Latham, J. A.; Park, H. J.; Yoon, U. C.; Langan, P.; Dunaway-Mariano, D.; Mariano, P. S. "Regioselectivity of enzymatic and photochemical single electron transfer promoted carbon-carbon bond fragmentation reactions of tetrameric lignin model compounds" *J. Org. Chem.* **2011**, *76*, 2840-2852.

(26) Nguyen, J.D.; Matsuura, B.S.; Stephenson, C.R.J. "A photochemical strategy for lignin degradation at room temperature" *J. Am. Chem. Soc.* **2014**, *136*, 1218-1221.

(27) Lim, S.H.; Lee, W.S.; Kim, Y.I.; Sohn, Y.; Cho, D.W.; Kim, C.; Kim, E.; Latham, J.A.; Dunaway-Mariano, D.; Mariano, P.S. "Photochemical and enzymatic SET promoted C-C bond cleavage reactions of lignin β-1 model compounds containing varying number of methoxy substituents on their arene rings" *Tetrahedron*, **2015**, *71*, 4236-4247.

(28) Luo, N.; Wang, M.; Li, H.; Zhang, J.; Liu, H.; Wang, F. "Photocatalytic oxidation-hydrogenolysis of lignin β-O-4 models via a dual light wavelength switching strategy" *ACS Catal.*, **2016**, *6*, 7716-7721.

(29) Guadix-Montero, S.; Sankar, M. "Review on Catalytic Cleavage of C-C inter-unit linkages in lignin model compounds: Towards lignin depolymerization" *Topics in Catalysis*, **2018**, *61*, 183-198.

(30) Fang, Z.; Meier, M.S.; "Toward the oxidative deconstruction of lignin: oxidation of β-1 and β-5 linkages" *Org. Biomol. Chem.*, **2018**, *16*, 2330-2341.

(31) Rinaldi, R.; Jastrzebski, R.; Clough, M.T.; Ralph, J.; Kennema, M.; Bruijnincx, P.C.; Weckhuysen, B.M., "Paving the Way for Lignin Valorisation: Recent Advances in Bioengineering, Biorefining and Catalysis" *Angew. Chem., Int. Ed.,* **2016**, *55*, 8164-8215.

(32) Kirk, T.K.; Nakatsubo, F. "Chemical mechanism of an important cleavage reaction in the fungal degradation of lignin" *Biochimica et Biophysica Acta*, **1983**, *756*, 376-384.

(33) Seeback, D.; Lapierre, J.M.; Greieldinger, G.; Skobridis, K. "Synthesis of chiral starburst dendrimers from PHB-derived triols as central cores" *Helvetica Chimica Acta* **1994,** *77*, 1673-1688.

(34) Baez, J.E.; Zhao, R.; Shea, K.J. "Synthesis of poly(methylene-*b*-*ε*-caprolactone) and poly(*ε*-caprolactone) with linear alkyl end groups: synthesis, characterization, phase behavior, and compatibilization efficacy" *Ind. Eng. Chem. Res.* **2017**, *56*, 10366-10383.

(35) Shea, K. J.; Walker, J. W.; Zhu, H.; Paz, M.; Greaves, J. "Polyhomologation. A living polymethylene synthesis" *J. Am. Chem. Soc.* **1997**, *119*, 9049-9050.

(36) Shea, K. J. "Polyhoologation: The living polymerization of ylides" *Chem. Eur. J.* **2000,** *6,* 1113-1119.

(37) Busch, B. B.; Paz, M. M.; Shea, K. J.; Staiger, C. L.; Stoddard, J. M.; Walker, J. R.; Zhou, X. Z.; Zhu, H. "The boron catalyzed polymerization of dimethylsulfoxonium methylide. A living polymethylene synthesis" *J. Am. Chem. Soc.* **2002**, *124*, 3636-3646.

(38) Luo, J..; Shea, K.J. "Polyhomologation. A living C1 polymerization" *Acc. Chem. Rev.* **2010**, *43*, 1420-1433.

(39) Luo, J.; Lu, F.; Shea, K.J. "Hydrocarbon waxes from a salt in water: the C1 polymerization of trimethylsulfoxonium halide" *ACS Macro Lett.*, **2012**, *1*, 560-563.

(40) Sperling, L. H. *Introduction to Physical Polymer Science*, 4th ed.; Wiley: Hoboken,

NJ, **2005.**

Supporting Information

DSC Curves of PMLM’s

a.

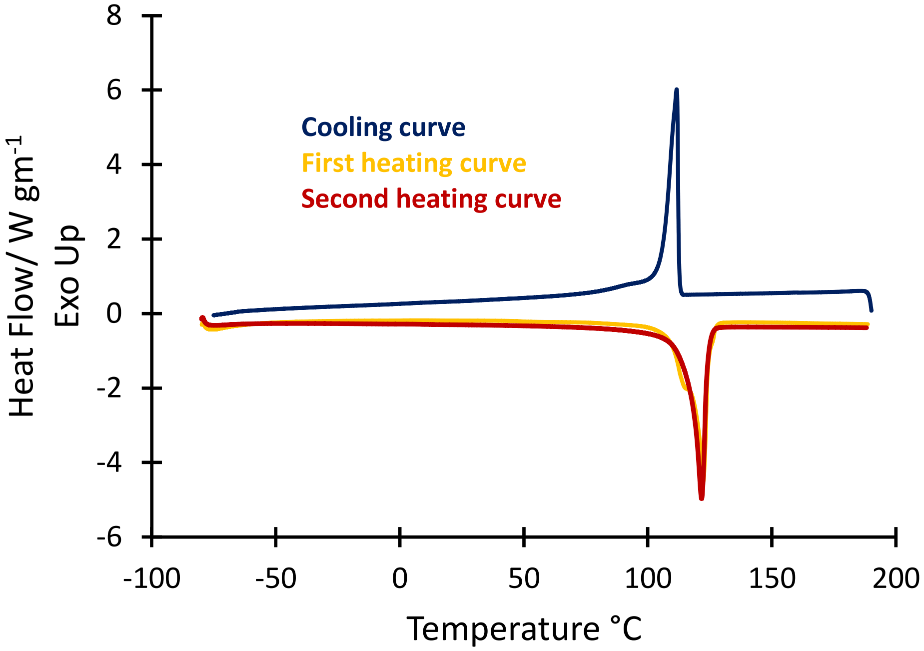

b.

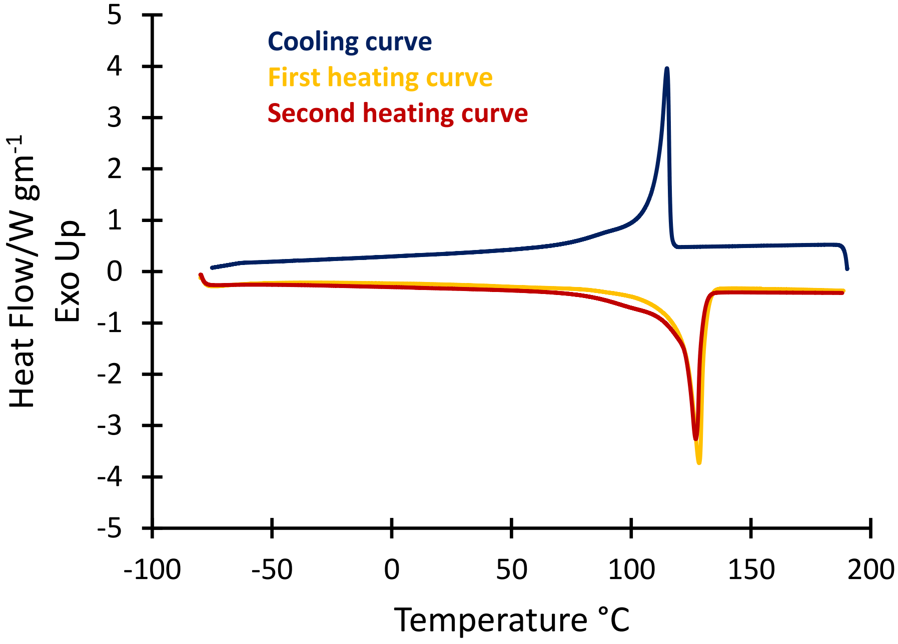
Cooling curve
First heating curve
Second heating curve
Heat Flow/W gm-1
Exo Up
Temperature °C
5
4
3
2
1
0
-1
-2
-3
-4
-5
-100
-50
0
50
100
150
200

c.

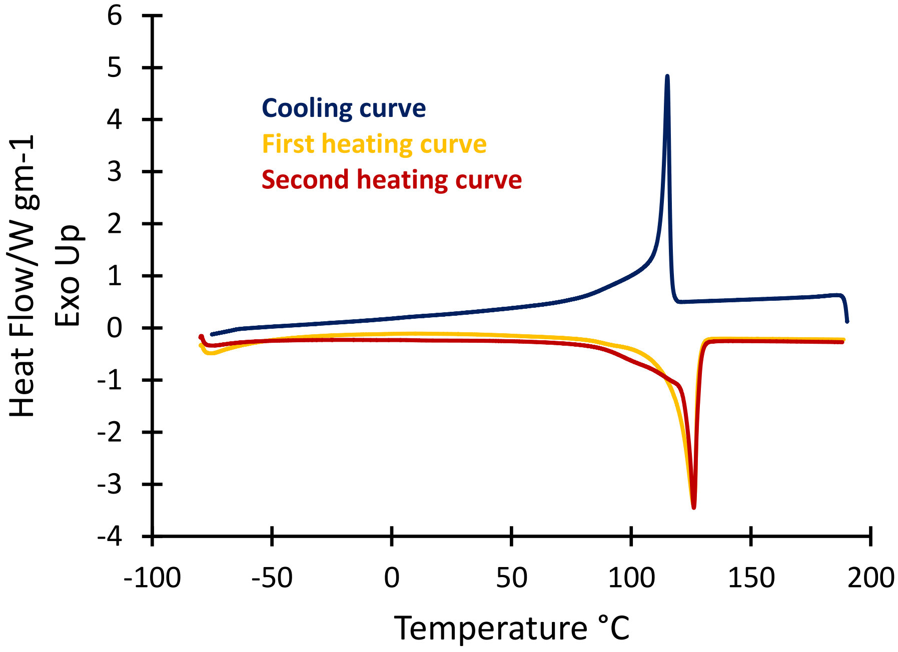
Cooling curve
First heating curve
Second heating curve
Heat Flow/W gm-1
Exo Up
Temperature °C
6
5
4
3
2
1
0
-1
-2
-3
-4
-100
-50
0
50
100
150
200

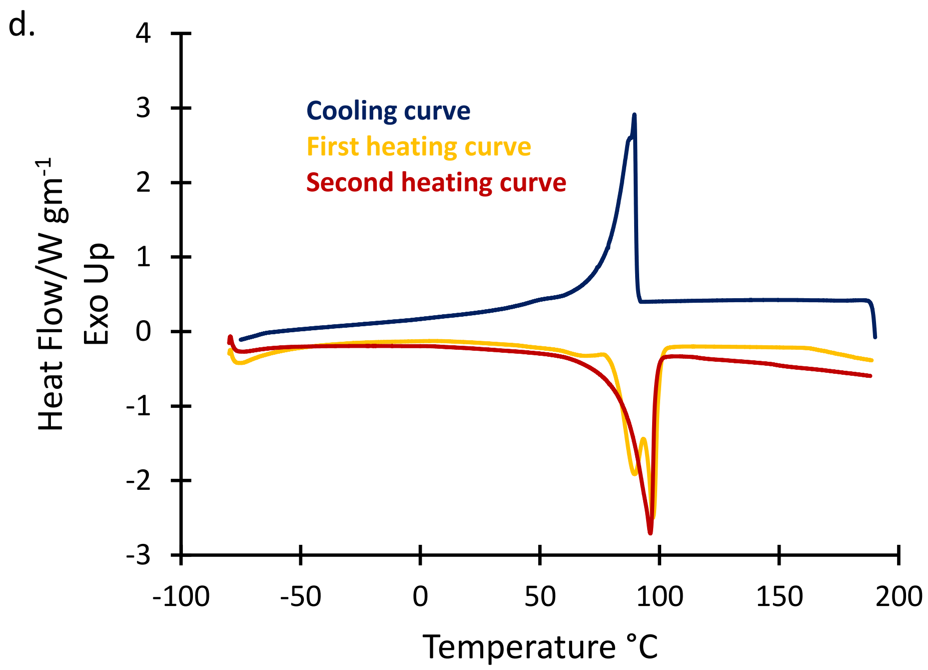

Figure S3.1: DSC traces of PMLM1 and PMLM2. Trace for PMLM1 synthesized under traditional conditions (a); Trace for PMLM1 synthesized under aqueous conditions. (b); Trace for PMLM2 synthesized under aqueous conditions. (c); Trace for PMLM2 synthesized under traditional conditions (d).